UNIVERSITÀ DI PARMA

UNIVERSITY OF PARMA

PhD in Biotechnology and Life Science

XXXII cycle

ANTI-AMYLOID-β OLIGOMER ACTIVITY OF HUMAN PHENYL-γ-VALEROLACTONE METABOLITES AND THE USE OF YEAST MODEL SYSTEMS TO STUDY AMYLOID NEURODEGENERATIVE PATHOLOGIES

Coordinator:

Prof. Simone Ottonello

Tutor:

Prof. Simone Ottonello

Prof. Roberta Ruotolo

PhD student:

Ilaria Minato

2016-2019

Index

ABSTRACT 1
INTRODUCTION 3
1. NEURODEGENERATIVE DISEASES 4
2. MISFOLDED PROTEINS IN NEURODEGENERATIVE DISEASES: PATHOLOGICAL FEATURES AND CLINICAL MANIFESTATION 7
2.1 Alzheimer's disease 8
2.2 Parkinson's disease 10
2.3 Huntington's disease 12
2.4 Amyotrophic lateral sclerosis 13
3. AN OLIGOMER-CENTRIC VIEW OF NEURODEGENERATION 14
3.1 Aβ oligomers: identity and mechanisms of toxicity 17
3.2 Amyloid oligomers in other NDs 19
3.3 Challenges in developing an oligomer-targeting therapy 19
4. YEAST AS MODEL SYSTEM TO STUDY AMYLOID-INDUCED TOXICITY 22
4.1 Yeast models for Alzheimer's disease 23
PART I 31
1. INTRODUCTION TO PART I 32
2. RESULTS (PART I) 41
2.1 A highly sensitive yeast model to assess β-amyloid oligomer-induced cytotoxicity 41
2.2 PVLs relieve β23-induced cytotoxicity in yeast 44
2.3 PVLs counteract β23-induced toxicity in human cells 48
2.4 (4'-OH)-PVL activity on human $A\beta_{42}$ 51
2.5 (4'-OH)-PVL prevents memory deterioration and attenuates neuroinflammation in an acute mouse model of AβO-induced neurotoxicity 55
3. DISCUSSION (PART I) 59
4. MATHERIAL AND METHODS (PART I) 63
PART II 73
1. INTRODUCTION TO PART II 74
2. RESULTS (PART II) 77
2.1 Different toxicity profiles were observed in yeast models of NDs 77

2.2 RNA-sequencing analysis 81
2.3 Enrichment analysis reveals common pathways associated to amyloid aggregate formation in yeast cells 84
2.4 Iron homeostasis is perturbed upon amyloid protein expression..... 88
2.5. Mitochondrial functionality is differentially altered in AD-like and PD models 90
2.6 An extreme alteration of the cell cycle regulatory pathways is a signature for AD-like model 95
2.7 Meiosis-regulatory genes are aberrantly activated in AD-like model..... 99
3. DISCUSSION (PART II) 102
4. MATERIALS AND METHODS (PART II)..... 107
CONCLUSIONS AND FUTURE PERSPECTIVES 115
ABBREVIATIONS..... 118
REFERENCES 121

ABSTRACT

Age-related neurodegenerative diseases (NDs) include a number of sporadic, and less frequently genetic, pathological conditions affecting the central or the peripheral nervous system, causing cognitive decline and motor symptoms. As the lifespan globally increases, NDs are becoming one of the most pressing medical and societal challenge worldwide, but no effective disease-modifying therapy is currently available. Despite their differences, NDs are associated with a decline in cellular proteostasis and the accumulation of insoluble deposits of misfolded proteins, which aggregate in highly ordered cross-β fibrils named amyloids. Even if amyloid deposits are the main histopathological hallmark of NDs, a series of evidences points to the soluble, prefibrillar amyloid oligomers as the ultimate neurotoxic species. Oligomers can act both extracellularly and intracellularly and induce various cytotoxic effects, including oxidative stress, mitochondrial damage, alterations in endoplasmic reticulum, vesicular trafficking and apoptotic signalling, eventually leading to neuroinflammation and cognitive impairment.

The aim of this thesis work is using *Saccharomyces cerevisiae*, an organism that has been extensively validated to study human diseases, as system to model amyloid oligomer toxicity, in order to identify molecules with anti-oligomer activity and investigate molecular pathways involved in amyloid neurodegenerative pathologies.

This PhD thesis consists of two parts. **Part I** introduces the development of a new yeast model of Alzheimer's disease (AD) oligomeropathy. Since yeast proved to be quite tolerant to the expression of the human amyloid peptide ($A\beta_{42}$), whose oligomerization is thought to be causal in AD, I resorted to an artificial polypeptide (β23) that forms amyloid-like oligomers and shows a dose-dependent toxicity in yeast cells.
Recently, flavonoids and flavan-3-ols, polyphenolic compounds deriving from dietary sources associated with a reduced incidence of NDs, are gaining attention for their neuroprotective properties, but they are characterized by a generally low bioavailability, as they undergo a broad host- and gut microbiota-assisted metabolism that complicates the identification of the most relevant bioactive species. I thus addressed this issue by examining the ability of phenyl-γ-valerolactones (PVLs), the main circulating flavan-3-ol metabolites in humans, to prevent amyloid-oligomer toxicity. Several PVLs, and particularly the monohydroxylated 5-(4'-hydroxyphenyl)-γ-valerolactone metabolite [(4'-

OH)-PVL], relived β23 oligomer-induced cell death in the 'AD-like' yeast model and in a human cell line. (4'-OH)-PVL also interfered with $A\beta_{42}$ oligomer formation *in vitro* and remodelled preformed AβOs into amorphous, non-toxic aggregates. Conversely, it did not show any significant effect on Aβ fibrillization. Importantly, treatment of AβOs with (4'-OH)-PVL prior to brain injection reduced recognition memory deterioration as well as neuroinflammation in a mouse model of AβO-induced memory impairment.

In **Part II**, a comparative transcriptomic analysis is carried out in the AD-like model and in the yeast models for Parkinson's disease (PD), Huntington's disease (HD) and amyotrophic lateral sclerosis (ALS), which are based on the inducible expression of the human amyloidogenic proteins underlying the pathogenesis of these disorders. I evaluated the transcriptional response at different time points, in order to identify both early and late changes associated with amyloid aggregate formation or aimed at their detoxification. RNA-sequencing revealed a fast and differentiated response of *S. cerevisiae* to the formation of different amyloid structures and the AD-like and PD models, along with a more toxic phenotype, presented the highest number of differentially expressed genes. In all strains, closely connected pathways associated with protein aggregation and proteotoxic stress resulted activated, which included responses to unfolded protein, oxidative stress and deficiency of essential metal ions like iron, corroborating previous findings about the role of these pathways in amyloid toxicity. Mitochondrial dysfunctions were evidenced in both the AD-like and PD models, but with an almost opposite gene modulation, and different alterations in mitochondrial morphology pointed to different implication of the mitochondrial fission and mitophagy processes. A strong decrease in transcripts for proteins involved in translation was characteristic of the PD model, while the downregulation of genes participating to mitotic cell division was a signature of the AD-like model. Even more, the activation of meiotic pathways that could induce haploid cells to sporulate were index of a profound damage of cellular division and DNA replication processes. Lastly, preliminary observation suggested the relevance of protein disordered regions in a context of cellular stress induced by amyloid-aggregate formation.

INTRODUCTION

1. NEURODEGENERATIVE DISEASES

Neurodegenerative diseases (NDs) are a heterogeneous group of chronic, highly debilitating diseases characterized by the progressive loss of neurons in specific areas of the central nervous system (CNS), a process referred to as neurodegeneration. Affecting the brain or the spinal cord and involving the peripheral nervous system as well, NDs cause cognitive decline (dementia), behavioural changes or motor symptoms (ataxia). NDs include, among others, Alzheimer's disease (AD), Parkinson's disease (PD), Huntington's disease (HD) and amyotrophic lateral sclerosis (ALS). They differ in prevalence, clinical manifestations and genes involved, either being solely genetic or existing in both sporadic and familial forms. Anyhow, the main risk factor associated with NDs is old age (Fig. 1). PD, for example, affects 1% of the population over the age of 60 and its prevalence reaches 5% over the age of 85[1].

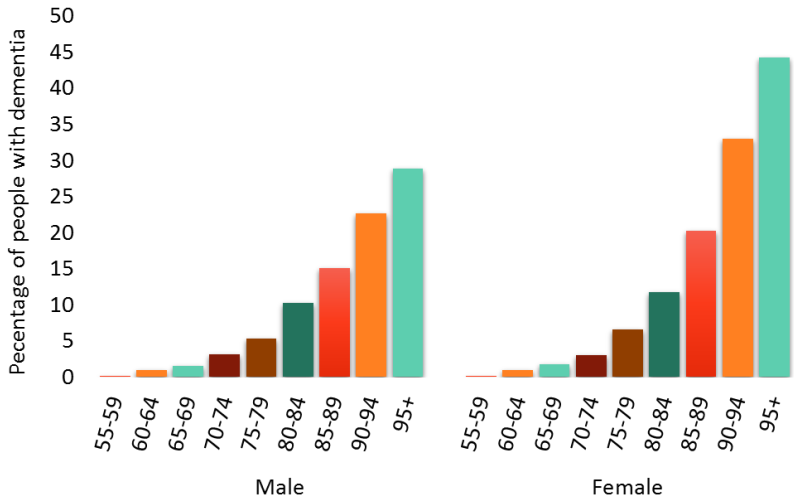

Figure 1. Risk of dementia increases with age. For each age group, percentage of people estimated to have dementia is indicated, separated by gender[2].

As average life expectancy is getting longer, populations are ageing[3] and consequently the prevalence/incidence of NDs is rising, becoming a major medical and societal challenge worldwide. People living with dementia were reported to be 50 million in 2018 and are predicted triplicate by 2050 (Fig. 2A), with not only a physical and psychological impact on their carers or families, but also with high health and social care costs (Fig. 2B). AD, which counts for 60%-70% of the cases of dementia, imposes a larger financial

burden than cancer or heart diseases - due to its long-term course - and its cost is forecast to double over the next 10 years[4].

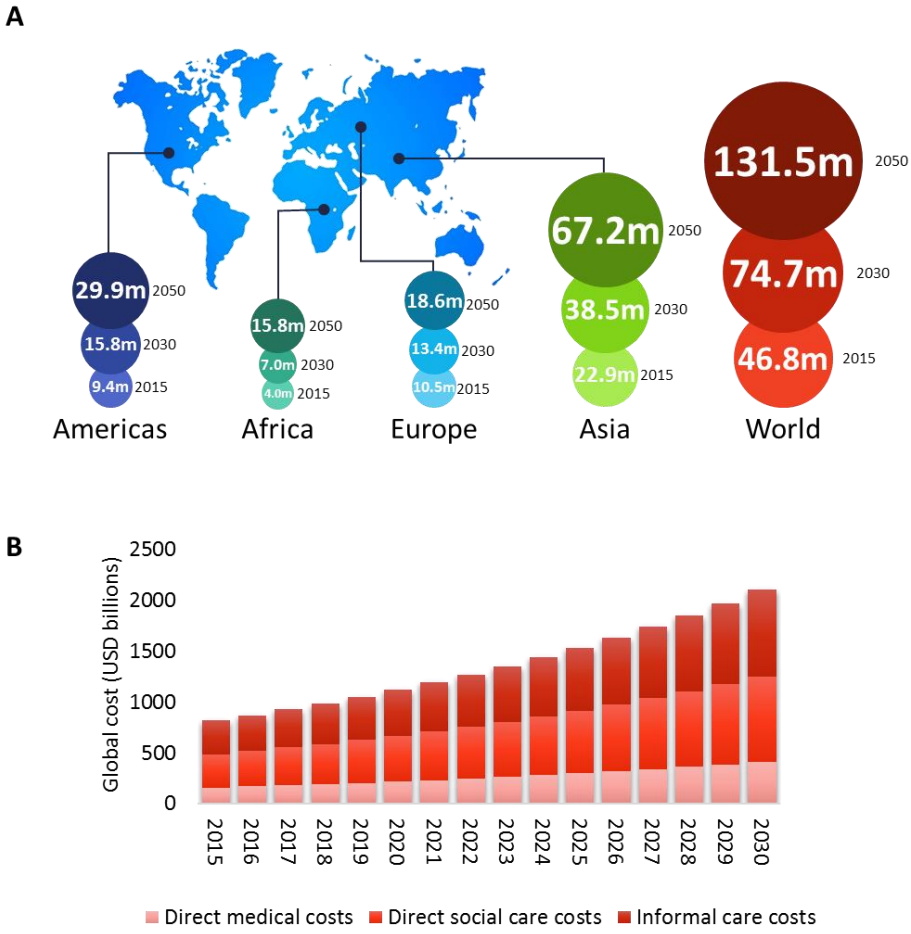

Figure 2. Global impact of dementia. A) People living with dementia around the world. B) Forecasted global costs of dementia 2015-2030[2].

There are no effective therapies or preventive strategies for NDs. This is the most regrettable consequence of the poor understanding of their ultimate aetiopathology, due at least in part to their multifactorial nature. Nonetheless, most NDs share a decline in cellular proteostasis that leads to the misfolding and aggregation of specific proteins, which accumulate in the brain as amyloid inclusions. Amyloids are defined as proteinaceous deposits of highly ordered fibrils, insoluble in aqueous buffer, 100-200 Å in diameter and composed of β-sheets running perpendicular to the fibril axis. They are

commonly recognized from their ability to bind specific dyes such as Congo Red or Thioflavin-T (Th-T)[5] (Fig. 3).

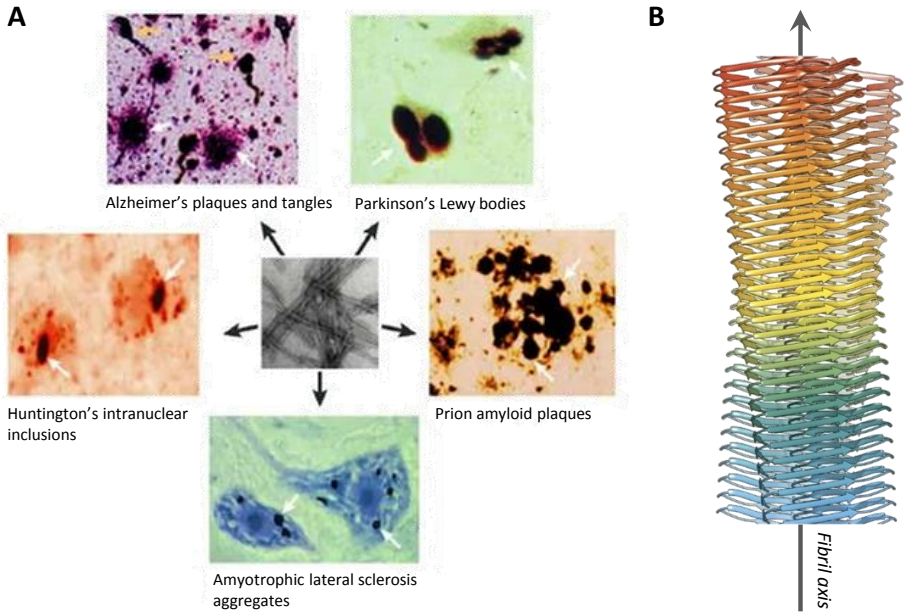

Figure 3. Cerebral amyloid aggregates in NDs. A) Extracellular senile plaques (white arrows) and intracellular neurofibrillary tangles (yellow arrows) are the pathological signature of AD. Intracytoplasmic aggregates are typically found in PD and ALS patients, while intranuclear inclusions of huntingtin are present in neurons of people affected by HD (white arrows). Amyloid plaques form also in some form of spongiform encephalopathies (modified from[6]). B) In spite of the different protein compositions, the ultrastructure of these deposits seems to be similar and composed mainly of a network of fibrillar polymers, made of β-sheets running perpendicular to the fibril axis (modified from[7]).

Although insoluble fibrillar aggregates represent the main histopathological hallmarks of NDs and were initially thought to be the causative agents, more recent findings showed that the smaller, soluble, prefibrillar oligomers may actually constitute the most proximal neurotoxic species. Oligomers, which exist in equilibrium with monomers and fibrils, are extremely dynamic in nature, range in size from dimers to higher-order aggregates and may be the triggers of the pathological events, especially at the early stages of the disease[8]. The deposition of misfolded proteins into larger and less reactive amyloid inclusions, on the other hand, could be considered as a protective mechanism to decrease the toxic oligomer levels[9].

2. MISFOLDED PROTEINS IN NDs: PATHOLOGICAL FEATURES AND CLINICAL MANIFESTATION

Since the aberrant folding of specific proteins is the molecular process thought to be at the basis of neurodegeneration, NDs are often classified as protein misfolding diseases[10].

Proteins need to assume a correct three-dimensional structure in order to fulfil their biological functions, but the majority of proteins is only marginally stable in its native state, a condition that allows the protein to maintain a certain degree of flexibility but also gives way to the transient occurrence of potentially dangerous unfolded conformations[11,12].

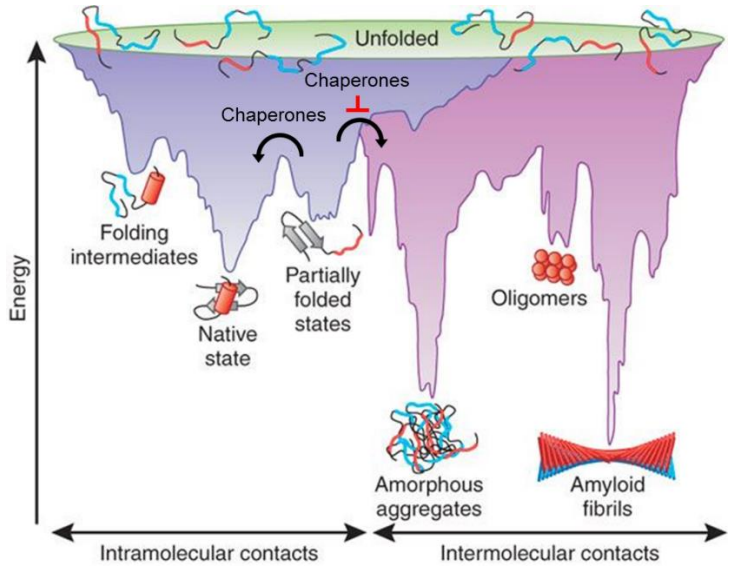

Figure 4. Energy landscape of protein folding and aggregation reactions. Partially folded conformations need to overcome a free-energy barrier to reach their native state, a step that *in vivo* is accelerated by molecular chaperones. When several molecules fold simultaneously in the same compartment, the formation of thermodynamically very stable amorphous aggregates, oligomers or amyloid fibrils can happen. Fibrillar aggregation is usually prevented by molecular chaperones (modified from[14]).

In physiological conditions proteins are kept in their proper folding by cellular quality control systems, which involve components - like molecular chaperones - that assist the correct folding of newly translated proteins or are induced in response to the

accumulation of misfolded proteins, to help them regain their correct conformation. When refolding cannot be achieved, mechanisms like proteasome, autophagy or degradation systems associated with the endoplasmic reticulum (ER) are deputed to protein degradation[13]. In a scenario of protein quality control decline associated with cellular aging or in presence of disease mutations that destabilize the correct fold or stabilize a misfolded protein state, proteotoxic stressors are exacerbated, promoting amyloidogenic protein escape form the quality control systems and their association into aberrant amyloid structures[13] (Fig. 4).

Even if disease-associated proteins typically have amino acid sequences or extended intrinsically disordered regions (i.e. regions without a stable secondary or tertiary structure) facilitating aggregation[12] and can assume a remarkably similar cross-β quaternary organization, they do not present obvious similarities in term of sequence, structure, size, function or cellular localization. AD is associated with amyloid-β (Aβ) peptide and tau accumulation, PD with abnormal α-synuclein (α-syn) aggregation, HD correlates with the intracellular accumulation of the huntingtin (Htt) protein with an expanded polyglutamine (polyQ) tract, while ALS is linked to altered localization and accumulation of TAR DNA-binding protein 43 (TDP-43). The downstream cytotoxicity of the misfolded protein can derive both from loss of the normal protein function and from a gain of function resulting from the formation of toxic aggregates and the engagement of aberrant interactions with other cellular elements[11]. The features of the pathological protein impact on the level of vulnerability of different types of neurons, on the brain regions in which neuronal death occurs and hence on the disease symptoms[15].

2.1 Alzheimer's disease

Auguste Deter was the first woman that, at the beginning of the XX century, around age of 50, was diagnosed by psychiatrist Alois Alzheimer with what is now known to be the most prevalent cause of senile dementia. AD patients are currently estimated over 40 million worldwide[2] (without taking account of the fact that the syndrome starts 2-3 decades before its full-blown manifestation) and the symptoms first described in Auguste - progressive memory loss and aphasia, disordered cognitive function, behavioural alterations and inability to perform basic daily activities - are attributed to the atrophy and degeneration of hippocampus (a brain area crucial for memory formation) and of some cortical and subcortical brain regions[16]. At the histological level, AD is mainly

characterized by the deposition of the Aβ peptide, which is the main constituent of large extracellular aggregates known as senile plaques, and of the microtubule-associated protein tau, which, in a hyperphosphorilated state, accumulates intracellularly in the so-called neurofibrillary tangles.

Aβ is a small (~4 kDa), intrinsically disordered peptide originating from the amyloid precursor protein (or APP), a transmembrane protein essential for neuronal development, survival and post-injury repair. APP is cleaved by intramembrane proteases named secretases. Its ectodomain first undergoes cut by either α- or β-secretases, then the intramembrane stub generated by β-secretase cleavage serves as substrate for the release of the Aβ peptide in biological fluids by γ-secretase scission (Fig. 5).

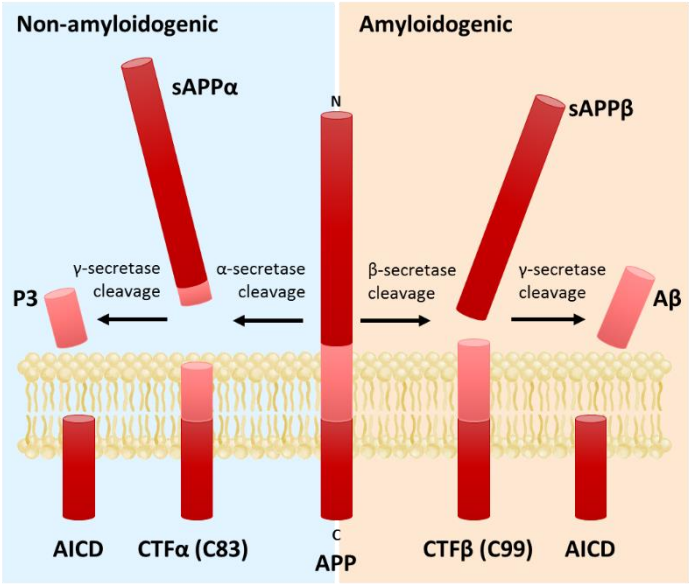

Figure 5. Human APP proteolysis in the non-amyloidogenic and amyloidogenic pathways. The non-amyloidogenic pathway involves processing of APP by membrane bound α-secretases, which cleave within the Aβ domain to yield a soluble N-terminal fragment (sAPPα) and the C-terminal fragment CTFα (C83), which is retained in the membrane, where it is cleaved by γ-secretases to generate extracellular P3 and the membrane-anchored APP intracellular domain (AICD). In the amyloidogenic pathway, APP is cleaved first by a different enzyme, β-secretase, generating the longer C-terminal fragment CTFβ (C99) and the N-terminal sAPPβ. CTFβ is then cleaved by γ-secretases into AICD and Aβ peptide[19].

The γ-secretase site of cleavage is variable and gives rise to fragments spanning approximatively from 36 to 43 amino acids in length, with different C-terminus hydrophobicity and distinct propensity to self-assemble[8]. The 40 amino acid-long Aβ peptide ($A\beta_{40}$) is the most abundant, while the amyloid-β peptide of 42 amino acids or $A\beta_{42}$ is the most aggregation-prone[8], possibly because of its more structured C-terminus[17]. Numerous putative physiological roles (protection against microbial infection amongst others[18]) have been proposed for Aβ peptide, but are yet to be fully elucidated.

According to the Aβ hypothesis, the dominant model in describing the complex AD pathogenesis, Aβ dyshomeostasis (i.e. imbalance between Aβ peptide production and clearance or increased $A\beta_{42}/A\beta_{40}$ ratio) is the AD initiating factor that may precede and even induce the hyperphosphorilation of tau and trigger the cascade of events driving the progressive neuronal and synaptic loss[9]. Aβ peptide can affect a wide array of neuronal functions and Aβ-mediated toxicity has been associated with alterations of signalling pathways[9], mitochondrial and oxidative damage[20], microtubule dynamic defects[21] and endosomal traffic jam[22], just to cite a few. Supporting the Aβ hypothesis, all dominant mutations causing early-onset AD occur in the Aβ-generating pathway, either in the genes coding for APP or for secretases, enhancing Aβ peptide production or its oligomerization propensity (e.g. determining secretase cutting site). The ε4 allele of apolipoprotein E (APOE), which has been shown to impair Aβ peptide clearance from the brain or facilitate its seeding, is a predisposing factor for AD[23] and the duplication of the wild-type APP gene (mapping on chromosome 21) in Down's syndrome leads to plaque formation and increased risk of developing Alzheimer's[24].

2.2 Parkinson's disease

Globally, people suffering from PD are about 3 million, making this neurodegenerative disease the second most common after AD. PD patients develop motor deficits - rigidity, resting tremor, bradykinesia (slowness of movement) and postural instability - that can be anticipated or followed by non-motor symptoms, like sleep disturbances, depression and dementia. The motor signs stem from the progressive loss of dopaminergic neurons projecting from the substantia nigra pars compacta to the striatum and the consequent deregulation of the motor circuitries due to the depletion of dopamine in the striatum[25]. Dopaminergic neurons display Lewy bodies, cytoplasmic inclusions formed by the

presynaptic protein α-syn, whose abnormal aggregation is thought to be pathogenic not only in PD but in a number of diseases collectively termed synucleinopathies.

α-Syn is a 140 amino acid protein (~14 kDa), abundantly expressed in the CNS and localizing mostly in presynaptic terminals, in close proximity with synaptic vesicles. Its precise role is unclear, but it is relevant to dopamine and vesicle release and ER/Golgi trafficking. α-Syn is a natively unfolded protein, composed of three distinct regions: i) an amphipathic N-terminal domain, binding lipids and with α-helical propensity; ii) a central hydrophobic domain, named NAC (non-Aβ component), with β-sheet potential and amyloidogenic; iii) a negatively charged C-terminal domain, prone to be unstructured[26] (Fig. 6). α-Syn can interact with membranes and be secreted, although lacking a signalling sequence to the secretory pathway. Extracellular vesicles can mediate the propagation of toxic α-syn aggregates between neurons[27].

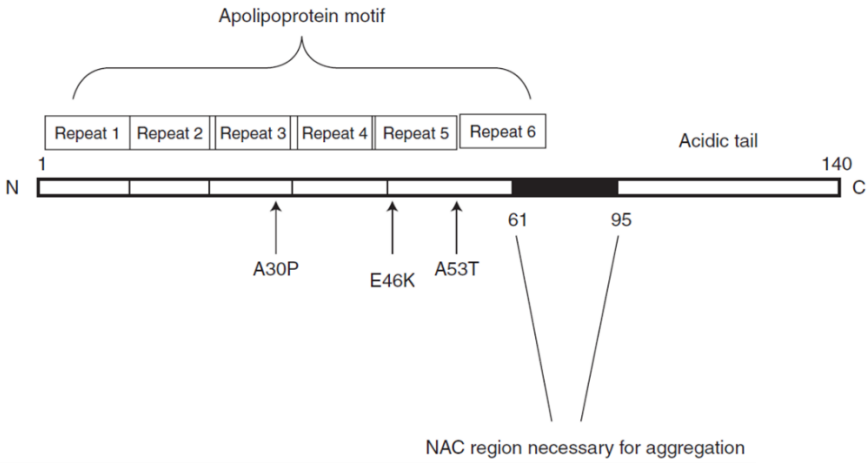

Figure 6. Schematic structure of α-Syn. The three regions in which the primary structure of α-syn is divided: the N-terminal region composed of 11-residue repeats (including the consensus sequence KTKEGV) similar to apolipoprotein binding domains (residues 1-60); the central region involved in aggregation (residues 61-95) and the C-terminal, highly acidic and proline-rich region (residues 96-140). Point mutations genetically linked to familial PD are indicated (modified from[26]).

The *SNCA* gene coding for α-syn is genetically linked both to rare but early-onset, autosomal dominant forms of PD and to sporadic PD, the majority of cases. Duplications or triplications of the gene *locus* have a dosage effect and point mutations, as the ones

specified in Figure 6, frequently destabilize the native conformation of α-syn N-terminus, affecting its aggregation propensity. α-Syn aggregates have been linked to mitochondrial fragmentation and dysfunction[28], impairment of the protein degradation system[29], cytoskeletal deformations and enhanced production of oxygen reactive species (ROS)[26]. Post-translational modifications like phosphorylation have been differentially associated with the pathology[26].

Mutations in other proteins have been related with recessive or dominant familial PD forms, e.g. mutations in parkin (an E3 ubiquitin ligase), in PINK1 (a mitochondrial serine/threonine-protein kinase involved in mitochondrial quality control), in the leucine-rich kinase 2 (LRRK-2) or in the glucocerebrosidase (GBA). In addition, environmental factors play an increasingly recognized role in determining dopaminergic neuron susceptibility[25].

2.3 Huntington's disease

HD is also known as Huntington's chorea, a term that defines the involuntary, brief, unpredictable body movements that manifest early in the disease. They are accompanied by other motor disturbances like bradykinesia, incoordination and rigidity, and by cognitive dysfunctions that impair executive functions, including language, but spare long-term memory and comprehension[30]. Unlike other NDs, HD is imputable to a single gene mutation: the expansion of the CAG triplet in the *HTT* gene, which produces an abnormally long polyQ stretch at the N-terminal portion (exon 1) of the Htt protein[30].

Htt is a 350-kDa protein whose mutated version gains toxic properties forming aggregates that are harmful to striatal GABAergic neurons and to neurons projecting from the cortex to the striatum, a critical brain area controlling voluntary movements. However, HD pathological events are likely to derive also from the loss of beneficial functions of the wild-type protein. Even if its role is not completely defined, Htt has been shown to be essential in development, to mediate endocytosis and vesicular trafficking, to associate with microtubules - coordinating cell division - and to interact with the molecular motor machinery. An involvement in autophagy has also been described[31].

The better characterized portion of Htt is the N-terminal region: it comprises 17 amino acids with α-helical structure, a prolin-rich domain (PRD) and, in between, the polyQ stretch, which is more flexible and can adopt several conformations (Fig. 7A). Heathy

subjects have usually 17-20 CAG repeats, while more than 40 repeats are associated with nearly full penetrance of the disease and 75 or more with juvenile onset (Fig. 7B). HD is inherited in an autosomal dominant manner[31].

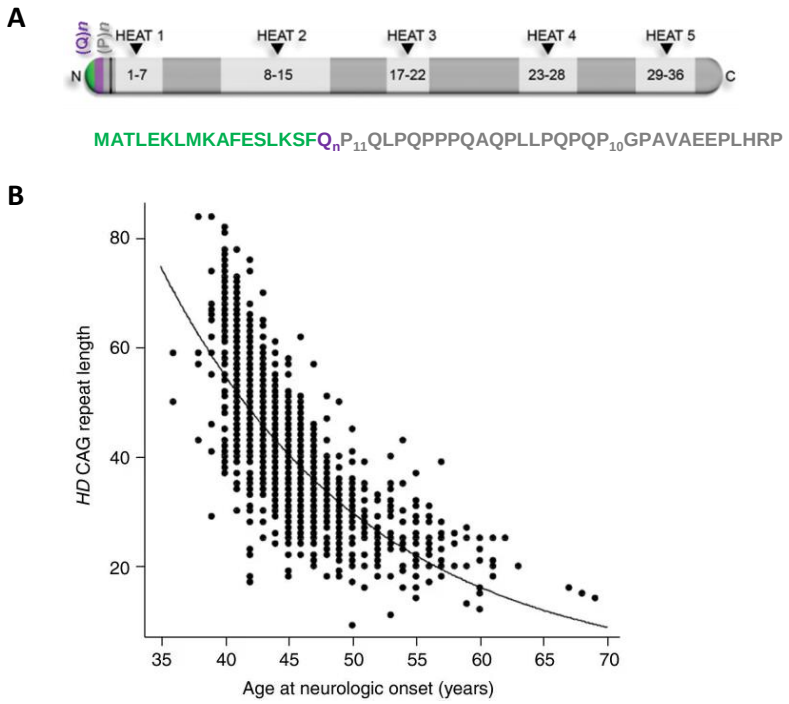

Figure 7. Htt protein and inverse correlation between polyQ length and age of HD onset. A) Full-length diagram of huntingtin. (Q)*n* indicates the polyQ tract, (P)*n* the proline-rich domain. The black line delimitates exon 1. Groups of HEAT repeats, 40-amino acid sequences involved in protein-protein interactions, are indicated. Underneath, the amino acid sequence of exon 1, comprising the first 17 amino acids (green), (Q)*n* (purple) and (P)*n* (grey), is reported (modified from[32]). B) Composite graph plotting age of HD onset against number of CAG repeats in blood DNA. Data points derive form 1200 HD subjects of known age at neurologic onset. The line represents the best-fit simple logarithmic regression to the data. About 67% of the overall variation in HD onset age is determined by the CAG repeat length[33].

2.4 Amyotrophic lateral sclerosis

ALS has traditionally been considered a neuromuscular disease, since it is characterized by the worsening of voluntary movements and a progressive paralysis that usually starts

from a specific body region and then spreads both locally and to neuro-anatomically connected regions, sparing only ocular movement and sphincter control[34]. The motor deficits develop within weeks or months and the average time of survival is three years from disease onset[35]. Yet, up to 50% of ALS cases presents also cognitive and behavioural impairments and recent studies have underlined a prominent involvement of the CNS[34]. ALS comprises a large number of clinical and pathological sub-phenotypes: several genetic and environmental factors have been proposed to contribute to disease development in the 85-95% of ALS patients, who do not have a familial history,[35] and more than 30 genes have been linked to familial forms of the disease. These genes include the gene coding for the antioxidant enzyme SOD1 (superoxide dismutase 1) and for the RNA-binding protein FUS (FUsed in Sarcoma) and some patients have inclusions positive for these proteins[34]. Although multiple mechanisms appear to be at play, ALS-associated genes participate to three main pathophysiological functions - RNA biology, protein turnover and axonal transport - and a recurring pathological feature is the presence of protein aggregates of TDP-43.

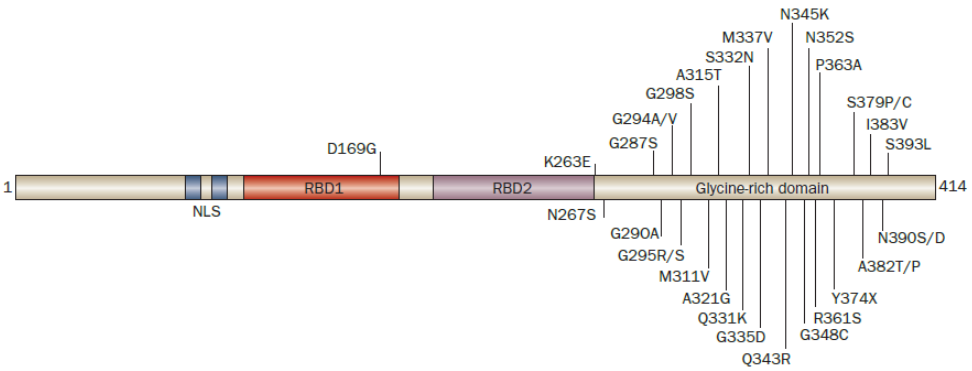

Figure 8. Schematic structure of TDP-43. TDP-43 sequence contains a nuclear localization signal (NLS) and two RDBs followed by a glycine-rich domain, that is a structural feature shared with different nuclear ribonucleoproteins. Mutations indicated by single letter amino acid code have been reported in human diseases, especially ALS (modified from[36]).

TDP-43 is a 43-kDa protein that in physiological conditions is predominantly nuclear, although able to shuttle between nucleus and cytoplasm, and has numerous functions in the transcription process, thanks to its capability to bind both DNA and RNA. It can act as transcriptional suppressor and is involved in the splicing of several genes. It

possesses two RNA-binding domains (RBDs) and a C-terminal glycine-rich region, where the majority of mutations found in ALS patients occurs[36] (Fig. 8). Post-translationally modified (e.g. phosphorylated) or cleaved forms present an altered aggregation propensity[37].

The cytoplasmic accumulation of TDP-43 in pathological conditions deplete the amount of TDP-43 available for mRNA transport[38], enhances its function of transcriptional suppressor[39] and alters levels of transcripts regulating chromatin assembly and histone processing[40]. Abnormal TDP-43 has also been shown to inhibit endocytosis (which regulates its turnover)[41], compromise the endo-lysosomal pathway[42], cause oxidative stress[43] and dysregulate metal ion homeostasis[44].

3. AN OLIGOMER-CENTRIC VIEW OF NEURODEGENERATION

Amyloid deposits, as senile plaques in AD, Lewy bodies in PD, inclusions formed by Htt in HD and TDP-43 in ALS, have long been considered as the signature of NDs. Anyway, a series of evidences has pointed out that these fibrillar, insoluble aggregates might actually act as a harmless or even protective reservoir for the truly toxic conformation, i.e. soluble oligomers. Oligomers can be described as non-monomeric assemblies that can be intermediary or end products of the amyloid aggregation process (summarized in Figure 9), typically smaller than fibrils and lacking the parallel β-sheet arrangement, but extremely variable in size, structure and stability[45].

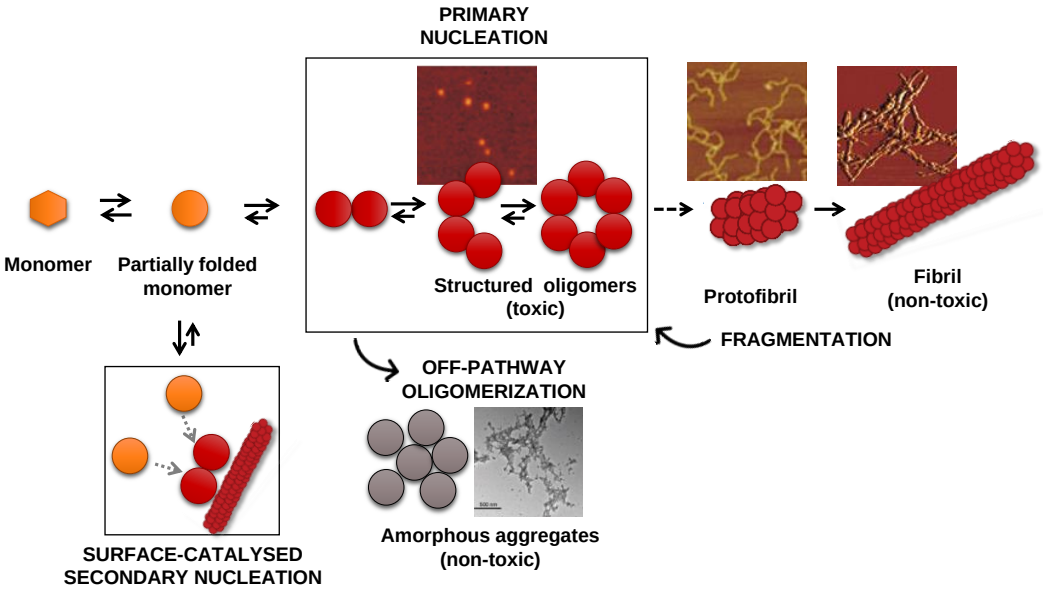

Figure 9. Overview of amyloid aggregation process. Natively unfolded monomers can assume partially folded conformations than can aggregate into transient, structured oligomers. Structured oligomers supposedly are the toxic conformations and, according to some aggregation models, can further grow into fibrils. Alternatively, amorphous, non-toxic aggregates can form ('off-pathway oligomerization'). Oligomers can also originate from secondary pathways, which include fibril fragmentation and oligomerization catalysed by interactions between monomers and fibril surface ('surface-catalysed secondary nucleation')[46].

3.1 Aβ oligomers: identity and mechanisms of toxicity

The prime example of the paradigm of toxicity shifting from fibrils towards smaller oligomers is given by Aβ peptide in AD, starting from observations that at first seemed to undermine the Aβ hypothesis itself. Significant amounts of amyloid deposits had been found in the cortex of apparently healthy old people and, as it turned out, the number of plaques poorly correlated with the entity of cognitive deficit[47], whereas a much better correlation was given by amyloid-β oligomer (AβO) levels[9]. Lambert and colleagues proposed the amyloid-β oligomer hypothesis after discovering that preparations of synthetic soluble AβOs - and not of monomers or fibrils - are potent CNS neurotoxins able to impair the maintenance of long term potentiation (LTP), one of the main form of synaptic plasticity thought to underlie memory and learning[48]. Supporting this hypothesis, memory consolidation is lost when AβOs are injected in the cerebrospinal fluid (CSF) of non-transgenic (non-Tg) animals[49] and AβO-selective antibody administration prevents this effect in AD Tg mice[50,51]. Likewise, the Osaka mutation (APP E693Δ), which is linked to a familial AD form with extensive cognitive impairment, leads to extremely low levels of senile plaques and, instead, enhances the formation of soluble oligomers[9].

AβOs clearly cannot be considered just as mere intermediates of the fibrillization pathway, but defining their properties in correlation with their toxicity is not obvious. Their transient nature makes challenging to characterize their structure and a high number of species have been described in literature[8,9]. Partly, this is due to oligomer inherent heterogeneity and it is plausible that more than one AβO species may be disease-relevant - since an elevated number of cellular pathways is involved in AD pathogenesis - but also some species may be artefacts introduced in non-physiological conditions. Some of the assemblies that have been identified include protofibrils (intermediates *en route* to fibril formation), annular aggregates, Aβ-derived diffusible ligands or ADDLs (small oligomeric forms of synthetic Aβ peptide) and globulomers. An apparent dodecamer of 56 kDa (Aβ*56), isolated from an APP Tg mouse line[52], was recently confirmed to exist also in human AD brain[53] and to be toxic to cultured neurons[54]. In most cases a direct structural comparison between oligomers formed *in vitro* and species found in the brain of animal models or AD patients has not been possible. Nevertheless, some brain-derived oligomeric species resemble synthetic AβOs in term of mass,

isoelectric point, immunoreactivity with conformation-specific antibodies and ability to induce pathological effects[55].

Overall, there is agreement on the hypothesis that Aβ peptide can aggregate in different oligomeric species able to interconvert, with distinctive toxicities and differentially related to fibrils, but among this variety of assemblies which species are the primary toxicity culprits in AD is still matter of debate. As reviewed by Cline *et al.*[9], toxic oligomers appear to be more than 50 kDa in size, reactive with the anti-amyloid oligomer antibody A11 (which does not recognize monomers or fibrils, but only soluble oligomers)[56] and unrelated to amyloid plaques, contrarily to the non-toxic species that are smaller and reactive with the anti-fibril antibody OC[57]. Some data seem to confirm that oligomerization and fibrillization are distinct and independent processes and the most toxic oligomeric species are off-pathway to fibril formation[58,59]. According to the fibril seeded model, though, a crucial part is played by monomer dissociation from fibrils and by secondary nucleation catalysed by fibril surface (see Fig. 9)[60]. Recently, the characterisation of the soluble aggregates present in the CSF of patients with established AD or mild-cognitive impairment has shown that aggregates of different sizes and with different mechanisms of toxicity (i.e. permeabilization of lipid membranes or induction of inflammatory response in glial cells) may be differentially relevant at different stages of the disease[61].

Molecular mechanisms leading to toxicity are also multiple. AβOs can act extracellularly, in CSF and interstitial fluids[62] where they are released from the APP cleavage, and are able to cause malfunction when added to neuronal cell cultures[54,63]. The simplest explanation of neuronal damage involves their direct insertion in the lipid bilayer and the formation of pores that alter its permeability[64]. This hypothesis, anyway, does not account for the population specificity of AβO neurotoxicity and a more selective binding to specific receptors could be required. NMDA (N-methyl-D-aspartate)[65] or AMPA (amino-3-hydroxy-5-methyl-4-isoxazole)[66] receptors have been proposed as candidate receptors through which AβOs could inhibit the persistence of hippocampal LTP. Alternatively, Aβ peptide can be uptaken[67] by neurons via endocytosis and its oligomerization may be promoted by retention and accumulation in lysosomes[68]. This way AβOs can directly interact with almost all intracellular organelles as well as with membrane-less cytosolic structures[69].

3.2 Amyloid oligomers in other NDs

Notably, the conformation specific antibody A11, produced against AβOs, detects also oligomers of α-syn or mutant Htt, implying that different aggregation-prone proteins can adopt similar cytotoxic conformation(s). Indeed, soluble oligomeric assemblies have been more or less confidently associated with a pathogenic activity also in other NDs.
For instance, there is no correlation between fibril burden and severity of PD[70] and early onset-PD mutations A30P and A53T in α-syn accelerate the formation of spherical prefibrillar aggregates *in vitro*, while slowing down their conversion into insoluble fibrils[71]. α-Syn oligomers can interact with cellular membranes, form membrane pores[72,73] and propagate throughout the brain using extracellular vescicles[27], thus being more harmful than insoluble conformations. Interestingly, dopamine can inhibit the conversion of protofibrils into mature fibrils, suggesting that the selective neuronal degeneration in PD may derive from the enhanced presence of oligomers in dopaminergic neurons[74]. In the same way, soluble polyQ-expanded Htt species induce higher cell mortality in comparison with large intracellular aggregates and several studies support their higher toxicity[75,76]. TDP-43 aggregation remains more elusive, but this protein as well can form neurotoxic oligomers that have been detected in the brain of animal models and patients[77]. Recently, the RBDs of TDP-43 have been found to primarily drive its early oligomerization and, notably, ALS-linked mutations (A315T and M337V) alter this process[78].

3.3 Challenges in developing an oligomer-targeting therapy

Oligomer characterization is crucial to develop both therapeutic strategies and diagnostic tools. As mentioned above, this goal is exceptionally difficult to achieve because of oligomer metastability and, despite some toxic species may expose the same A11-reactive epitopes and act through common mechanisms[56], the oligomer heterogenic nature hinder the univocal identification of the primary toxic forms. Oligomeric species can interconvert to one another in a rapid equilibrium that can be easily perturbed in experimental conditions. Due to the non-covalent nature of the interaction between monomers, the denaturing conditions of techniques that are commonly used to detect protein sizes, like SDS-PAGE and Western blotting, could alter oligomeric species distribution. Additionally, SDS could induce the formation of dimers, trimers or other

artefacts[79,80] producing misleading results when characterizing toxic conformations or evaluating the effects of candidate therapeutic compounds. Native or 'non-denaturing' PAGE, in which proteins migrate depending both on their charge and hydrodynamic size, shows a higher percentage of high molecular weight oligomers compared to SDS-PAGE, but high molecular weight species often result in a gel smear with difficult discrimination of similar sizes[81,82]. An expedient for covalently stabilizing AβO mixture is the photo-induced crosslinking of unmodified proteins (PICUP)[83], but this method revealed to be less successfully applicable to $A\beta_{42}$ peptide compared to $A\beta_{40}$[84], probably because the reactive Tyr10 is less accessible, producing an incomplete cross-linking of oligomeric species[85]. Size-exclusion chromatography (SEC) could as well result in a low resolution of the sample[86] and the relative abundance of peaks detectable in the eluate are likely to not accurately reproduce the oligomeric population existing prior to analysis, since aggregates may dissociate because of long separation times, uneven interaction with the column matrix or because of their perturbed concentrations. The disordered nature and the high aggregation propensity of Aβ peptides have made difficult to characterize oligomer tertiary and quaternary organization and no atomic level resolution structure is available, hampering the design of therapeutic drugs specifically targeting oligomeric species. Moreover, targeting individual molecular entities could not represent the best strategy, as multiple conformations have been found in the brain of AD patients and could be responsible of toxicity[87].

When studying the mechanism of action of therapeutic compounds, *in vitro* analyses using synthetic or recombinant Aβ peptide offer the advantage of excluding influences of external factors in a simplified environment. Nonetheless, producing Aβ aggregates of defined size distribution and morphology can be difficult, several oligomer formation protocols are found in literature and multiple operating conditions complicate result comparison. It should be also considered that recombinant peptides usually aggregate faster than the synthetic Aβ forms, probably due to the presence of small amounts of impurities or racemized conformations that cannot be avoided in synthetic preparations and may impede the incorporation of Aβ monomers in higher-order aggregates[88].

All the above observations highlight the relevance of animal or cellular models, which can be used to monitor oligomer formation *in vivo* (in some cases directly, e.g. by fluorescence microscopy) and evaluate toxic properties of different oligomeric

conformations. In therapeutic molecule screenings, cellular assays, that use cellular toxicity as readout, allow the immediate discard of toxic compounds and can be exploited to identify compounds simultaneously targeting multiple oligomeric species and, importantly, both *cis*- and *trans*-acting compounds. The ability to cope with multiple pathological features is advisable since AD, as other NDs, is a complex multi-factorial disease which may require treatment with equally multi-targeting approaches.

4. YEAST AS MODEL SYSTEM TO STUDY AMYLOID-INDUCED TOXICITY

A useful platform to screen drugs or small molecules and get a basic mechanistic insight of amyloid-toxicity is represented by the budding yeast *Saccharomyces cerevisiae*. Protein folding is essential in every cell type and the same issues arising in human cells from amyloid protein misfolding can occur also in an organism as simple as *S. cerevisiae*. The fundamental cellular pathways underlying neurodegeneration, such as autophagy, vesicular and ER-to-Golgi trafficking, protein quality control, mitochondrial function and cellular aging, are conserved in yeast cells[89]. *S. cerevisiae* was the first eukaryotic organism to have its genome - about 6000 open reading frames (ORFs), only 4% of which with introns - fully sequenced and the encoded proteins have been extensively characterized by functional analyses[11]. Thanks to the amenability of genetic and environmental manipulations, its cost-effective laboratory maintenance and short generation time, *S. cerevisiae* has been successfully used to uncover basic aspects of cellular biology and biochemistry (e.g., cell cycle progression, DNA replication, protein folding and intracellular transport[11]) and lend itself as a powerful toolbox to study human diseases, including NDs. As exemplified in Table 1 and 2, disease models in *S. cerevisiae* are created following one of two main approaches: i) if the protein responsible for the pathological outcome has a yeast homologue, the gene can be directly deleted or overexpressed to evaluate how it impacts on cellular biology; ii) when the disease-implicated gene does not have an obvious counterpart in yeast, the human transgene can be heterologously expressed, obtaining a so-called humanized yeast model. It is the case, for example, of AD, PD, HD and ALS yeast models, where $A\beta_{42}$, α-syn, polyQ-expanded Htt or TDP-43, respectively, have been (over)-expressed producing viability defects and cellular changes associated with amyloid aggregation.

Amyloid structures formed in yeast have analogous biochemical properties to those formed in human cells and low-*n* oligomeric species reacting with the same conformation-specific antibodies have been observed[90,91]. Yeast models have been exploited for high-throughput screenings of genetic- or small molecule-modifiers of amyloid toxicity and validation of key hits in mammalian cells or animal models have confirmed *S. cerevisiae* as a simple and reliable system to study ND pathobiology.

Table 1. Yeast models based on yeast orthologues of human proteins (modified from[89])

Disease	Human gene	Protein(s) involved	Yeast orthologue(s)	Refs
Batten's disease	*CLN3*	CLN3	YHC3/BTN1	92
Friedreich's Ataxia	*FXN*	Frataxin	YFH1	93,94
Ataxia-telangiectasia	*ATM*	ATM	TEL1, MEC1	95,96
Niemann-Pick disease	*NPC1*	NPC1	NCR1	97,98
Hereditary Spastic Paraplegia	*SPG1*	mAAA-proteases (Afg312 and paraplegin)	mAAA-proteases (Yta10 and Yta12)	99
Amyotrophic lateral sclerosis	*SOD1*	SOD1	SOD1	100

Table 2. Yeast models based on heterologous expression of human proteins (modified from[89])

Disease	Human gene	Protein(s) involved	Yeast orthologue(s)	Refs
Creutzfeldt-Jakob disease	*PRNP*	PrP	-	101–104
Amyotrophic lateral sclerosis	*TARDBP*	TDP-43	-	105
	FUS	FUS/TLS	-	106,107
Parkinson's disease	*SNCA*	α-Synuclein	-	108–113
	PARK8	Lrrk2	-	114
Alzheimer's disease	*APP*	Amyloid-β	-	91,115–120
	MAPT	Tau	-	121
Huntington's disease	*HTT*	Huntingtin	-	122,123

4.1 Yeast models for Alzheimer's disease

As the most prevalent ND, understanding mechanisms underlying AD is essential and developing good AD models could help take forward the slow progresses made so far. *S. cerevisiae* models were initially used to dissect APP processing. For example, a system based on the simultaneous expression of a fusion of APP with an invertase and of the human β-secretase has been generated to monitor β-secretase activity and identify β-secretase inhibitors from yeast ability to grow on selective plates, depending on whether APP-invertase was cleaved or not by β-secretase[119]. Although this model - and others with similar aims - offered a way to understand Aβ generation pathway and

screen compounds for their ability to interfere with it, they are not informative about the effects of the β-amyloid peptide, which have been evaluated with other systems.

Following APP cut, $A\beta_{42}$ is released in the extracellular space. In mammalian cell lines its extracellular toxicity cannot be completely isolated from other effects, as $A\beta_{42}$ is a physiological product of APP detectable also intracellularly[124]. In yeast, instead, $A\beta_{42}$ extracellular impact has been assessed through the supplementation of the culture medium with different peptide conformers and AβOs were found to be significantly more toxic than fibrils[125]. Stress induced by exposure to $A\beta_{42}$ oligomers was also documented in a strain expressing a reporter protein (the red fluorescent protein mCherry) under the control of the *HSP42* promoter that is activated during heat-shock response[126].

Intracellular effects of $A\beta_{42}$ are not less important: evidences exist that APP processing can occur inside the cell, during its maturation across the trans-Golgi network[127,128], and $A\beta_{42}$ may cover a prominent role in AD pathogenesis once internalized by interaction with cellular membranes or receptors[9,129]. Intracellular effects have been studied in yeasts heterologously expressing human $A\beta_{42}$ as either a cytosolic or a secretory peptide. Since it is conceivable that mainly prefibrillar aggregates are formed in yeast cells, such models could serve to address genetic or small molecule screens against these species starting from the early stages of research.

Nevertheless, the creation of a yeast model of $A\beta_{42}$ oligomerization and toxicity has been more challenging compared to other ND models, since Aβ expression *per se* is well tolerated by yeast cells[118,130,131], which likely degrade it as fast as it is produced[117].

Models based on cytosolic $A\beta_{42}$ expression

By means of its fusion to reporter proteins that prevent its degradation, different groups have developed yeast models showing high cytoplasmic accumulation of oligomeric $A\beta_{42}$, which can be used to study $A\beta_{42}$ aggregation dynamics and localization. In these models, however, $A\beta_{42}$ causes only a very weak - if not insignificant - toxicity.

- $A\beta_{42}$ fusion to GFP (Fig.10A)

  Caine *et al.* expressed $A\beta_{42}$ in yeast as a fusion product with the green fluorescent protein (GFP)[117]. A slight reduction of cellular viability (4-5% compared to the control) and a mild induction of the heat shock response, attributed to misfolded or aggregated $A\beta_{42}$-GFP[117], were observed. The $A\beta_{42}$-

GFP fusion caused the suppression of GFP fluorescence, visible only in a small percentage of cells as punctuated *foci*, likely as a consequence of its degradation following GFP misfolding induced by Aβ properties[132]. Using this system, folate was validated as an inhibitor of Aβ misfolding, which deduced by the increased green fluorescence in the treated cells[132], similarly to what had been observed in screening previously carried out in *Escherichia coli*[133,134].

More recently, the *S. cerevisiae* genome-wide deletion library has been transformed with the $A\beta_{42}$-GFP fusion and phospholipid metabolism, along with mitochondrial function and transcriptional/translational regulation, has emerged as one of the main processes affected by $A\beta_{42}$-GFP aggregation. These processes were identified by assessing $A\beta_{42}$-GFP fluorescence in the deleted strains, which inversely correlated with the formation of insoluble aggregates[135]. On the contrary, in another study, the significant reduction of fluorescence intensity in a ROS sensitive strain treated with some phenolic compounds[136] was explained as an increased GFP-$A\beta_{42}$ removal by proteolysis due to the anti-aggregating activity of the tested compounds. This highlights how phenotype-modifying effects in such systems are susceptible of different interpretations.

Recently, the same readout - but in aged cells, reported to less efficiently clear $A\beta_{42}$-GFP thus exhibiting an higher green fluorescence - has been used to study the effects of a statin (simvastatin) on $A\beta_{42}$ turnover[137].

- <u>$A\beta_{42}$ fusion to Sup35</u> (Fig. 10B)

  Using a different method to monitor $A\beta_{42}$ aggregation, Bagriantsev and Liebman fused $A\beta_{42}$ to MRF (the yeast prion Sup35 lacking the non-essential N-terminal domain) and expressed the fusion protein in a yeast strain carrying the *ade1-14* non-sense mutation that introduces a premature stop codon. MRF works as a termination factor and, in the mutant strain, causes the generation of a truncated version of Ade1. As a result, yeast cannot grow on synthetic medium lacking adenine (-Ade) and accumulates a red intermediate of the adenine synthesis. If the efficiency of translational termination at the premature stop codon is compromised because $A\beta_{42}$-MRF aggregates into low-*n*, SDS-stable oligomers, cells gain the ability to grow on -Ade and do not accumulate the red pigment[91]. The $A\beta_{42}$-MRF fusion as well as the $A\beta_{42}$-GFP fusion is not toxic. Firstly, this system showed that the prion curing agent guanidine hydrochloride (GuHCl)

stimulated Aβ$_{42}$-MRF oligomerization, enabling cellular growth on -Ade. This effect was not mediated by GuHCl effect on the Hsp104 chaperone, since, inversely to what expected, Hsp104 deletion inhibited Aβ oligomerization. On the contrary, Hsp104 was hypothesized to have a role in preventing Aβ$_{42}$-MRF disaggregation and degradation[91]. Next, this system was adapted for high-throughput screening of drugs or genetic modifiers affecting Aβ oligomerization[138,139] and the overexpression of *YAP1802*, a gene involved in clathrin cage assembly and the yeast orthologue of the human AD-risk factor *PICALM*, was found to reduce Aβ$_{42}$-MRF oligomerization[139].

Adopting a similar approach, Von Der Haar and colleagues fused Aβ$_{42}$ to prion Sup35 replacing the region between amino acid 5 and 112[118]. In this work, anyway, no change in the aggregating ability of Aβ$_{42}$-Sup35 was observed upon treatment with GuHCl.

All the models described above require the fusion to a reporter protein to monitor oligomer formation, being unfeasible the use of the native peptide that would be otherwise degraded. As Von der Haar *et al.* pointed out, both quantitative and qualitative differences may exist between the aggregates mediated by Aβ$_{42}$ and the aggregates formed by the wild type prion protein Sup35, since Aβ$_{42}$-Sup35 aggregates are less stable, do not need seeding to start aggregating and more weakly suppress the *ade1* mutation[118]. Hence, it could be questioned if structural differences may exist also between aggregates formed by native Aβ$_{42}$ peptide and the non-toxic Aβ-Sup35 oligomers. This underlines the importance of the *in vivo* and *in vitro* experiments that were carried out to furtherly assess the results obtained in these models and how the ability of anti-aggregative compounds to protect from toxicity should always be confirmed in other experimental settings.

Models based on secretory Aβ$_{42}$ expression

A mild-toxic phenotype induced by Aβ$_{42}$ oligomers was achieved in yeast drawing inspiration from Aβ$_{42}$ fate in AD neurons: the complex APP metabolism is difficult to reproduce in yeast, but Aβ$_{42}$ fusion to a secretory signal is enough to affect its toxic properties.

- Aβ$_{42}$ expression with Kar2 signal sequence (Fig. 10C)

As showed by Treusch *et al.*[120], $A\beta_{42}$ fusion to an ER targeting signal (Kar2) forces the fusion protein to transit through the secretory pathway, thus mimicking APP metabolism. Secreted peptides are retained by yeast cell wall and from the periplasmic space they can re-enter the cell by endocytosis. Yeast stably expressing secretory Kar2-$A\beta_{42}$ from multiple tandem copies integrated in the genome exhibited a mild-toxic phenotype. This model was used to screen for both toxicity enhancers and suppressors and it emerged that several toxicity modifiers were involved in endocytosis or were functionally related to the cytoskeleton. Many hits presented a human homologue and among these, *YAP1802* counteracted Aβ-induced toxicity when overexpressed - in agreement with the reduction in Aβ oligomerization subsequently established by Park *et al.* in the $A\beta_{42}$-MRF model[139] - and partially restored endocytosis. Aβ peptide was found to specifically interfere with the endocytic trafficking of membrane receptors and, in a further high-throughput screening, clioquinol was identified as a promoter of AβO degradation in a copper-dependent manner, ultimately reducing Aβ levels and restoring endocytic traffic[90].

The same signal sequence was used by another group, but they decided to constitutively express $A\beta_{42}$ peptide[140]. The rationale behind this choice was that Aβ peptide production in AD neurons is constitutive and the use of an inducible promoter determines an acute cytotoxicity that prevents from discovering implications of cumulative effects and cellular ageing. Besides a shorter chronological life span, this strain showed an impaired respiration capacity, accompanied by increased ROS production and decreased proteasomal activity[140]. In a follow-up study, the same model was used in batch cultivation in bioreactors to better control environmental parameters and transcriptome analysis evidenced ER stress and unfolded protein response activation[141].

- <u>$A\beta_{42}$ expression with MFα signal sequence</u> (Fig. 10D)

  D'Angelo *et al.* tested the toxicity of a series of chimeric constructs in which a secretion signal derived from the precursor of the *S. cerevisiae* mating factor α (MFα) was fused with $A\beta_{42}$ and/or GFP sequences[130]. The expression of MFα-$A\beta_{42}$-GFP reduced cellular viability, but removing GFP clearly lowered the toxicity and the expression level: GFP probably stabilized Aβ, which was then responsible of the toxic properties of the chimeric protein. As expected,

construct toxicity was exacerbated by the substitution of $A\beta_{42}$ with Aβ peptide carrying the arctic mutation linked to familial AD ($A\beta_{ARC}$). It should be noted that the presence of a signal sequence impacted on the nature of the aggregates, not only because Aβ-GFP caused no toxicity, but also because in absence of a signal sequence some fluorescent *foci* could be seen, while expression through the secretory pathway completely suppressed GFP fluorescence. It suggests that aggregation in these conditions may cause complete GFP unfolding and, more importantly, creates a link between aggregating properties and toxicity. Nevertheless, the insertion of a long linker sequence between $A\beta_{42}$ and GFP (MFα-$A\beta_{42}$-linker-GFP) was sufficient to restore fluorescence, preserving the same level of toxicity.

In the MFα-$A\beta_{42}$-linker-GFP model, *HSP104* deletion partially restored viability[130], confirming a deleterious role of Hsp104 in amyloid oligomerization, in agreement with Bagriantsev and Liebman[91]. However, Bagriantsev and Liebman, indirectly observing an oligomerization reduction in the deleted strain, concluded that Hsp104 inhibited disaggregation[91]. D'Angelo *et al.*, instead, observed a filamentous distribution of the chimeric protein in the deleted strain that, coupled with the decreased toxicity, led them to hypothesize that Hsp104 promoted disaggregation of larger aggregates into smaller and more toxic ones[130].

In addition, D'Angelo *et al.* detected an impairment of mitochondrial respiration and especially put in evidence the central involvement of endocytosis not as a final target but as a mean of Aβ-induced toxicity and how disturbance of ER traffic pathways could reduce deleterious effect[130]. The deletion of *YAP1801* and *YAP1802* (both yeast homologues of *PICALM*), clearly lowered growth inhibition induced by MFα-$A\beta_{42}$-GFP, an opposite effect to what observed by Treusch *et al.*[120]. These discrepancies could be due to the use of different signal sequences or to the different expression levels of Aβ peptide, which could determine the beneficial or detrimental role of endocytosis.

These results were supported by Fruhmann *et al.*, who overexpressed the chimeric construct in the yeast knockout collection searching for genes that reduced or enhanced $A\beta_{42}$ toxicity[142]. They found a lowered toxicity in strains defective in ER-Golgi traffic and mitochondrial function, but also in strains

deleted in genes connected to the cell cycle and the DNA replication stress response. Increased toxicity was observed in strains affected in the actin cytoskeleton organization, endocytosis and the formation of multivesicular bodies, including key factors of the ESCRT (Endosomal Sorting Complexes Required for Transport) machinery. In a strain lacking the ESCRT accessory factor Bro1, $A\beta_{42}$ severely compromised the plasma membrane integrity, along with inducing strong growth defect and enhanced loading of lipid droplets.

In all these cases, the complete processing through the secretory pathway proved to be instrumental in unleashing cytotoxic potential of $A\beta_{42}$ peptide. Importantly, the processes triggered by $A\beta_{42}$ expression in yeast, such as mitochondrial and ER stress, matched with the AD signature in neurons or peripheral tissues of patients. The outcome of validation experiments and the correspondence with results previously reported in other models highlights the high conservation of the pathways implicated in neurodegeneration and supports the relevance of the data obtained in yeast.

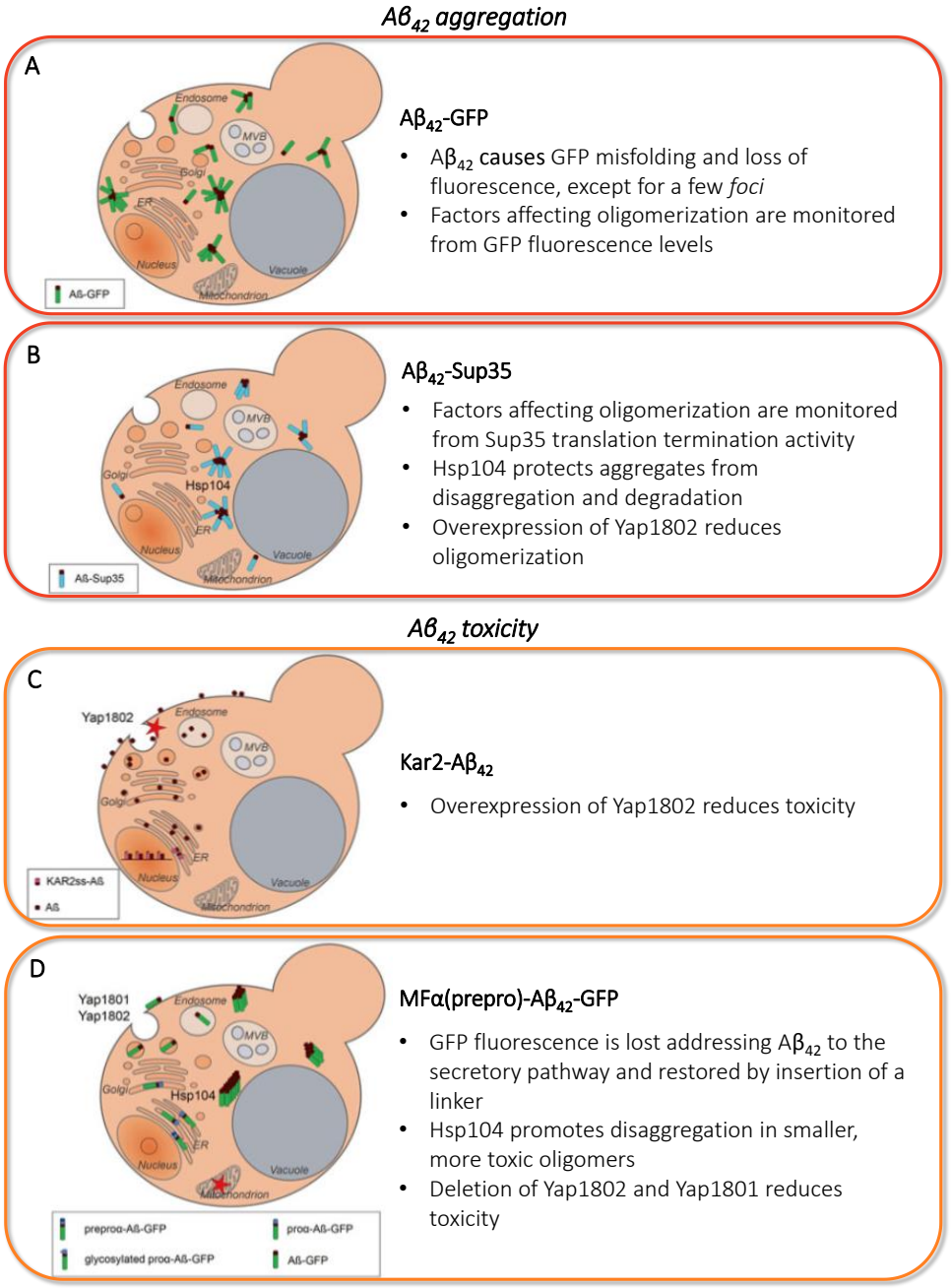

Figure 10. *S. cerevisiae* to model Aβ42 aggregation and toxicity. This Figure resumes some of the results obtained with different yeast models (modified from[143]). Aβ42 can be expressed in yeast as a cytosolic peptide fused to scaffold proteins (GFP, panel A; Sup35, panel B) or addressed to secretory pathway (panel C and D).

PART I

Anti-amyloid-β oligomer activity of phenyl-γ-valerolactone metabolites

1. INTRODUCTION TO PART I

Age-related neurodegenerative diseases, which include sporadic AD as one of the most prevalent, represent a major public and biomedical challenge. Although the ultimate pathogenesis of many of these disorders is only partially known, most of them share the presence of soluble prefibrillar oligomers, considered the most proximal neurotoxic species[8,9]. In presence of environmental factors or genetic mutations, β-amyloid peptide can switch to a partially folded state and can spontaneously establish intermolecular interactions[46], forming a wide set of structurally and functionally polymorphic AβOs. Toxic AβOs are associated with various cellular detrimental effects: disturbance of receptor-mediated functions, membrane oxidative damage, disruption of mitochondrial activity, Ca^{2+} dyshomeostasis and endoplasmic ER-apoptotic stress[9,144], leading to neuroinflammation and cognitive impairment. AβOs can be in a dynamic equilibrium with fibrillar aggregates and amyloid plaques, which are currently considered as potentially harmless Aβ storage forms, but they may act as nucleation site or release oligomers[9]. According to this view, AβO build-up resulting from drug-induced interference with plaque formation and/or promotion of their disaggregation, has been proposed as a possible explanation of the failure of many candidate AD-drugs (above all, monoclonal antibodies; mAbs) that primarily target large Aβ aggregates rather than AβOs[145,146]. The high dosage requirements of AβO-targeting mAbs (like aducanumab or crenezumab), as well, may be a consequence of the lack of a stringent discrimination between oligomers and fibrils that leads to the establishment of off-target engaments[9,146]. Another recently added complexity may stem from the unexpectedly high diversity of Aβ peptide variants found in the brain of AD patients, including truncated forms, that may hamper recognition of many of their aggregated species by sequence-specific monoclonal antibodies[87].

The high rate of negative clinical trials and projections pointing to a striking rise in AD incidence, as life expectancy globally increases, bring out a largely unsatisfactory outlook. The multifactorial nature of AD, still poorly deciphered, suggests that an effective treatment might require a multi-target approach[9] and an early or preventive intervention would be appropriate since neurodegeneration starts way before the diagnosis. All these reasons, coupled with epidemiological studies showing a correlation between certain alimentary habits and a decreased risk of chronic diseases[147–149], have aroused great interest in various natural compounds (Fig. 11), especially polyphenols.

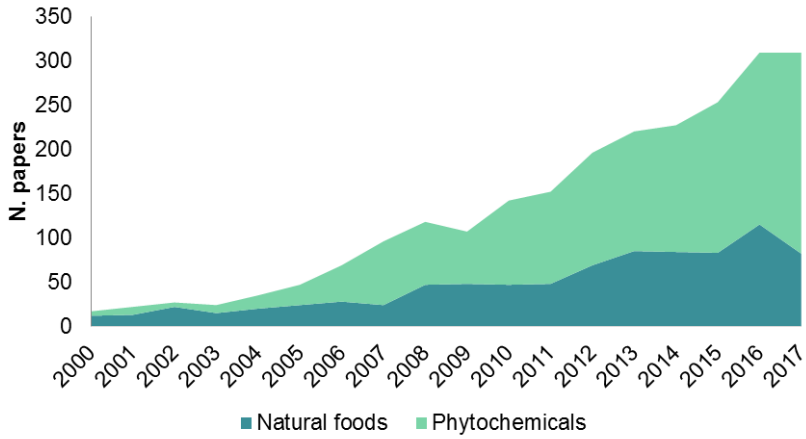

Figure 11. Number of articles dealing with plant foods or phytochemicals in relation to AD, published since 2000. The streaking increase in the number of publications in recent years shows the increasing interest in using natural foods or compounds to deal with chronic diseases.

In various experimental set-ups, different polyphenols have proven capable of modifying different neuropathological features of AD and promoting AβO detoxification by either impeding oligomer formation and/or redirecting them to higher-order, amorphous aggregates devoid of toxicity[59,150–153]. Special attention, in this context, has been given to flavan-3-ols, polycyclic flavonoids including monomeric [e.g. epicatechin, EC and (-)-epigallocatechin gallate, EGCG] and polymeric (e.g. procyanidins) compounds that are particularly abundant in plant-derived foods and beverages, such as dark chocolate, tea, berries and red wine[154–159]. In addition to a direct anti-Aβ action and other cellular effects (e.g. antioxidant and neuritogenic activity) of specific flavan-3-ols[150,151,153,160,161], more general, multi-target effects have been reported for extracts of the above plant foods. For example, a cognitive enhancement effect of cocoa has been documented in a human study and ascribed primarily to an improved brain circulation[162]. As pointed out in Figure 12, much less investigated, instead, have been the human metabolites of flavan-3-ols, some of which (e.g. 3-hydroxyphenylpropionic acid, 3-HPP) have nevertheless been shown to mitigate Aβ (including AβO) toxicity[163].

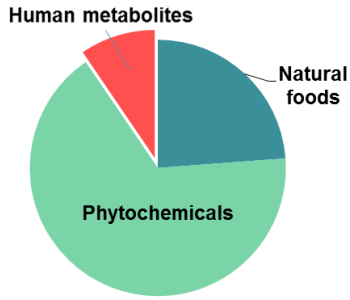

Figure 12. Number of articles dealing with plant foods, phytochemicals or human metabolites in relation to AD, published since 2000. Articles concerning human metabolites are still a minority.

Phenyl-γ-valerolactones (PVLs) are the major group of human flavan-3-ol metabolites, representing by far the most abundant circulating compounds in humans after intake of sources of this subclass of flavonoids[158,164–167]. As outlined in Figure 13, PVLs can originate from the flavan-3-ol (-)-epicatechin but also from condensed epicatechins such as the dimeric procyanidin B2, through 5-carbon side-chain ring fission catalysed by gut microbial enzymes and subsequent phase II metabolic conversion by the host, mainly through colonic and hepatic enzymes[158,167]. According to recent metabolic profiling studies in humans[167], approximately 42% of ingested (-)-epicatechin was converted within 4 to 12 h to PVLs, which reached peak plasma levels within 6 h and were still detectable after 24 h[165]. PVLs and other human flavan-3-ol metabolites are characterized by generally better pharmacokinetic/bioavailability properties than their *in planta* precursors, whose beneficial effects have been studied *in vitro* utilizing compound concentrations that are hardly reached under *in vivo* conditions. These data highlight the need to rather consider PVLs as potential bioactive compounds responsible for, or at least contributing to, the anti-neurodegenerative effects of dietary flavan-3-ols. With the perspective of a potential clinical translation, another concern to take into account is the inter-individual variations in PVL production in association with different composition of the colonic microbiota, responsible for the initial step of flavan-3-ol metabolism[158].

In order to focus on bioavailable compounds and overcome individual differences in gut microbial biotransformation, we set out to evaluate the anti-AβO action of a comprehensive set of chemically-synthetized PVLs representative of human flavan-3-ol metabolism[158,168], flanked by 16 additional human metabolites of dietary polyphenols plus three plant metabolites (Table 3).

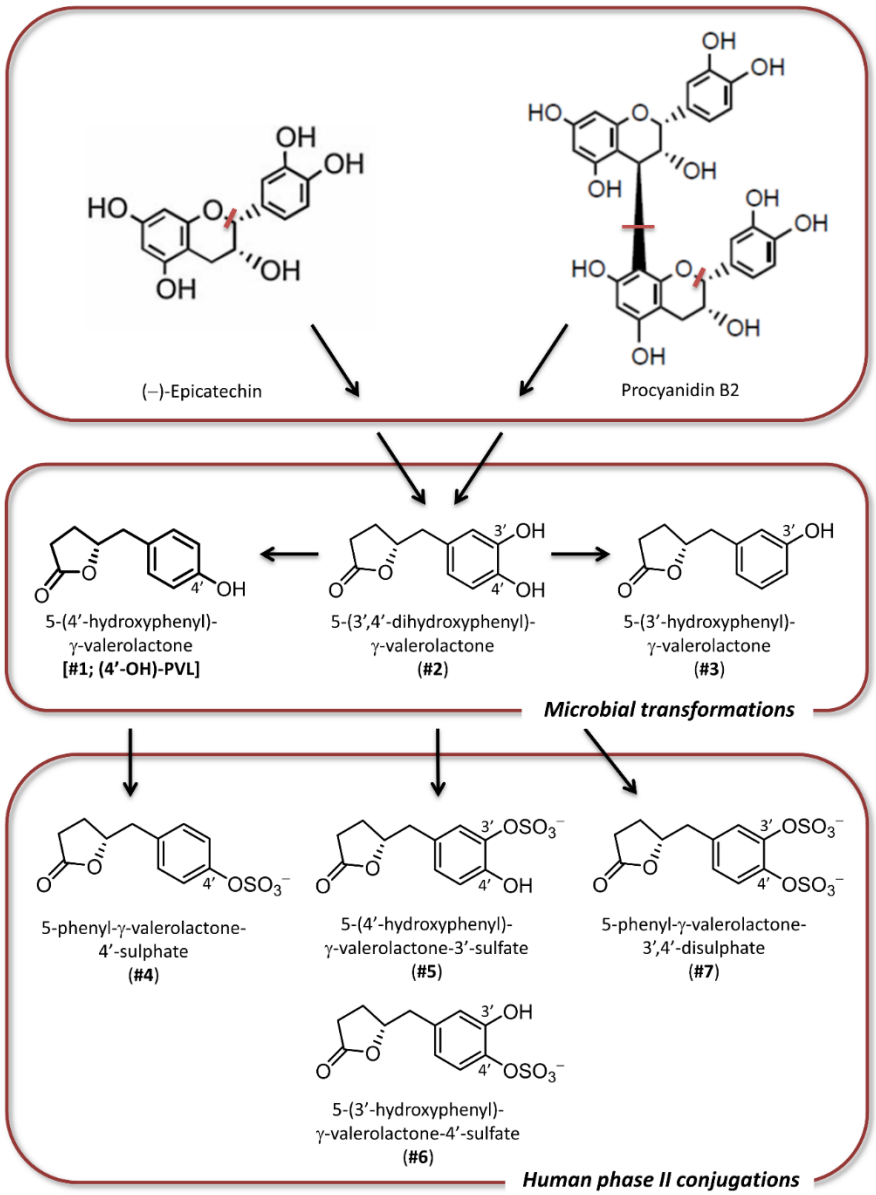

Figure 13. Outline of human flavan-3-ol metabolism and PVL formation. Starting from (–)-epicatechin and procyanidin B2, chosen as representative plant polyphenol precursors, after 5-carbon side-chain ring fission and initial transformation catalysed by gut microbial enzymes, compounds #1-2 serve as precursors for subsequent phase II metabolism as indicated. The latter is catalysed by host colonic and hepatic enzymes and generates the indicated sulfated PVL derivatives (compounds #4-7) as major phase II products that are then released into the circulation.

Table 3. Polyphenolic compounds tested.

FLAVONOIDS	
Flavan-3-ols	
Phenyl-γ-valerolactones (PVL)	
(–)-5-(4'-Hydroxyphenyl)-γ-valerolactone [#1; (4'-OH)-PVL]	Gut microbial metabolite
(–)-5-(3',4'-Dihydroxyphenyl)-γ-valerolactone (#2)	Gut microbial metabolite
(–)-5-(3'-Hydroxyphenyl)-γ-valerolactone (#3)	Gut microbial metabolite
(–)-5-Phenyl-γ-valerolactone-4'-sulfate (#4)	Human phase II metabolite
(–)-5-(4'-Hydroxyphenyl)-γ-valerolactone-3'-sulfate (#5)	Human phase II metabolite
(–)-5-(3'-Hydroxyphenyl)-γ-valerolactone-4'-sulfate (#6)	Human phase II metabolite
(–)-5-Phenyl-γ-valerolactone-3',4'-disulfate (#7)	Human phase II metabolite
(–)-Epigallocatechin gallate (EGCG)	Plant metabolite
3-(3′-Hydroxyphenyl)propionic acid (3-HPP)	Gut microbial metabolite
NON-FLAVONOIDS	
Hydroxycinnamic acids	
Caffeic acid (CA)	Plant metabolite
Ferulic acid (FA)	Plant metabolite
Dihydrocaffeic acid (DC)	Gut microbial metabolite
Dihydroferulic acid (DF)	Gut microbial metabolite
Isoferulic acid (IF)	Gut microbial metabolite
Caffeic acid 3-O-glucuronide (CA 3-gluc)	Human phase II metabolite
Caffeic acid 4-O-glucuronide (CA 4-gluc)	Human phase II metabolite
Dihydrocaffeic acid 3-O-sulfate (DC 3-S)	Human phase II metabolite
Dihydrocaffeic acid 3-O-glucuronide (DC 3-gluc)	Human phase II metabolite
Ferulic acid 4-O-sulfate (FA 4-S)	Human phase II metabolite
Isoferulic acid 3-O-glucuronide (IF 3-gluc)	Human phase II metabolite
Hydroxybenzoic acids	
3-Hydroxybenzoic acid (3-HBA)	Gut microbial metabolite
Ellagitannins	
Urolithin A (Uro A)	Gut microbial metabolite
Urolithin B (Uro B)	Gut microbial metabolite
Urolithin C (Uro C)	Gut microbial metabolite
Urolithin D (Uro D)	Gut microbial metabolite
Urolithin B 3-O-glucuronide (Uro B gluc)	Human phase II metabolite

A tabulated summary of the studies in which these metabolites have already been tested for their neuroprotective activity (with special reference to AD) can be found in Table 4.

Table 4. Neuroprotective effects documented for some polyphenolic metabolites tested in this work.

Compound/neuroprotective effect[a]	Ref(s)
5 (3',4' Dihydroxyphenyl)-γ-valerolactone (#2)	
Positive correlation between plasma levels of #2 and NORT memory performance of 3xTg-AD mice supplemented with polyphenolic extract	169
(-)-Epigallocatechin gallate (EGCG)	
Anti-$A\beta_{42}$ fibrillization activity and remodelling *in vitro*	136,150,170
Remodelling of preformed fibrils and oligomers *in vitro* and in APP overexpressing cell line	151
Metal chelating activities against various metals, attenuation of metal-catalysed amyloid formation *in vitro*	171
Decreased Aβ levels and plaques in Aβ/Tg2576 mice	172
Decreased plaque burdens, reduced soluble and insoluble $A\beta_{40}$ and $A\beta_{42}$, reduced phosphorylated tau, improved working memory in Tg2576 mice	173
Protection against Aβ toxicity attributed to antioxidant activity in cultured hippocampal neurons	174
Iron chelating activity, resulting in modulation of APP translation via an IRE present in the 5'-UTR of APP, in human SH-SY5Y neuroblastoma cells	175
Neuroprotective action (inhibition of apoptosis, aggregation, formation of ADDLs) against Aβ-derived peptides toxicity in primary cultures of rat hippocampal cells	176
Formation of small oligomers, structured but unable to seed fibril growth and not toxic *in vitro*	168
Increased neuronal survival and neurogenesis on the adult hippocampus of C57B/6 mice and on adult hippocampal precursor cells *ex vivo*	177
Increased secretion of neprilysin (Aβ degrading enzyme) in cultured rat astrocytes	178
Elevated neprilysin expression in AD mouse model	179
3-(3'-Hydroxyphenyl)propionic acid (3-HPP)	
Anti-Aβ42 oligomerization and anti-Aβ42 fibrillation activities *in vitro*	163
Positive correlation between plasma levels of 3-HPP and NORT memory performance of 3xTg-AD mice supplemented with polyphenolic extract	169

Table 4 (continued).

Caffeic acid	
Reversed neurotoxicity by attenuation of the elevation of intracellular calcium levels and tau phosphorylation in PC12 cells pre-treated with caffeic acid before treatment with $A\beta_{42}$	180
Inhibition of cholinesterase (acetylcholine cleaving enzymes) activity and decrease in malondialdehyde content (caused by pro-oxidants) in rat brain (*in vitro*)	181
Anti-$A\beta_{42}$ fibrillization activity and remodelling *in vitro*	136
Protection from cytotoxicity of HFIP-pretreated $A\beta_{42}$ in *Candida glabrata* cells	136
Ferulic acid	
Protection from cognitive impairment, ameliorated cortical acetylcholine level, suppressed hippocampal neuroinflammation in $A\beta_{42}$ ICV injected mice following long-term administration	182
Inhibition of $A\beta_{42}$ fibril formation and elongation and fibril remodelling *in vitro*	183
Interaction with $A\beta_{40}$ in the initial stage of the aggregation process; inhibition of Aβ monomer/oligomer self-assembly and formation of amorphous aggregates *in vitro*	184
Decreased expression levels of BACE-1 and APP and increased MMP-2 and MMP-9 (metallopeptidase involved in neuronal plasticity) expression in SHSY5Y-APP cells	185
Restored mitochondrial function and antioxidant activity in $A\beta_{42}$ treated cells	186
Decreased β-amyloid deposits and Aβ oligomer abundance; reversed and behavioural memory deficits in Aβ/APP/PS1 mice	187
Protection against Aβ-induced learning and memory deficits in $A\beta_{42}$ ICV injected mice following long-term administration of ferulic acid	188
Prevention of low-order oligomer formation *in vitro*	189
Inhibition of $A\beta_{42}$ monomer to oligomer transition *in vitro*	190
Prevention of $A\beta_{42}$-induced activation of astrocyte cells in $A\beta_{42}$ ICV injected mice following long-term administration of ferulic acid	191
Reduction of cortical $A\beta_{40}$ levels, but slight effect on $A\beta_{42}$ deposition in APP/PS1 (APPswe/PS1dE9) Tg mice	192
Inhibition of cholinesterase activity in cell free *in vitro* system	193
Reduced average fibril length in *Caenorhabditis elegans* $A\beta_{42}$ Tg strain (CL2006)	194
Dihydrocaffeic acid	
Protection against oxidative stress in human neuroblastoma SK-N-MC cells	195

Table 4 (continued).

Dihydroferulic acid	
Protection against oxidative stress in SK-N-MC cells	195
3-Hydroxybenzoic acid (3-HBA)	
Anti-$A\beta_{42}$ oligomerization and anti-$A\beta_{42}$ fibrillation activity *in vitro*	163
Urolithin A	
Anti-$A\beta_{42}$ fibrillization activity *in vitro*	196
Protection against oxidative stress and antiglycative activity (advanced glycation is an effect of hyperglycemia, that has a significant role in AD) in SK-N-MC cells	195
Urolithin B	
Anti-$A\beta_{42}$ fibrillization activity *in vitro* and increased maximum survival/motility in $A\beta_{42}$Tg *C. elegans*	196
Protection against oxidative stress and antiglycative activity in SK-N-MC cells	195

[a]NORT, novel object recognition test; Tg, transgenic; $A\beta_{42}$, amyloid-β 42; APP, amyloid precursor protein; IRE, iron responsive element; 3'-UTR, 3'-untranslated region; ADDLs, Aβ derived diffusible ligands; AD, Alzheimer's disease; HFIP, hexafluoroisopropanol; ICV, intra-cerebroventricular; BACE1, β-secretase 1; MMP, matrix metalloproteinase; PS1, presenilin 1.

For the initial screening, compound activity was assessed using a sensitive assay based on a newly developed yeast model of amyloid oligomer-induced toxicity, based on the heterologous expression of an artificial polypeptide named β23. It derives from a combinatorial library of peptides designed to form cross-β-structures[197] and was selected for its high cytotoxicity to human cells[198]. Its sequence comprises patterns of seven polar-nonpolar alternating amino acids (joined by four-amino acids linkers) (Fig. 14), a periodicity that accurately mimic the sequence of amyloid peptides and dictate the formation of amphipathic β strands predisposing to oligomerization[197]. Distinguishing features of using β23 polypeptide as target toxicant in yeast cells are: i) it preferentially forms β-amyloid oligomeric species[197,198]; ii) it is extremely toxic to yeast cells, but, at the same time, its dose-dependent toxicity allows to select a window suitable to screen molecules able to restore cell viability.

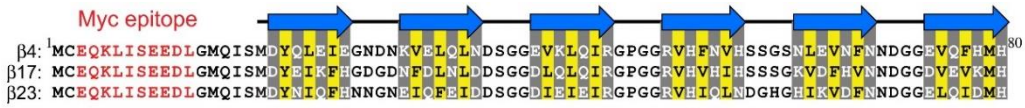

Figure 14. Amyloidogenic synthetic peptides identified to form β-sheet fibrils. The amino acid sequences of β23 and two other amyloidogenic peptides (β4 and β17) identified by Olzscha et al.[198] are reported. Polar and nonpolar amino acids are indicated in grey and yellow, respectively, and regions forming β strands are indicated by blue arrows. Among the selected peptides, β23 is extremely toxic when expressed in human cells[198].

Multiple PVLs, and particularly the monohydroxylated metabolite 5-(4'-hydroxyphenil)-γ-valerolactone [(4'-OH)-PVL], emerged as highly effective β23-oligomer detoxifying compounds, capable of preventing β23-induced cell growth inhibition at sub-nanomolar concentrations. A similar efficacy profile was observed in β23-overexpressing human cells and in other assays involving AβOs but not fibrils. Importantly, (4'-OH)-PVL also displayed a dose-dependent neuroprotective and anti-neuroinflammatory effect in an acute mouse model of AβO-induced memory impairment.

2. RESULTS (PART I)

2.1 A highly sensitive yeast model to assess β-amyloid oligomer-induced cytotoxicity

The yeast *S. cerevisiae* was chosen as the initial model system in which to assess the anti-amyloid oligomer activity of PVLs.

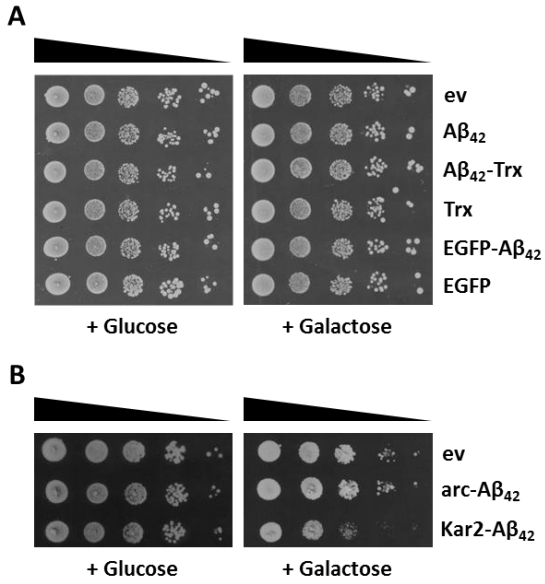

Figure 15. Cytosolic expression of Aβ$_{42}$ does not affect cell viability in yeast. A) Yeast cells (BY4742 strain) were transformed with multicopy expression plasmids harbouring galactose-inducible genes coding for the human Aβ$_{42}$ peptide alone or the same peptide fused with the indicated scaffold proteins (thioredoxin, Trx; enhanced green fluorescent protein, EGFP). Yeast cells transformed with the empty vector (pYES2; ev) or with constructs for the expression of the Aβ$_{42}$-lacking forms of Trx and EGFP served as controls. Serial dilutions (ten-fold increments) of the indicated transformants were spotted on agar plates under repressive (+ Glucose) or inducing (+ Galactose) conditions and cell growth was assessed after 2 days at 30°C. B) Yeast cells (W303α strain) were transformed with pYES2 plasmids expressing an E22G arctic variant of the human amyloid peptide (arc-Aβ$_{42}$) and a fusion derivative of Aβ$_{42}$ that due to the presence of an ER-targeting peptide is forced through the secretory pathway (Kar2-Aβ$_{42}$). Kar2-Aβ$_{42}$ expression causes a detectable reduction of the yeast cell viability under inducing conditions. Serial dilution spot assay conditions were the same as in panel (A).

In accordance with previous reports[118,130,131], yeast cells confirmed to easily cope with the human $A\beta_{42}$ peptide when expressed as a free cytosolic peptide or fused to scaffold proteins such as thioredoxin or EGFP (enhanced-GFP)[130] under the control of a galactose-inducible promoter (Fig. 15A). This was true not only for the wild-type allele, but also for the 'arctic' $A\beta_{42}$ variant (Fig. 15A), i.e. $A\beta_{42}$ carrying one of the known mutations (E22G) causing familial AD through an increased formation of Aβ protofibrils[199]. A more stringent but still relatively weak phenotype is obtained by targeting $A\beta_{42}$ to the secretory pathway[120,139] using a yeast multicopy vector to express the $A\beta_{42}$ peptide N-terminally fused to an ER-targeting signal (Kar2-$A\beta_{42}$; Fig. 15B).

To obtain a more sensitive cellular β-amyloid toxicity readout, we resorted to β23, a reportedly highly toxic artificial polypeptide with a β-sheet structure and a marked propensity to form soluble prefibrillar oligomeric aggregates both *in vitro*[197] and *in vivo*[198]. Indeed, when expressed from a multicopy vector under the control of a galactose-inducible promoter, β23 caused a readily detectable but exceedingly strong cell-death phenotype (Fig. 16A, upper panel). We thus switched to a stably integrated form of β23 and inserted either one copy or two copies of a galactose-inducible β23-coding sequence into the genome of an efflux-deficient yeast strain (*pdr1Δpdr3Δ*, conveniently reducing compound efflux during screening). As shown in Figure 16A (lower panel), these integrative transformants displayed copy number-dependent cell growth inhibition with different severity phenotypes. In serial dilution assays, a rather weak growth inhibition phenotype was observed with the one-copy β23 transformant, whereas a marked reduction of cell viability was apparent with the two-copy β23 transformant starting from the first input cell dilution (Fig. 16A) and a similar growth impairment was observed under liquid culture conditions (Fig. 16B).

Because of the severe but still manageable growth inhibition caused by stable integration of two copies of β23, which may afford optimal sensitivity in the detection of phenotype modifying compounds, this integrative transformant was selected for the subsequent screening of PVLs (Table 3 and Figure 13). Importantly, as revealed by an immuno-dot blot analysis performed with an antibody (A11) that selectively recognizes toxic Aβ oligomers[56,152], induction of β23 expression upon switch to a galactose-containing medium was accompanied by the accumulation of A11-immunoreactive, amyloid oligomeric material (Fig. 17).

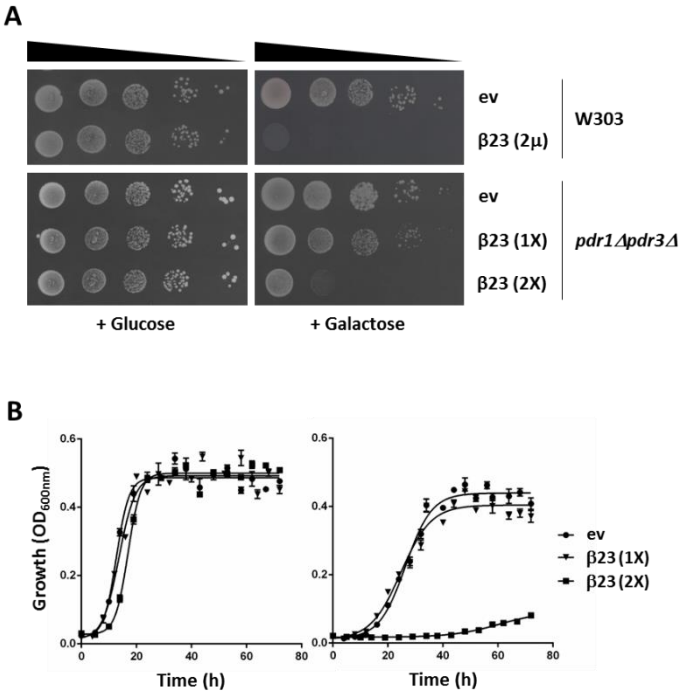

Figure 16. β23 toxicity in yeast. A) Serial dilution assays (10-fold input cell dilutions ranging from 10^1 to 10^4) were performed on yeast cells transformed with either episomal (2μ) or integrative β23 [one-copy (1X); two-copy (2X)] constructs; empty-vector (ev) transformants served as controls. Cells were spotted on glucose- or galactose-containing agar plates and growth was assessed after 2 days at 30°C. B) Growth curves of the 1X and the 2X β23 integrative transformants cultured under β23 expression repressive (+ glucose; left) or inducing (+ galactose; right) conditions.

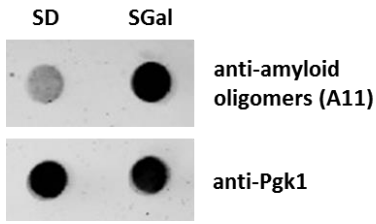

Figure 17. β23 toxic oligomer formation in yeast. Immuno-dot blot analysis performed with the anti-amyloid oligomer antibody A11 on whole cell extract samples derived from the 2X β23 integrative transformant strain cultured in SD (glucose-containing) or SGal (galactose-containing) liquid medium. Immunoreactivity with the constitutively expressed phoshoglycerate kinase (Pgk1) enzyme served as a loading control.

2.2 PVLs relieve β23-induced cytotoxicity in yeast

The above described β23 integrative transformant was employed for the screening of the whole set of polyphenol-related compounds (Table 3) using cell viability as readout (see 'Materials and Methods' for details). PVLs and other compounds were selected and synthetized thanks to the collaboration with Prof. Daniele Del Rio (Department of Veterinary Science, University of Parma) and Prof. Claudio Curti (Department of Food and Drug, University of Parma). The metal-chelator clioquinol (CQ), for which different anti-Aβ and AD protective effects have previously been documented in various experimental settings[200–203], including yeast cells expressing Kar2-Aβ$_{42}$[90], was also included as an additional reference compound.

As shown in Figure 18 and Table 5, all PVL metabolites prevented β23-induced growth inhibition to some extent. However, the magnitude and dose-dependency of this effect varied significantly for the different PVLs (Fig. 18 and Table 5).

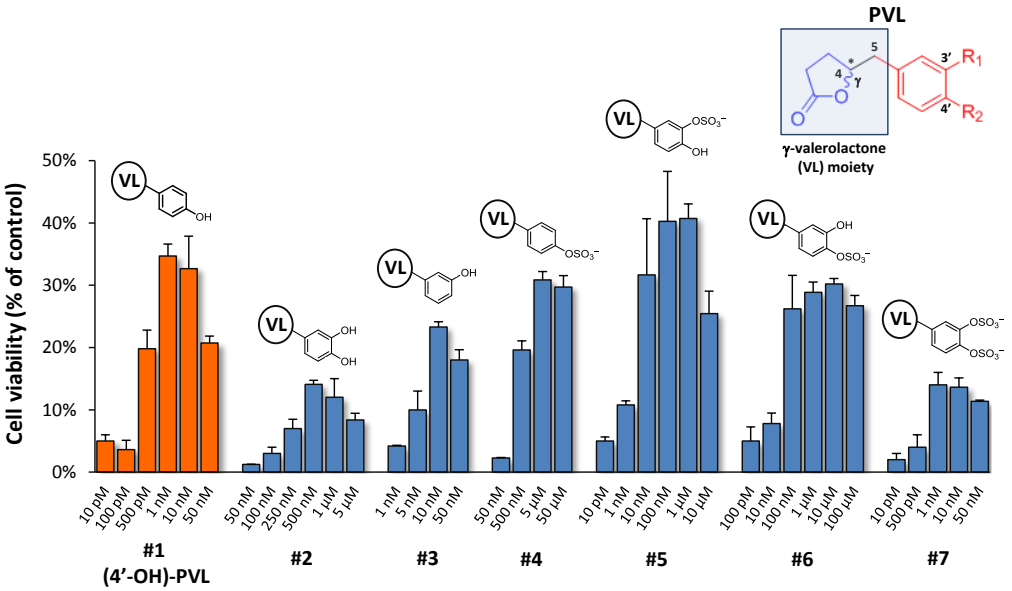

Figure 18. PVLs protect yeast cells against β23 toxicity. Dose-response plots of the protective effects of the different PVLs against β23 toxicity. The results (see 'Materials and Methods' for details) are expressed as percentage of cell viability relative to the DMSO vehicle control (arbitrarily set to 0%); data are the mean ± standard deviation of three replicates. A schematic representation of the chemical structures of the tested PVLs is shown above individual bar-plots.

Preservation of cell viability ranged from approximately 14% for the 3',4'-dihydroxylated and the 3',4'-disulfated PVLs (#2 and #7 in Fig. 13) to up to 41% for the 3'-sulfated PVL metabolite (#5). Intermediate values were obtained with the other PVLs, the most effective of which was the monohydroxylated (4'-OH)-PVL metabolite (#1), which improved cell viability by 35% compared to the DMSO vehicle and also featured the lowest half-maximal effective concentration (EC_{50} = 498 pM; Table 5).

Table 5. Cytoprotective efficacy of compounds antagonizing β23 proteotoxicity in yeast.

Compounds[a]		EC_{50}	Maximum response (% cell viability rescue)[b]
PVLs	#1 [(4'-OH)-PVL]	498 pM	35% ± 1.9%
	#2	250 nM	14% ± 0.7%
	#3	5 nM	23% ± 0.8%
	#4	369 nM	31% ± 1.4%
	#5	2 nM	41% ± 2.4%
	#6	31 nM	30% ± 0.9%
	#7	533 pM	14% ± 1.5%
CA		157 nM	12% ± 2%
FA		95 nM	14% ± 0.5%
DF		5 nM	14% ± 1%
CA-gluc		254 nM	15% ± 0.5%
EGCG		5 nM	26% ± 0.3%
3-HBA		18 nM	29% ± 0.5%
3-HPP		10 nM	21% ± 1%
CQ		254 nM	23% ± 0.7%

[a]EGCG, (–)-epigallocatechin gallate; 3-HBA, 3-hydroxybenzoic acid; 3-HPP, 3-hydroxyphenylpropionic acid; CQ, clioquinol; see Figure 13 for the chemical structures of the PVLs.

[b]Cell viability rescue data were normalized with respect to the DMSO vehicle control (arbitrarily set to 0%) and are the mean ± standard deviation of three independent replicates, from which the indicated EC_{50} values were derived.

The other tested polyphenol compounds, including the plant metabolite EGCG and the human metabolites 3-HPP and 3-hydroxybenzoic acid (3-HBA), which have previously

been shown to interfere with Aβ aggregation and to mitigate β-amyloid toxicity in various model systems[151,163,174,204], also scored positive in the yeast β23 assay but with lower activities and apparently higher (10- to 20-fold) EC_{50} values compared to (4'-OH)-PVL (Table 5 and Fig. 19). Similar results (23% rescue of cell viability with an EC_{50} of 254 nM) were obtained with the metal chelator CQ (Table 5 and Fig. 19). Altogether, these results validate the β23-based yeast assay as a reliable tool for detecting compounds capable of relieving β-amyloid oligomer-induced cytotoxicity and point to PVLs as highly protective compounds.

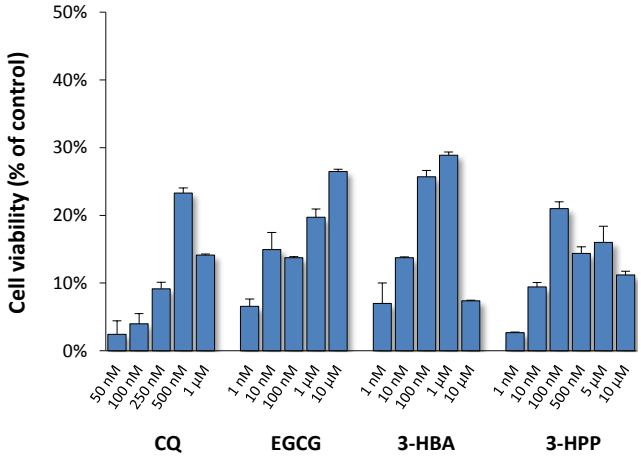

Figure 19. Anti-proteotoxic effect of a subset of $A\beta_{42}$-active compounds in the yeast β23 system. Dose-response analysis (as described in Fig. 18) of clioquinol (CQ), the plant polyphenol metabolite (-)-epigallocatechin gallate (EGCG), and the human flavonoid metabolites 3-hydroxyphenylpropionic acid (3-HBA) and 3-hydroxyphenylpropionic acid (3-HPP).

Other bioactive human polyphenol metabolites such as urolithins (Table 3) proved to be only marginally effective in our yeast model (Fig. 20). Urolithins are the main colonic metabolites of ellagitannins and ellagic acid and the most abundant circulating compounds after the intake of pomegranates, berries, nuts, oak-aged wines and tisanes. *In vitro* preliminary research has shown anticarcinogenic, antiglycative and antioxidant effects of urolithins and their glucuronide and sulfate metabolites[205]. Attenuation of the neuroinflammation caused by abnormal microglia activation has been reported[206,207], as well as more specific anti-neurodegenerative effects. For example, Yuan *et al.* have shown that methyl-urolithin B prevents Aβ fibrillation *in vitro* and protects *Caenorhabditis*

elegans against $A\beta_{42}$ induced neurotoxicity and paralysis *in vivo*[196]. The absence of a protective effect in our yeast model could be due, at least in part, to their high toxicity in yeast in our experimental conditions (Fig. 20).

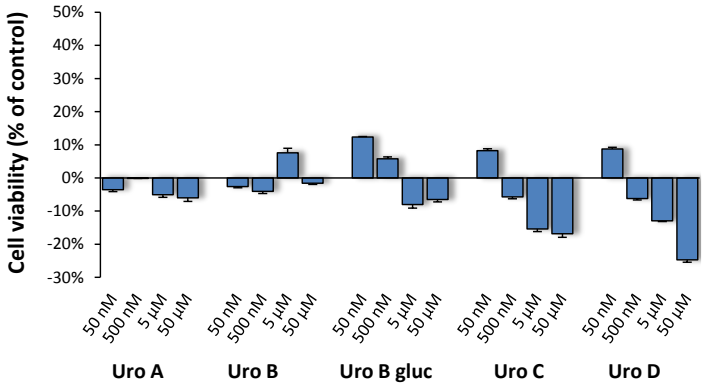

Figure 20. **Urolithins do not protect yeast cells against β23 toxicity.** Dose-response analysis (as described in Fig. 18) of a subset of urolithins: urolithin A (Uro A), urolithin B (Uro B), urolithin B glucuronide (Uro B gluc), urolithin C (Uro C) and urolithin D (Uro D).

On the other hand, (4'-OH)-PVL did not restore growth at appreciable levels in a yeast model of PD overexpressing the α-synuclein protein (Fig. 21). Thus, this compound appears not to be simply a generalized modulator of cellular stress.

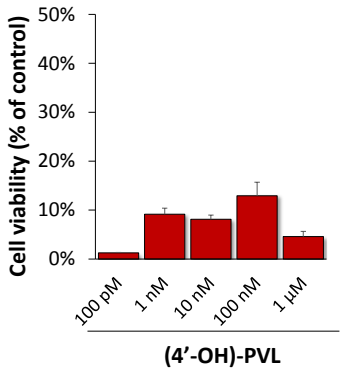

Figure 21. Effect of (4'-OH)-PVL in the Parkinson's disease yeast model. Dose-response analysis of the effect of (4'-OH)-PVL in a yeast model of PD based on α-syn-induced toxicity. Yeast cells bearing two integrated copies of the coding sequence for α-syn under the control of a galactose-inducible promoter were culture in liquid SGal medium in the presence of the indicated concentrations of (4'-OH)-PVL**.** The results are expressed as percentage of cell viability relative to the DMSO vehicle control (arbitrarily set to 0%); data are the mean ± standard deviation of three replicates.

All PVLs (as well as other polyphenol metabolites) displayed bell-shaped dose-response curves (Fig. 18 and 19), suggesting that these flavan-3-ol metabolites may become toxic above a certain threshold concentration. Based on this observation and on the sub-nanomolar EC_{50} value displayed by (4'-OH)-PVL, we selected this particular monohydroxylated flavan-3-ol metabolite as lead for subsequent analyses and asked whether (4'-OH)-PVL treatment interfered with the accumulation of A11-reactive, β23 oligomeric species. As shown in Figure 22, (4'-OH)-PVL and other PVLs (e.g., #5 and #6) markedly reduced A11 immunoreactivity in β23-expressing cells. This suggests a direct mode of action, involving either β23 aggregation inhibition or β23 oligomer detoxification. We cannot exclude, however, the possible co-existence of additional indirect effects (e.g., antioxidant) ultimately leading to an increased proteotoxic stress tolerance.

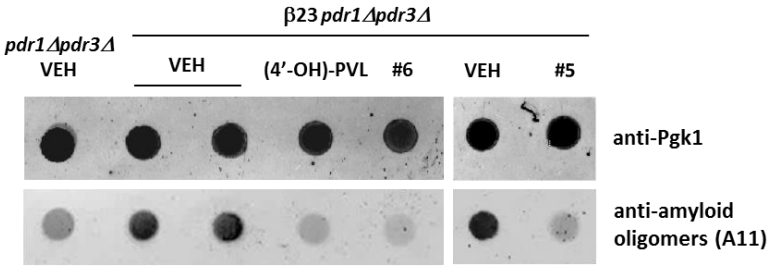

Figure 22. **PVLs reduce the accumulation of A11-reactive amyloid oligomers in yeast cells.** Representative results of an immuno-dot blot analysis performed with the pan-amyloid oligomer antibody A11 on total lysates derived from 2x β23 cells cultured for 8 h under inducing (+ galactose) conditions in the presence of the indicated PVLs. The untransformed *pdr1Δpdr3Δ* strain and the corresponding 2x β23 transformant treated with the DMSO vehicle only served as references; Pgk1 immunoreactivity was used as a loading control (see 'Materials and Methods' for details).

2.3 PVLs counteract β23-induced toxicity in human cells

We next wished to find out whether the anti-β23 oligomer activity of PVLs observed in yeast also applies to human cells. To this end, we transferred the β23 coding sequence, along with sequences coding for human $A\beta_{42}$ fused to EGFP[198] and its aggregation-prone 'arctic' variant, into a mammalian cell expression vector. This was followed, in collaboration with Prof. Gaetano Donofrio (Department of Veterinary Science, University

of Parma), by transient transfection, constitutive expression and viability testing in human embryonic kidney (HEK293) cells - the same cells employed for the initial characterization of the molecular bases of β23 cytotoxicity[198].

Also in human cells, β23 proved to be significantly more toxic than the $A\beta_{42}$ peptide[198] and caused an approximately 50% lethality 72 h after transfection (Fig. 23).

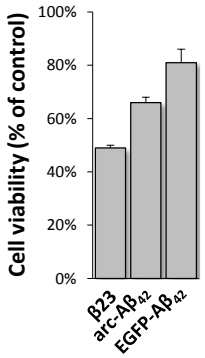

Figure 23. **β23 and $A\beta_{42}$ cytotoxicity in human cell line.** HEK293 cells were transiently transfected with plasmids (pCMV) expressing β23, EGFP-$A\beta_{42}$ fusion protein and its E22G arctic variant (arc-$A\beta_{42}$) under the control of the constitutive CMV promoter. 72 h after transfection, the MTT assay was used to assess cell viability; the results are expressed as percentage of cell viability relative to control cells transfected with the empty pCMV vector (arbitrarily set to 100%).

Using this β23 expression set-up, we then examined the anti-proteotoxicity (and cell survival-promoting) activity of the different PVL metabolites.

As shown in Figure 24, also in HEK293 cells, PVLs exerted a positive effect on the viability of β23 expressing cells. (4'-OH)-PVL, which preserved cell viability by 96% compared to the DMSO vehicle control, was the second most effective compound, again with a very low half-maximal effective concentration (EC_{50} = 0.1 pM; see Fig. 24 and Table 6). The main deviation from the yeast data was observed for the 5-(3',4'-dihydroxyphenyl)-γ-valerolactone metabolite (#2 in Fig. 13), which was the worst performing in the yeast β23 assay, whereas it afforded full viability in HEK293 cells although with an EC_{50} several orders of magnitude higher than that of (4'-OH)-PVL. Whether these differences in efficacy are due to cell-specific differences in metabolite mode of action, or merely reflect different internalization and/or intracellular stability properties is presently unknown.

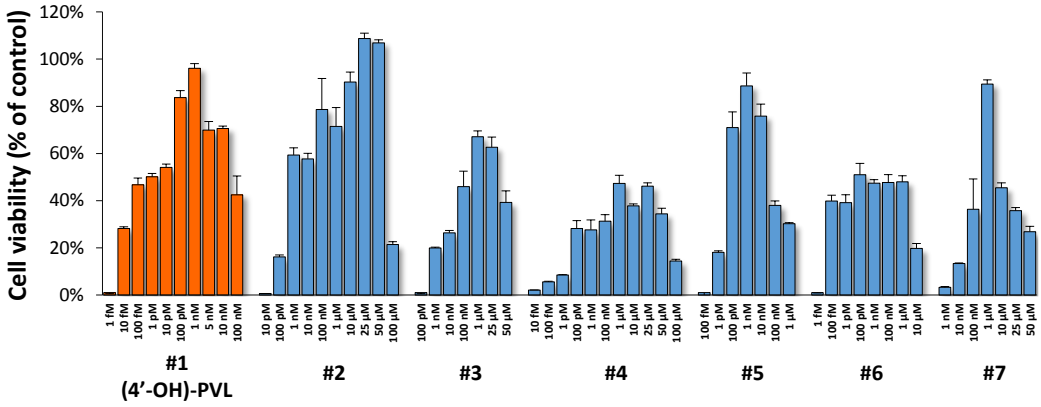

Figure 24. Cytoprotective activity of PVLs in a β23-expressing human cell line. The MTT cell viability assay was used to assess the ability of the indicated PVLs to protect against β23 cytotoxicity in HEK293 cells. Cell viability assays were performed 72 h after transfection with the pCMV-β23 plasmid (see 'Materials and Methods' for details). Results are expressed as percentage of cell viability relative to the DMSO vehicle control (arbitrarily set to 0%); data are the mean ± standard deviation of three replicates.

Table 6. **Anti-β23 activity of PVLs and other compounds in HEK293 cells.**

Compound		EC_{50}	Maximal response (viability rescue; % of control ± standard deviation)[a]
PVLs	#1 [(4'-OH)-PVL]	0.1 pM	96% ± 2%
	#2	3 nM	109% ± 2.2%
	#3	10 nM	67% ± 2.4%
	#4	49 pM	47% ± 3.5%
	#5	5 pM	89% ± 5.5%
	#6	0.6 pM	51% ± 1%
	#7	93 nM	89% ± 1.8%
CQ		57 pM	61% ± 2.6%
3-HBA		823 pM	74% ± 3.7%
3-HPP		661 pM	85% ± 2.4%

[a]Cell viability rescue data were normalized with respect to the DMSO vehicle control (arbitrarily set to 0%) and are the mean ± standard deviation of three independent replicates, from which the indicated EC_{50} values were derived.

We then compared (4'-OH)-PVL activity with that of a subset of the anti-$A\beta_{42}$ reference compounds previously shown to relieve β23 cytotoxicity in the yeast system (Table 5). As shown in Table 6 and Figure 25, also in human cells (4'-OH)-PVL was apparently more active than CQ and the polyphenol metabolites 3-HPP and 3-HBA, with a higher maximal protective capacity (91% viability vs. an average value of 73% for the other compounds) and a considerably lower (2-3 orders of magnitude) EC_{50} value.

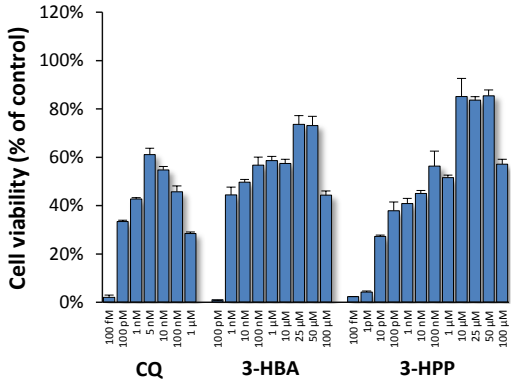

Figure 25. Anti-proteotoxic effect of a subset of anti-$A\beta_{42}$ active compounds in β23-expressing human cell line. Dose-response analysis (as described in Fig. 24) of a subset of reference anti-Aβ compounds performed in pCMV-β23 transfected HEK293 cells.

2.4 (4'-OH)-PVL activity on human $A\beta_{42}$

We then examined the activity of (4'-OH)-PVL on the human $A\beta_{42}$ peptide. We first investigated the ability of (4'-OH)-PVL to relieve cytotoxicity caused by Kar2-$A\beta_{42}$ (Fig. 15B), a fusion derivative of $A\beta_{42}$ that due to the presence of an ER-targeting peptide is forced into the secretory pathway, thus mimicking secretory APP processing and $A\beta_{42}$ production as it occurs in neurons[120]. As shown in Figure 26, also in this assay (4'-OH)-PVL dose-dependently ameliorated the viability of yeast cells conditionally expressing Kar2-$A\beta_{42}$. Its maximum protective effect (22% cell viability rescue relative to untreated controls) was similar to, but with a lower EC_{50} (29 pM) compared to that of CQ (113 nM).

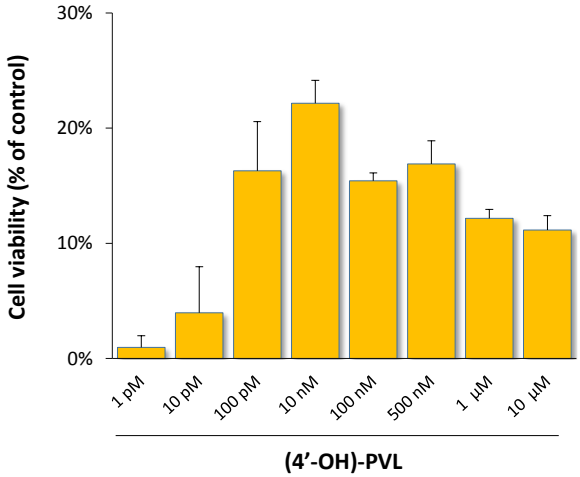

Figure 26. Cytoprotective effect of (4'-OH)-PVL in the Kar2-Aβ$_{42}$ yeast model of amyloid toxicity. Dose-response analysis of the effect of (4'-OH)-PVL in the secretory model of Kar2-Aβ$_{42}$-induced cytotoxicity. Yeast cells transformed with a multicopy plasmid expressing Kar2-Aβ$_{42}$ under the control of a galactose-inducible promoter were culture in liquid SGal medium in the presence of the indicated concentrations of (4'-OH)-PVL**.** The results are expressed as percentage of cell viability relative to the DMSO vehicle control (arbitrarily set to 0%); data are the mean ± standard deviation of three replicates.

To further investigate the apparently oligomer-specific action of (4'-OH)-PVL, we examined the ability of (4'-OH)-PVL to interfere with Aβ$_{42}$ aggregation using atomic force microscopy (AFM). Two distinct incubation conditions of the synthetic Aβ$_{42}$ peptide, carried out in the presence of (4'-OH)-PVL or the DMSO vehicle, were utilized for these experiments: a 24 h incubation at 4°C (pH 7.4) for Aβ oligomers and a longer (4 days) incubation at 37°C under acidic conditions for fibril formation (see 'Materials and Methods' for details). As shown in Figure 27, (4'-OH)-PVL, at a 3:1 molar ratio with respect to monomeric Aβ$_{42}$, significantly reduced both AβO abundance and size compared to the vehicle alone. In contrast, the same (4'-OH)-PVL molar ratio only slightly interfered with Aβ$_{42}$ fibril formation (Fig. 27C).

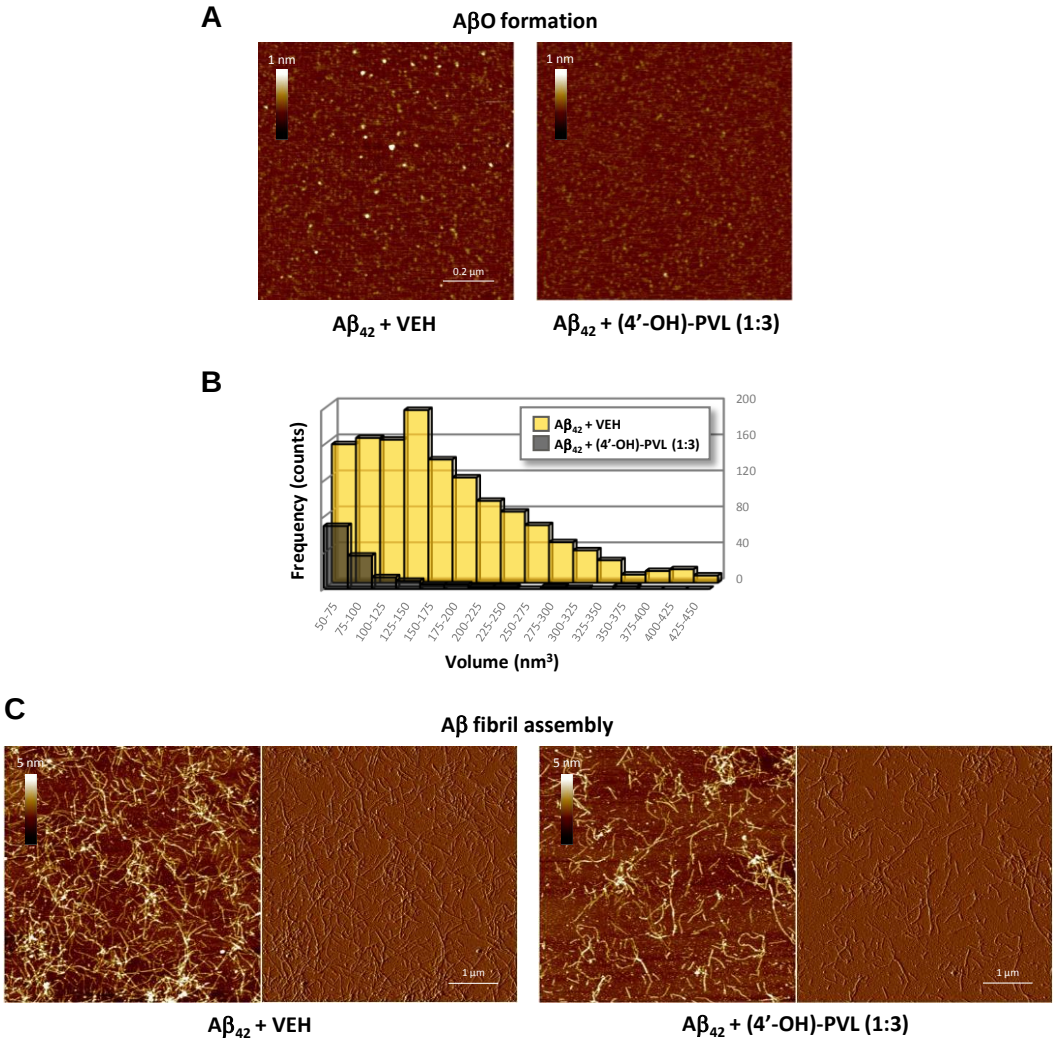

Figure 27. (4'-OH)-PVL interferes with Aβ$_{42}$ oligomer formation. A) AβOs were produced by incubating the synthetic human Aβ$_{42}$ depsipeptide (100 µM monomer concentration) for 24 h at 4°C (pH 7.4) in the presence of the DMSO vehicle only or (4'-OH)-PVL (1:3 Aβ$_{42}$:PVL molar ratio) (see 'Materials and Methods' for details). AβOs were diluted to a final concentration of 100 nM prior to deposition. B) A histogram quantification of the number ('frequency') and size ('volume') of the AβOs formed in the presence or absence of (4'-OH)-PVL. C) Same experimental set-up as in (A), but with a 4-days incubation at 37°C (pH 5.0) to allow for fibril formation. For each sample, height and amplitude AFM images are shown (colour scale bars correspond to a range of +500/-500 mV for amplitude images).

In line with this result, no significant effect of (4'-OH)-PVL on fibril formation was detected in kinetic assays in presence of Th-T (Fig. 28), in a kinetic assay conducted in collaboration with Prof. Michele Vendruscolo (Department of Chemistry, University of Cambridge).

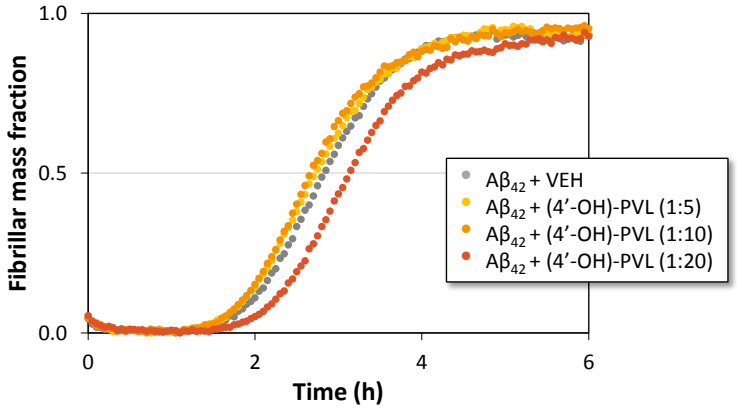

Figure 28. (4'-OH)-PVL does not interfere with recombinant Aβ$_{42}$ fibril formation. Recombinant Aβ$_{42}$ peptide was incubated at 37°C in presence of Th-T and different molar ratio of (4'-OH)-PVL or vehicle (VEH); variations in Th-T fluorescence were monitored over 24 hours (see 'Material and Methods' for details). The fibrillar mass fraction is calculated as the ratio between Th-T fluorescence intensity measured at a specific time point and the maximal fluorescence reached in each sample.

Given prior reports documenting the ability of polyphenol aglycones of different size and chemical structure to remodel soluble AβOs into large-size, unstructured and non-toxic aggregates[151,152,208], we next examined the remodelling activity of (4'-OH)-PVL. To this end, preformed AβOs were treated with either vehicle (DMSO) or (4'-OH)-PVL (3 h at 22°C) and were imaged by AFM. As shown in Figure 29A, a clear remodelling of AβOs into large-size aggregates was observed upon treatment with (4'-OH)-PVL (3:1 molar ratio with respect to monomeric Aβ$_{42}$) but not with vehicle. Under the same experimental conditions, treatment with (4'-OH)-PVL caused a strong reduction of immunoreactivity with the oligomer conformation-specific antibody A11 (Fig. 29B).

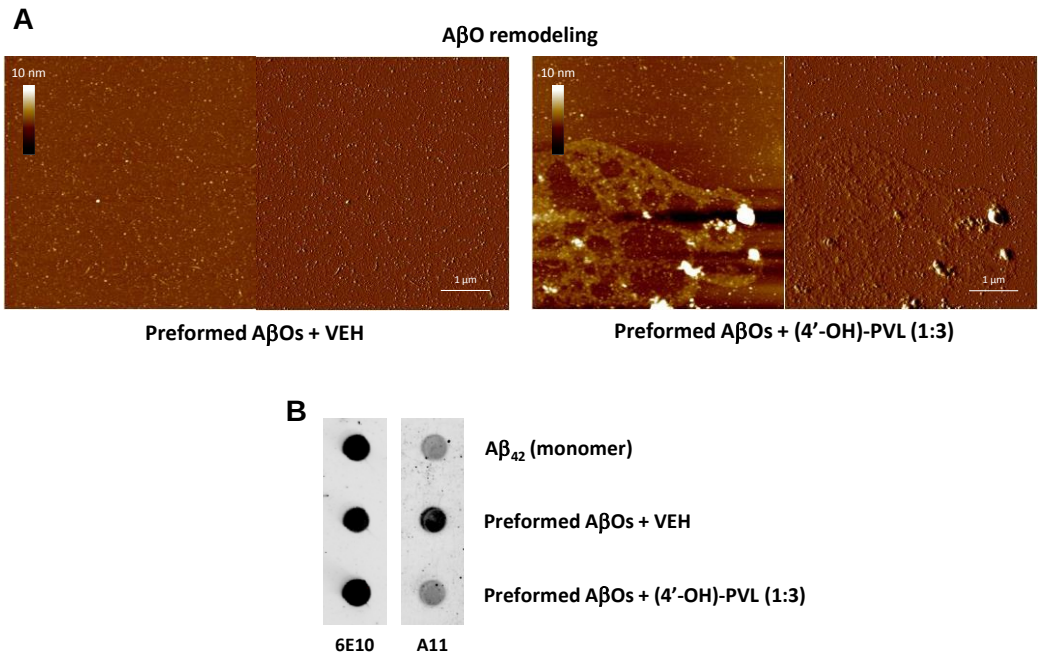

Figure 29. (4'-OH)-PVL remodels preformed AβOs. A) Preformed AβOs were diluted 10-fold with PBS supplemented with either DMSO or (4'-OH)-PVL (1:3 monomeric $A\beta_{42}$:PVL molar ratio) and incubated at 22°C for 3 h prior to AFM analysis (see 'Materials and Methods' for details). For each sample, height and amplitude AFM images are shown (colour scale bars correspond to a range of +30/-30 mV for amplitude images). B) Immuno-dot blot analysis of preformed AβOs treated with the DMSO vehicle or (4'-OH)-PVL as in (A). The Aβ sequence-specific (6E10) and the toxic oligomer-specific (A11) antibodies were used as primary loading control and test antibodies, respectively (see 'Materials and Methods' for details). The monomeric (freshly dissolved) $A\beta_{42}$ peptide served as a negative control for A11-immunoreactivity.

2.5 (4'-OH)-PVL prevents memory deterioration and attenuates neuroinflammation in an acute mouse model of AβO-induced neurotoxicity

Results obtained with β23 and Kar2-$A\beta_{42}$, whose cellular toxicity is due to prefibrillar β-oligomeric species rather than to amyloid fibrils, as well as the *in vitro* data obtained with synthetic $A\beta_{42}$, point to an apparently anti-AβO-specific action of (4'-OH)-PVL. Such action may rely on interference with early steps of oligomer formation, but it may also result from AβO remodelling (Fig. 29). The latter mode of action might also lead to AβO

surface shielding and prevention of aberrant interactions with essential cellular proteins as originally proposed by Olzscha et al.[198]. In addition, although AβOs can also act intracellularly[9], their neurotoxic action *in vivo* starts extracellularly upon interaction with neuronal cell surface receptors.

We addressed this issue - and followed-up the AβO detoxification activity revealed by *in vitro* experiments - by investigating the effect of (4'-OH)-PVL in an acute mouse model of AβO-induced memory impairment that mimics one of the earliest steps of $A\beta_{42}$ amyloidotic neurodegeneration[49], in collaboration with Prof. Gianluigi Forloni and Claudia Balducci (Department of Neuroscience, Mario Negri Institute for Pharmacological Research, Milan).

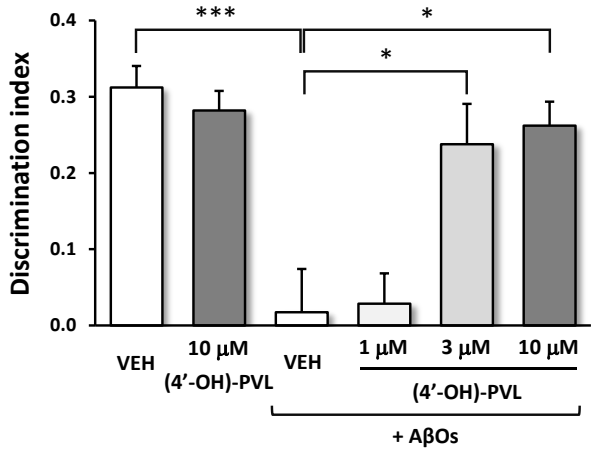

Figure 30. (4'-OH)-PVL antagonizes AβO-mediated memory impairment. Histogram representation (mean ± standard error of mean) of the Discrimination Index (see 'Materials and Methods') measured by NORT in C57BL/6 naïve mice ICV-injected with AβOs (1 μM $A\beta_{42}$ monomer concentration) preincubated for 15 min with the DMSO vehicle (VEH) (n=18) or the indicated concentrations of (4'-OH)-PVL [1 μM (4'-OH)-PVL, n=7; 3 μM (4'-OH)-PVL, n=21; 10 μM (4'-OH)-PV, n=10]. Two additional groups of animals, ICV-injected in parallel with the DMSO vehicle (n=21) or with the highest concentration (10 μM) of (4'-OH)-PVL (n=8) without AβOs served as controls. The significant memory deficit observed in the AβOs+VEH group compared to the VEH only group, was dose-dependently antagonized by (4'-OH)-PVL (* $p<0.05$, *** $p<0.001$; Tukey's test). The difference between the VEH and the (4'-OH)-PVL+VEH groups was not statistically significant, indicating the absence of any detrimental effect of (4'-OH)-PVL at the highest tested concentration. AβOs for these experiments were prepared and characterized as detailed in 'Materials and Methods'.

Memory impairment, measured with the 'novel object recognition test' (NORT) in mice intra-cerebroventricularly (ICV) injected with preformed AβOs (see 'Materials and Methods' for details), was used as readout to evaluate a possible neuroprotective effect of (4'-OH)-PVL in this *in vivo* system. To this end, C57BL/6 naïve mice were ICV microinjected with untreated AβOs, or AβOs preincubated for 15 min with (4'-OH)-PVL at monomeric Aβ42:PVL molar concentration ratios ranging from 1:1 to 1:10. As shown in Figure 30, AβOs caused a statistically significant memory impairment that was dose-dependently relieved by (4'-OH)-PVL. At the maximal concentration (10 μM), (4'-OH)-PVL preserved 'novel object recognition' capacity by up to 84% of the vehicle control value, without any significant detrimental effect on the NORT performance when injected alone.

Given the causal relationship between AβOs, glia and astrocyte activation[209], neuroinflammation and AD[210], we finally asked whether the above processes could also be modulated by (4'-OH)-PVL. To this end, C57BL/6 mice were separately microinjected with the vehicle, (4'-OH)-PVL (3 μM), preformed AβOs (1 μM) alone or preincubated for 15 min with 3 μM (4'-OH)-PVL - a submaximal PVL concentration that proved to be already quite effective in preventing AβO-induced memory deterioration. After 4 h, mice were sacrificed and hippocampal brain sections from animals belonging to the different treatment and control groups were immunostained with antibodies directed against the microglia/macrophage-specific protein Iba1 and the glia/astrocyte intermediate filament protein GFAP. The post-treatment 4 h time-point was chosen for neuroinflammation assessment because a significant AβO-mediated glial activation was previously observed at this particular time-point[209]. As shown in Figure 31, Iba1 and GFAP immunoreactivity significantly increased in AβOs-injected mice - compared to ones injected with vehicle or (4'-OH)-PVL - and both biomarkers were reduced in brain sections from mice injected with (4'-OH)-PVL-preincubated AβOs compared with untreated AβOs. The reduction in Iba1 immunoreactivity proved to be statistically significant (p-value=0.0236; Fig. 31A), whereas a visible but statistically non-significant trend toward a reduced immunoreactivity (p-value=0.1057) was observed in the case of the astrocyte activation biomarker GFAP (Fig. 31B). The anti-AβO and memory preservation effect of (4'-OH)-PVL may thus also rely on a positive modulation of AβO-induced neuroinflammation.

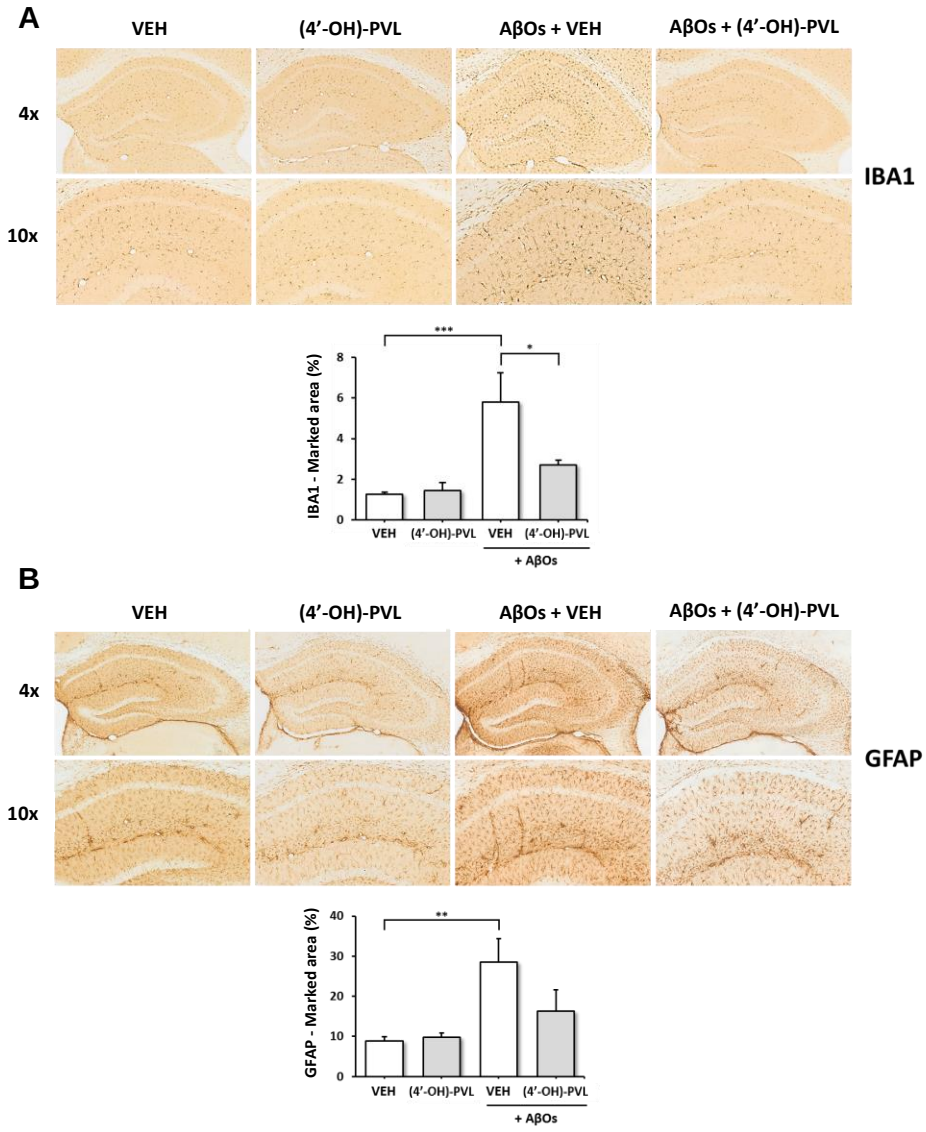

Figure 31. (4'-OH)-PVL treatment reduces glial activation in AβO-treated mice. A) Hippocampal slices from C57BL/6 mice microinjected with the DMSO vehicle (VEH, n=8), 3 μM (4'-OH)-PVL (n=8), preformed AβOs (1 μM monomeric $A\beta_{42}$) + VEH (n=9), or AβOs preincubated for 15 min with 3 μM (4'-OH)-PVL (n=9), were immuno-stained with an antibody against the microglia/macrophage-specific protein Iba1. Immunoreactivity quantitation data (mean ± standard error of mean) are reported in the histogram shown below the immuno-microscopy images (* $p<0.05$, *** $p<0.001$; Tukey's test). B) Same as (A) except for the use of an antibody directed against the glia/astrocyte intermediate filament protein GFAP for immunostaining (** $p<0.01$).

3. DISCUSSION (PART I)

Based on a cross-species exploration focused on β-amyloid oligomer-induced cytotoxicity, this thesis work documents the anti-AβO action of the PVL metabolites of flavan-3-ols, the major class of flavonoids in the human diet[158,167].

A cell-based assay built on a self-assembling, highly cytotoxic artificial polypeptide (β23)[197,198] was validated and used for the initial screening of PVLs. Due to its binary pattern of alternating polar and nonpolar residues (a structural feature also present in a number of natural human proteins[211]) this polypeptide has been shown to adopt a cross-β structure that leads to the formation of amyloid fibril aggregates *in vitro* and small-size prefibrillar oligomers when expressed in human HEK293 cells[197,198]. The observed immunoreactivity of cell lysates derived from β23-expressing yeast cells with the oligomer-specific antibody A11, but not with the fibril-specific dye Th-T, indicates that toxic oligomers rather than fibrils are the main, if not the only, proteotoxic species formed by β23 also in our yeast model system.

We found that multiple PVLs alleviate β23 toxicity in yeast and HEK293 cells at sub-nanomolar concentrations, with an efficacy (i.e., a dose-dependent rescue of cell viability) generally higher than that of previously known natural or synthetic anti-Aβ compounds (e.g., the flavan-3-ol metabolites EGCG, 3-HPP and 3-HBA[150,163]). The monohydroxylated metabolite (4'-OH)-PVL proved to be particularly effective in preventing β-amyloid oligomer toxicity in both β23-based cellular systems as well as in a secretory yeast model based on human $A\beta_{42}$. Importantly, in an acute mouse model of AβO-induced neurotoxicity[49], (4'-OH)-PVL relieved memory impairment and neuroinflammation, which are both considered as the earliest and most detrimental effects of AβOs, ultimately leading to synaptic loss and microgliosis[8,9,212]. The beneficial effects exerted by (4'-OH)-PVL in such different model systems suggest that PVLs directly interfere with β-amyloid oligomer formation or toxicity, although we cannot exclude additional indirect effects resulting from positive modulation of conserved (i.e., operating in both yeast and mammalian cells) anti-proteotoxic stress responses.

Compared to previously described β-amyloid toxicity assays in yeast[90,142], a distinguishing feature of the β23-based screening is the ability of β23 to cause severe cellular toxicity also when expressed outside of the ER-Golgi secretory system. *S. cerevisiae* unicellular nature cannot account for complex, systemic effects typical of AD pathogenesis and for specialized neuronal functions, but the yeast model system rather

serves as a reductionist tool to focus on the intracellular effects of AβOs for the initial molecule screening. While clearly distinct from secretory APP processing and extracellular release of the monomeric Aβ peptide as it occurs in Aβ-producing cells, this mode of expression mimics the deleterious effects associated with endocytosed or intracellularly released (e.g., via lysosomal/endosomal leakage) AβOs[9,213,214]. Furthermore, the oligomer-focused configuration of the β23 assay may explain the marked target specificity of PVLs compared to other more promiscuous compounds, as EGCG, 3-HPP and 3-HBA[150,163], which also inhibit fibrillogenesis of $A\beta_{42}$[59]. In fact, while devoid of any major effect on $A\beta_{42}$ fibril formation, (4'-OH)-PVL effectively relieved the toxicity of intracellularly produced β23 oligomers as well as the neurotoxic effects caused by preformed, exogenously administered AβOs in the mouse system.

Since prefibrillar oligomeric aggregates and fibers (and even more so amyloid plaques) have been increasingly viewed as opposite ends of the Aβ peptide toxicity range[9], selective action on AβOs (regardless of possible amino acid variations in the sequence of the Aβ peptide[87,215]) is currently considered a highly desirable feature of Aβ toxicity modifiers. Although we mainly focused on (4'-OH)-PVL, other PVLs (especially the sulfated metabolites #5 and #6; see Fig. 13) were nearly as effective in relieving β23 oligomer toxicity in cell-based assays, and preliminary evidence indicates a similar anti-AβO selective activity *in vitro* also for these phenyl-γ-valerolactones. However, since sulfated PVL metabolites were chemically synthesized in the form of ammonium salts, we were concerned about possible neurotoxic effects caused by the ammonium counterion and for this reason we did not test them in the AβO *in vivo* mouse system.

As revealed by AFM analysis (Fig. 27 and 29), (4'-OH)-PVL interfered with, although it did not abolish, AβO formation when added to *in vitro* oligomerization reactions. Importantly, it converted preformed AβOs into large-size non-toxic aggregates, with no evidence of oligomer disassembly. This remodelling effect, which has previously been observed with different polyphenol aglycones and shown to coincide with AβO detoxification[151,152,208], may underlie the memory preservation and anti-neuroinflammatory activity of (4'-OH)-PVL. Based on the AβO remodelling activity of chemically diverse polyphenol compounds, and the lack of such activity for the phenolic monomer resorcinol, a structure-activity relationship hypothesis has been proposed[152]. According to this hypothesis, the presence of two phenolic rings would appear to be minimally required for AβO remodelling. This seems at variance with the observed

remodelling activity of the small-sized (4'-OH)-PVL metabolite, which contains only one monohydroxy phenolic ring but fused to the γ-valerolactone moiety via a one-carbon bridge. Interestingly, the relative efficacy of the different PVLs observed in cell-based assays suggests that while the presence of two hydroxyl groups (as in metabolite #2) does not appear to confer a superior anti-proteotoxic activity, the presence of at least one hydroxyl group (preferably at position 4', as in metabolites #1 and #5) seems to correlate with a stronger efficacy. Still, the significant residual activity displayed by hydroxyl-lacking PVLs such as #4 and #7 points once again to the potentially important contribution of the γ-valerolactone unit.

Additional biological activities have been documented for PVLs[158], some of which may be relevant to their ability to relieve AβO-induced memory impairment and neuroinflammation. These include pro-neuritogenic[161], anti-inflammatory[216] and antioxidant activities[160]. These activities should be taken into account especially considering we resorted to an acute mouse model of AD that, although exhibiting a symptom (impaired memory) shared with conventional transgenic AD animal models, does not strictly reproduce AD pathogenesis, characterized by chronic neuronal deterioration and progressive decline in cognition. In 3xTg-AD mice, for example, cognitive impairment and microglia activation are exacerbated in a progressive and age-dependent manner[217,218], while in the non-Tg model a single AβO injection impairs memory consolidation within 24 hours[49] and rapidly activates glial cells and pro-inflammatory cytokine expression[209]. Furthermore, even if a mouse model incorporating all the features of the disease has not been developed yet, such young animals (18-week old) may lack possible co-actors of AD pathogenesis like capillary dysfunction. Thus, it is conceivable that the memory defect, which is transient and spontaneously disappears after 10 days, is determined by neuroinflammation rather than by a persistent neurodegenerative phenomenon[49,209]. With this in mind, the value of this model should not be identified in its utility for preclinical drug testing, but rather for studies aimed at dissecting mechanisms, where it can helpfully isolate some phenotypes from others.

The existence of a positive correlation between intake of flavanol-3-ol rich foods (especially cocoa[155,156]) and cognitive performance has also been documented[157,159]. Notably, an enhancement of dentate gyrus function and cognition, attributed to an improved brain microcirculation, has been reported in healthy 50-69 year-old subjects who consumed a high cocoa flavan-3-ol containing diet for three months[162]. This effect

may be relevant in the framework of treatments aimed at contrasting AβO-induced pathology, since a causal relationship between oligomeric $A\beta_{42}$ presence and capillary constriction has recently been hypothesised from observations both in human brain sections and in murine models[219].

An important issue not addressed in the present study regards the ability of the tested PVLs to cross the blood-brain barrier (BBB) and to accumulate in the brain at concentrations sufficient for target(s) engagement and anti-AβO action. We note, however, that different PVLs scored positive in an artificial BBB model system, in which 5-(3',4'-dihydroxyphenyl)-γ-valerolactone (#2) displayed the highest penetration capacity[161]. Although actual brain PVL levels are difficult to predict, the bioavailability and prevalence of PVLs as long-lasting flavan-3-ol metabolites (elimination half-life ~6 h) along with their sub-micromolar peak plasma concentrations (>500 nM)[165,167] suggest that potentially effective, cumulative brain PVL levels might be reached, at least in response to a flavan-3-ol rich diet. In keeping with this possibility, which is definitely worth of further investigation, plasma concentrations of 5-(3',4'-dihydroxyphenyl)-γ-valerolactone and other PVLs were found to positively correlate with memory performance in 3xTg-AD mice fed with a flavan-3-ol-enriched diet[169]. Also relevant, in this regard, is the validation of PVLs as urine biomarkers of the intake (and prospective AD-preventing/anti-neurodegenerative effects) of flavan-3-ols in ongoing epidemiological studies[158,166,167].

Since microbial enzymes are responsible of the initial ring fission reaction that gives rise to PVLs, the gut microbiota may play a key role in brain pathophysiology[220]. Increasing evidences suggest an antibacterial action of (-)-epicatechin-based PVL precursors[221] and it is possible that polyphenol compounds could modulate the composition of the microbiota by inhibiting some bacterial populations and stimulating others[222–224]. Then, future studies will also need to address the relationship between gut microbiota composition and PVL production - and so the crosstalk between the gut and the brain (the 'gut-brain axis') - as well as the potential nutraceutical use of synthetic PVLs as AD-preventive compounds.

4. MATHERIAL AND METHODS (PART I)

PVLs and other tested compounds

PVL metabolites #1, #2 and #3 (see Table 3 and Figure 13) were produced by asymmetric synthesis as described previously[225], while compounds #4, #5, #6 and #7 were synthesized by functionalization of the corresponding aglycones according to Brindani *et al.*[168]. CQ, EGCG, 3-HPP, 3-HBA, caffeic acid, ferulic acid, dihydrocaffeic acid and isoferulic acid were purchased from Sigma-Aldrich. Dihydroferulic acid, caffeic acid 3-O-glucuronide, caffeic acid 4-O-glucuronide, dihydrocaffeic acid 3-O-sulfate, dihydrocaffeic acid 3-O-glucuronide, ferulic acid-4-O-sulfate, isoferulic acid 3-O-glucuronide were purchased from Toronto Research Chemicals Inc.. Urolithin A, urolithin B, and urolithin B-glucuronide were kindly provided by Dr. Olivier Dangles (INRA, Avignon; France), while urolithin C and urolithin D were purchased from Dalton Pharma Services. All tested compounds were dissolved in DMSO as either 10 or 20 mM stock solutions.

Yeast strains expressing the human $A\beta_{42}$ peptide

A previously constructed pET28-based plasmid expressing human $A\beta_{42}$ fused to *E. coli* thioredoxin (Trx)[226] was utilized as template for the PCR-assisted construction of yeast vectors expressing the unfused human $A\beta_{42}$ peptide or the $A\beta_{42}$-Trx fusion polypeptide, using, respectively, the oligonucleotide pairs #A-#B and #C-#D as amplification primers (see Table 7). The resulting amplicons were cloned into the *Hind*III-*Xba*I restriction sites of the pYES2 vector (Thermo Fisher Scientific) to produce the pYES2-$A\beta_{42}$ and pYES2-$A\beta_{42}$-Trx plasmids. A pYES2-based plasmid only containing the Trx coding-sequence (PCR-amplified from pET28-$A\beta_{42}$-Trx using oligonucleotides #C and #D as primers) was also constructed and used as a control.

To produce the EGFP-$A\beta_{42}$ fusion protein, a variant EGFP sequence lacking a terminal stop-codon and containing an extra-sequence coding for a four-amino acids spacer to be interposed between the C-terminus of EGFP and the N-terminus of $A\beta_{42}$, was PCR-amplified using plasmid pYX212-EGFP as template[227] and oligonucleotides #E and #F as primers (Table 7). The resulting amplicon was then cloned into the *Hind*III restriction site of pYES2-$A\beta_{42}$ to generate plasmid pYES2-EGFP-$A\beta_{42}$.

Overlap extension PCR[228] was used to produce an additional $A\beta_{42}$ fusion derivative, in which the human $A\beta_{42}$ peptide is preceded by the ER-targeting signal peptide Kar2

(Table 8). To this end, the Kar2-coding sequence of the gene coding for the ER chaperone Kar2 was first retrieved by PCR using genomic DNA from the BY4742 strain (Dharmacon) as template and the oligonucleotide pair #G-#H (Table 7) as amplification primers. The sequence coding for the human $A\beta_{42}$ peptide was amplified from the pYES2-$A\beta_{42}$ plasmid using a pair of oligonucleotide primers (#I and #L in Table 7), one of which (#I) bears a 3'-end complementary to 3'-end of the #H primer previously employed for Kar2 amplification. The Kar2 and $A\beta_{42}$ coding amplicons were then mixed and after annealing of the complementary ends corresponding to oligonucleotides #I and #H and addition of the far-end primers (#G and #L), a third amplification reaction was performed to generate the Kar2-$A\beta_{42}$ fusion product. The latter amplicon was then cloned into the *Hind*III-*Xba*I sites of the pYES2 vector to generate plasmid pYES2-Kar2-$A\beta_{42}$.

Yeast codon-optimized sequences coding for the human $A\beta_{42}$ peptide and its aggregation-prone, E22G 'arctic' variant, N-terminally fused to the c-myc tag sequence, were produced by gene synthesis (Eurofins Genomics) and cloned into the *Hind*III-*Xba*I restriction sites of the pYES2 vector.

The above plasmids, except for pYES2-Kar2-$A\beta_{42}$, were individually transferred into the wild-type yeast strain BY4742 (See Table 9) and transformants were selected on synthetic defined dextrose (SD) medium containing 2% (w/v) glucose plus histidine, leucine and lysine, but lacking uracil. The pYES2-Kar2-$A\beta_{42}$ plasmid was transformed into the wild-type *S. cerevisiae* strain W303α and transformants were similarly selected on SD medium lacking uracil.

Yeast strains expressing the β23 polypeptide

A yeast codon-optimized β23 coding sequence (see Table 8[198]) was produced by gene synthesis (Eurofins Genomics) and inserted into the *Hind*III-*Xba*I restriction sites of the multicopy yeast expression vector pYES2 (*URA3* selectable marker) under the control of a galactose-inducible (*GAL1*) promoter. After sequence verification, the resulting construct was transformed into the wild-type *S. cerevisiae* strain W303α (ATCC, see Table 9) using a standard, lithium acetate-based transformation protocol[229]. Yeast transformants were selected under non-inducing conditions on SD medium containing 2% (w/v) glucose plus histidine, leucine, adenine and tryptophan, but without uracil. The same yeast strain transformed with the empty pYES2 vector served as a control.

For integrative transformant construction, a β23 expression cassette (β23 coding sequence under the control of the *GAL1* promoter and the *CYC1* terminator) was

generated by PCR-amplification using the pYES2-β23 plasmid as template and oligonucleotides #M and #N as primers (see Table 7). The resulting β23 expression cassette was then inserted into the *Sma*I restriction site of the integration vector pFL26 (ATCC; *LEU2* selectable marker). Following sequence verification, the one-copy β23 cassette was integrated into the *leu2* locus of the *pdr1Δpdr3Δ*, low-efflux mutant strain (W303α genetic background; kindly provided by the laboratory of Susan Lindquist[230]; see Table 9) and the resulting 1X β23 transformants were selected on SD medium lacking leucine. The β23 expression cassette was separately cloned into the *Not*I-*Sal*I restriction sites of the pMW#2 vector (Addgene; *HIS3* selectable marker) and integrated into the *his3* locus of the previously generated one-copy β23 integrative transformant. Two-copy (2X) β23 transformants were thus generated and selected on SD medium lacking leucine and histidine. Integrative yeast transformants harbouring the pFL26 and pMW#2 empty vectors were also produced and used as control strains.

Table 7. Oligonucleotides used for the cloning strategy.

Primer name	Primer sequence[a]
#A	FW: 5'-TAAATATAAAAAGCTTGCCACCATGGATGCAGAATTCCGACATGAC-3'
#B	RE: 5'-AATTATTTTATCTAGATTACGCTATGACAACACCGCCCACC-3'
#C	FW: 5'-TAAATATAAAAAGCTTGCCACCATGAGCGATAAAATTATTCACCTGAC-3'
#D	RE: 5'-AATTATTTTATCTAGATTACGCCAGGTTAGCGTCGAGGAACTC-3'
#E	FW: TAAATATAAAAAGCTTGCCACCATGAGTAAAGGAGAAGAACTTTTC-3'
#F	RE: 5'-AATTATTTTAAAGCTTTTTGTATAGTTCATCCATGCCATG-3'
#G	FW: 5'-TAAATATAAAAAGCTTGCTAGCGCCACCATGTTTTTCAACAGACTAAGCGCTG-3'
#H	RE: 5'-ATCCAGAGTCATGTCTAAACTCAGCATCACCTCTAACTAAAACATTGGAGGAG-3'
#I	FW: 5'-TTCCACTCCTCCAATGTTTTAGTTAGAGGTGATGCTGAGTTTAGACATGACTC-3'
#L	RE: 5'-ATTTTATTAATCTAGATTATCAGGCAATGACCAC-3'
#M	FW: 5'-GATGATCCACTAGTACGGATTAGAAG-3'
#N	RE: 5'-ATAAATAGGGACCTAGACTTCAGGTTG-3'
#O	FW: 5'-TGCCGGCTCTGCCGGCTCCGATGCAGAATTCCGACATGACTC-3'
#P	RE: 5'-AATTATTTTAGGATCCTCACGCTATGACAACACCGCCCAC-3'
#Q	FW: 5'-TAAATATAAAAAGCTTCCGGCTCCGCCGGCTCCGCTGCCGGCTCTGCCGGCTCC-3'

[a]FW, forward primer; RE, reverse primer.

Table 8. Nucleotide sequences of the Kar2-Aβ$_{42}$ and β23 coding regions.

Gene name	Nucleotide sequence[a]
Kar2-Aβ$_{42}$	**ATGTTTTTCAACAGACTAAGCGCTGGCAAGCTGCTGGTACCACTCTCCG TGGTCCTGTACGCCCTTTTCGTGGTAATATTACCTTTACAGAATTCTTTC CACTCCTCCAATGTTTTAGTTAGAGGT**GATGCTGAGTTTAGACATGACTC TGGATACGAAGTTCATCATCAAAAGCTGGTCTTTTTCGCCGAAGATGTCG GTTCCAATAAGGGAGCTATCATCGGTCTGATGGTGGGAGGAGTGGTCAT TGCCTGATAA
β23	ATGGAGCAAAAACTGATCTCCGAGGAGGATTTGGGAATGCAGATCTCCA TGGACTACAACATCCAGTTTCATAACAATGGAAACGAGATTCAGTTCGAG ATTGACGATTCCGGAGGTGATATCGAGATTGAAATCAGAGGTCCAGGAG GTAGAGTGCATATCCAACTGAATGACGGACATGGACATATCAAAGTGGA CTTCAACAATGACGGTGGAGAACTGCAGATCGACATGCATTGATAA

[a]The sequence encoding the ER-targeting signal peptide derived from the *KAR2* gene is shown in *bold italics*. The sequence coding for the c-myc tag is *underlined*.

Table 9. *S. cerevisiae* background strains used in this work.

Strain	Genotype
BY4742	*MATα his3Δ1 leu2Δ0 lys2Δ0 ura3Δ0*
W303α	*MATα can1-100, his3-11,15, leu2-3,112, ade2-1, trp1-1, ura3-1*
pdr1Δpdr3Δ W303α	*MATα can1-100, his3-11,15, leu2.3,112, ade 2-1, TRP1, Gal vector, URA3, Gal vector, pdr1::KAN, pdr3::KAN*

β23 cytotoxicity assays in yeast

For growth curve analysis, yeast cells were cultured at 30°C in SD medium for 24 h, washed, transferred to 96-well plates and diluted to an OD_{600} of 0.1 with 'inducing' selective minimal medium [2% galactose plus a non-repressing glucose concentration (0.005% w/v)]; cells diluted with 'non-inducing' (2% glucose) SD medium served as controls. Cell growth was monitored for three days by OD_{600} measurements performed with a TriStar² LB 942 Microplate Reader (Berthold Technologies). Growth curves were determined in triplicate for each condition and analysed with the GraphPad Prism software.

The two-copy β23 integrative transformant utilized as test strain for compound screening was similarly cultured overnight under non-inducing conditions, followed by washing and

dilution to an OD_{600} of 0.1 with 'inducing' selective minimal medium as above. Aliquots of cells (198 µl each) were then dispensed into 96-well plates and 2 µl of each compound (from a 100X stock solution in DMSO) or DMSO only ('vehicle') were added and assayed in triplicate upon incubation at 30°C for 48 h without agitation, followed by OD_{600} determination as above. The anti-β23 toxicity effect exerted by individual compounds is expressed as percentage of cell viability relative to the 'vehicle' control (arbitrarily set to 0%). EC_{50} values, i.e., compound concentrations causing a 50% maximal protective effect, were extrapolated from dose-response curves (determined in triplicate for each compound) using GraphPad Prism.

For serial dilution 'spot' assays performed on solid media, yeast pre-cultures were washed, adjusted to an OD_{600} value of 1.0 and serially diluted in ten-fold increments, prior to spotting (4 µl aliquots for each dilution) onto glucose- or galactose-containing, selective minimal medium agar plates. Yeast growth was examined by visual inspection (and photographically recorded) after incubation at 30°C for two days.

Identical liquid-medium assay conditions were applied to the Kar2-$Aβ_{42}$ transformant and to yeast transformants expressing other $Aβ_{42}$ derivatives, including the aggregation-prone 'arctic' variant of $Aβ_{42}$, or α-synuclein.

Immuno-dot blot analysis of β23-expressing yeast cells

Cell extracts for immuno-dot blot analysis were prepared by inoculating a pre-culture of the two-copy β23 strain into 'inducing' (2% galactose) selective synthetic medium at an OD_{600} of 0.3, followed by an 8 h at 30°C. Cells were harvested by centrifugation, resuspended in ice-cold lysis buffer (25 mM Tris-HCl pH 7.5, 50 mM KCl, 1 mM $MgCl_2$, 1 mM EDTA, 1% Triton X-100, 10% glycerol, plus protease inhibitors) supplemented with an equal volume of glass beads (0.5 mm diameter), and lysed by five rounds of vigorous vortexing (1 minute stroke followed by 1 minute incubation on ice) with a Mini-Beadbeater-16 (Bio Spec Products Inc.). The resulting lysates were clarified by centrifugation (10000 rpm, 30 minutes at 4°C) and the total protein concentration of supernatant fractions was determined with the Bradford reagent (Bio-Rad).

Aliquots of the above supernatants (10 µg total protein each in a final volume of 100 µl) were used for immuno-dot blot analysis. This was performed in a 96-well plate format using a Bio-Dot® microfiltration apparatus (Bio-Rad) for vacuum-transfer of the samples to nitrocellulose membranes (0.2 µm pore-size; Bio-Rad) pre-wetted with Tris-buffered saline (TBS; 20 mM Tris-HCl pH 7.5, 0.8% NaCl). Sample-loaded membranes were then

blocked by incubation for 2 hours at room temperature in TTBS buffer (TBS supplemented with 0.1% Tween 20) containing 5% (w/v) BSA and 1% (w/v) fish skin gelatin. After blocking, replica stripes of the same membranes were incubated overnight at 4°C with the anti-amyloid oligomer antibody A11 (Thermo Fisher Scientific; 1:1000 dilution) and with an anti-Pgk1 antibody (Abcam; 1:2000 dilution) as housekeeping/loading control. Following washing with TTBS, membranes were incubated for 2 h at room temperature with IRDye-labled goat anti-rabbit (for A11) or goat anti-mouse (for anti-Pgk1) secondary antibodies (LI-COR Biosciences; 1:10000 dilution), washed once more with TTBS, dried, and visualized with an Odyssey® fluorescence infrared imaging system (LI-COR Biosciences).

Proteotoxicity assays in mammalian cells

For $A\beta_{42}$ expression in HEK293 cells, a construct coding for an EGFP-$A\beta_{42}$ fusion protein was generated by a two-step PCR strategy that also allowed to introduce a 12-amino acids spacer between the two polypeptides. The sequence coding for human $A\beta_{42}$ was first amplified using the $A\beta_{42}$-Trx plasmid as template and the #O-#P oligonucleotides (see Table 7) as primers. After clean-up of the reaction mixture, the resulting $A\beta_{42}$ amplicon was used as template for a second PCR with the #Q-#P oligonucleotides (Table 7) as primers. The product of this second amplification was then cloned into the *Hind*III/*Bam*HI restriction sites of the pEGFP-C1 (Addgene) vector in-frame with the EGFP coding sequence, under the control of the human cytomegalovirus (CMV) immediate early promoter.

Human codon-optimized sequences coding for the E22G 'arctic' variant of the $A\beta_{42}$ peptide and for the β23 polypeptide–were produced by gene synthesis (Eurofins Genomics) and cloned into the pEGFP-C1 vector, pre-digested with *Nhe*I and *Xba*I in order to remove the EGFP coding sequence.

Human embryo kidney 293T (HEK293; ATCC) cells were cultured in Dulbecco's modified essential medium (DMEM) containing 10% foetal bovine serum (FBS), 2 mM L-glutamine (Gibco, Thermo Fisher Scientific), 50 IU/ml penicillin (Gibco), 50 µg/ml streptomycin (Sigma-Aldrich) and 2.5 µg/ml amphotericin B (Gibco) and were incubated at 37°C/5% CO_2 in a humidified incubator. Confluent cells in 48-well plates were transiently transfected with the above pC1 plasmids, expressing the EGFP-$A\beta_{42}$ fusion protein, the arctic variant of $A\beta_{42}$ and the β23 polypeptide, using a polyethylenimine (PEI)-based transfection reagent (Polysciences) as per manufacturer's instructions.

Cell viability was measured 72 h after transfection with the MTT assay. Reduction of MTT by viable cells and formation of the purple-coloured formazan product was determined by measuring absorbance at 540 nm (using absorbance at 690 nm as reference). Three biological replicates (each comprising eight technical replicates/compound plus controls) were performed for each compound. EC_{50} values (i.e., compound concentrations causing 50% maximum protection) were determined as described above for yeast proteotoxicity assays.

In vitro Aβ$_{42}$ oligomer and fibril formation

A depsipeptide derivative of the human Aβ$_{42}$ peptide (#RP10017 from GenScript; or in-house synthesized[231]) was used to prepare seed-free solutions of monomeric Aβ$_{42}$ as described previously[49,232]. Briefly, the depsipeptide was dissolved in 0.02% trifluoroacetic acid (TFA) at a 1 mg/ml concentration, and following extensive ultracentrifugation (100,000 x *g* for 7 h at 4°C), the monomeric depsi-Aβ$_{42}$ peptide contained in the supernatant was quantified with the Qubit Protein Assay (Thermo Fisher Scientific). Following Aβ$_{42}$ release by addition of 3 mM NaOH, the resulting Aβ$_{42}$ peptide solution (200 µM) was diluted with PBS to a final concentration of 100 µM and immediately used for AβO or fibril formation. AβOs for pre- and post-assembly assays and for ICV brain injection, were produced by incubating the above Aβ$_{42}$ monomer solution for 24 hours at 4°C. To test for the effect of (4'-OH)-PVL on AβO formation, (4'-OH)-PVL or the DMSO vehicle were added to the above Aβ$_{42}$ solution (100 µM) immediately after dilution with PBS. For post-assembly assays, AβOs preformed as described above were diluted 10-fold with PBS, supplemented with either (4'-OH)-PVL or the DMSO vehicle, and incubated at 22°C for three hours prior to AFM analysis. A similar experimental set-up was employed for immuno-dot blot analysis of the effect of (4'-OH)-PVL on preformed AβOs. This was performed using 6E10 (BioLegend; 1:2000 dilution) and A11 (1:1000 dilution) as reference and test (i.e., AβO-specific) primary antibodies, respectively, followed by secondary antibody incubation and visualization as described above for the immune-dot blot assays performed on yeast cell extracts. For fibril formation, the Aβ$_{42}$ monomer solution was incubated for 4 days at 37°C under acidic conditions (pH 5.0) in presence of (4'-OH)-PVL or the DMSO vehicle. Before ICV brain injection, all AβO preparations were checked by AFM and SEC as described previously[49,232].

Atomic Force Microscopy

Multimode AFM analysis was performed with a NanoScope V microscope (Bruker) operated in tapping mode using 0.01–0.025 Ohm–cm Antimony (n) doped Si probes (thickness range, 3.75 µm; length, 125 µm; width, 35 µm; spring constant, 40 N/m) and a scan rate proportional to the scanned area (0.5–0.9 Hz), as described previously[232]. Freshly cleaved muscovite mica discs (Agar Scientific) were used for sample deposition. Twenty microliters of AβOs or fibrils were added to freshly cleaved mica at room temperature, after 10 min the samples were washed with MilliQ water and dried under a gentle stream of nitrogen. AFM images were analysed for diameter and length with the Scanning Probe Image Processor (SPIP data analysis package 5.1.6 v.; Image Metrology). Untreated freshly cleaved mica and freshly cleaved, buffer-soaked mica were used as controls. Topographic patterns and SPIP characterization were confirmed by independent measurements performed on a minimum of 4 different, spatially separated areas.

Thioflavin-T kinetic assay

Recombinant $A\beta_{42}$ peptide was expressed in *E. coli* BL21 Gold (DE3) strain (Stratagene) and purified as described previously[233]. After dissolving lyophilized peptide in 6M GuHCl, pre-formed aggregates and salt were removed using a Superdex 75 10/30 GL column (GE Healtcare) at a flow rate of 0.5 ml/min and the peptide was eluted in 20 mM sodium phosphate buffer (pH 8) supplemented with 200 µM EDTA and 0.02% NaN_3. The concentration was calculated from the absorbance at 280 nm using extinction coefficient ε_{280} = 1,490 $L \cdot mol^{-1} \cdot cm^{-1}$. The working solution for kinetic experiments was prepared diluting monomeric $A\beta_{42}$ to 2 µM concentration and adding 20 µM Th-T from a 20 mM stock solution. Compounds (or DMSO vehicle) were added from 100X stock solutions to a final volume of 250 µl. Only-buffer controls were prepared to exclude any effect of the vehicle on $A\beta_{42}$ aggregation. All samples were prepared in low-binding Eppendorf tubes on ice using careful pipetting to avoid introduction of air bubbles. 80 µl per well for each sample ware then pipetted in triplicate into 96-well black half-area, low-binding, clear-bottomed PEG coating plates (Corning). Assays were performed at 37°C without agitation in a Fluostar Omega microplate reader (BMGLabtech). Th-T fluorescence was measured through the bottom of the plate with a 440-nm excitation filter and a 480-nm emission for 12 h.

Animals

Eight-weeks-old C57BL6/N male mice (Charles River Laboratories) were used for *in vivo* studies. Mice were all drug and behavioural test naïve and experiments were conducted during the light cycle. Prior to brain surgery, animals were housed in a SPF facility in groups of four in standard mouse cages containing sawdust plus food (2018S Harlan diet) and water *ad libitum*, under conventional laboratory conditions (20±2°C; 60% humidity) with a 12/12 hour light/dark cycle (7:00 am – 7:00 pm). The IRFMN (Istituto di Ricerche Farmacologiche Mario Negri) adheres to the principles set out in the following laws, regulations, and policies governing the Care and Use of Laboratory Animals: Italian Government Law (D. lgs 26/2014; Authorization n.19/2008-A issued by the Ministry of Health on March 6, 2008); Mario Negri Institutional Regulations and Policies providing internal authorization for persons conducting animal experiments (Quality Management System Certificate – UNI EN ISO 9001:2015 – Reg. N° 6121); the NIH Guide for Care and Use of Laboratory Animals (2011 edition) and EU directives and guidelines (EEC Council Directive 2010/63/UE). The statement of Compliance (Assurance) with the Public Health Service (PHS) Policy on Human Care and Use of Laboratory Animals has been reviewed (9/9/2014) and will expire on September 30, 2019 (Animal Welfare Assurance #A5023-01).

Behavioural and glial-histochemical analyses on AβO-injected mice

For ICV brain microinfusion of AβOs, a 7-mm long, stainless steel guide cannula was implanted by a stereotaxic surgery apparatus (model 900, David Kopf Instruments) into the cerebral lateral ventricle (L ± 1.0; DV-3.0 from dura) of forane (IsoFlo®, Zoetis)-anesthetized mice. Recognition memory was measured on mice injected with AβOs alone, AβOs supplemented (and preincubated for 15 min) with different concentrations of (4'-OH)-PVL or the DMSO vehicle, and on mock-injected (PBS+DMSO) control animals using an open-square grey arena (40 x 40 cm; 30 cm high) and different objects as described previously[49]. The familiarization phase of the novel object recognition task (NORT) was started 2 h after AβO injection and was followed 24 h later by the 'test phase', both conducted according to a previously described protocol[49]. Memory performance was expressed as discrimination index, i.e., (seconds spent on novel object – seconds spent on familiar object)/(total time spent on both objects). At the end of the experiments, mice were sacrificed and the correct placement of the cannula into the lateral ventricle was verified histologically.

For neuro-histochemical analysis, brain slices from AβO-injected mice were incubated with 1% H_2O_2 for 10 min followed by a 1 h incubation at 4°C in blocking solution (3% normal goat serum plus 0.3% or 0.4% Triton X-100 for GFAP and Iba1, respectively) as described previously[234]. Brain sections were then incubated overnight with anti-GFAP (Merck Millipore; 1:3500 dilution) and anti-Iba1 (FUJIFILM Wako Pure Chemical Corporation; 1:500 dilution) primary antibodies. Following incubation with the appropriate biotinylated secondary antibodies (Vector Laboratories; 1:200 dilution), immunostaining was developed and visualized using an avidin/biotin blocking kit (Vector Laboratories) and diaminobenzidine as chromogen. Diaminobenzidine tissue analysis and image acquisition were performed with an Olympus image analyser (VS-ASW 2.8 v.; Olympus). Quantitative analysis was conducted with the use of an operator-blind-to-treatment, Fiji software, with normalization on the quantified area.

Quantification and statistical analysis

Statistical significance of the differences measured in cell-based toxicity assays conducted on the different test compounds was evaluated by ANOVA.

NORT and histological data were analysed using a one-way between-subjects ANOVA; Student's t-test was used for comparisons of only two groups, whereas the Tukey's posthoc test was used for multiple comparisons. The numbers of animals (n) utilized for each experiment/condition are specified in the corresponding figure legends. No specific method was employed for mice randomization being mice simply C57BL/6 naïve of very similar ages (7/8 weeks).

Statistical analysis was performed with the GraphPad Prism v6.0. For all analyses significance was defined as $* p < 0.05$, $** p < 0.01$, $*** p < 0.001$.

PART II

Use of yeast model systems to study amyloid neurodegenerative pathologies

1. INTRODUCTION TO PART II

Advances in genetics and the identification of disease-linked mutations have been the breakthrough for the creation of animal and cellular models for several human diseases, including NDs[8,235–238]. Among cellular models, *Saccharomyces cerevisiae* can count on an extensive characterization from the genetic and functional point of view and on high feasibility of manipulation[239]. Despite the obvious limitations in terms of specialized neuronal functions, the reduced complexity of this unicellular organism, coupled the high conservation in eukaryotic evolution of the cellular pathways implicated in NDs[239], represents a convenient feature that prompted scientists to use it to dissect fundamental disease-associated mechanisms.

The yeast expression of the amyloidogenic (poly)peptides causally related to NDs recapitulates central aspects of protein pathobiology, including aggregation and toxic phenotype, and when the protein of interest can be fused with a fluorescent partner - like the EGFP - without affecting its amyloidogenicity, aggregate formation and their subcellular distribution can be easily tracked[105,108,122]. The yeast model for PD, based on the overexpression of α-syn, manages to reproduce the dose-dependent toxicity shown in humans, in which duplications or triplications of α-syn locus are related to early onset in familial PD. In the yeast model, overexpression confers higher aggregation propensity to α-syn, that switches from being associated with lipid membranes to forming cytoplasmic inclusions[108]. Similarly, intracellular tight inclusions (*foci*) of Htt can be observed in the HD yeast model based on the expression of Htt fragments bearing a polyQ longer than 25Q. Indeed, 25Q corresponds to the normal, non-pathogenic polyQ length, while Htt expression with 72Q or 103Q expansions grant a proportional tendency to form detrimental aggregates[122]. Mirroring what happens in human cells, where TDP-43 localizes into the nucleus in normal conditions, while it accumulates in the cytoplasm of ALS-affected neurons, in yeast this protein aberrantly forms toxic cytoplasmic aggregates when overexpressed[105].

On the other side, even if researchers were able to develop AD yeast models reproducing Aβ aggregation[91,130,132], $A\beta_{42}$ expression in yeast fails to cause a strong impairment of cellular viability[117,130], both when expressed as a free peptide or fused to protein scaffolds like Trx or EGFP[117,130] (Fig. 15A). Moreover, $A\beta_{42}$-EGFP fusion abolishes EGFP fluorescence[130]. A slight toxicity increment can be obtained addressing $A\beta_{42}$ to the secretory pathway (Kar2-$A\beta_{42}$), mimicking APP metabolism and Aβ endocytic

reuptake occurring in neuronal cells[120] (Fig. 15B). As described in Part I of this PhD thesis, the overexpression of the artificial polypeptide β23[198] proved to be a valid alternative to generate amyloid-like toxic aggregates in yeast.

Nevertheless, the simplicity of a unicellular organism as *S. cerevisiae* could raise questions about its ability to discriminate between proteotoxic stresses induced by different (poly)peptides that form amyloid aggregates with similar ultrastructural features. The discovery of novel susceptibility factors and therapeutic targets for ND using *S. cerevisiae* models[10], in addition to our results (see Part I of this PhD thesis, in particular Figs. 18, 20, 21) showing that polyphenol metabolites have a specific action on different yeast models, seems to suggest a certain degree of strain-specificity. Therefore, we decided to analyse whole-transcriptome changes in four humanized yeast models to identify differential molecular pathways associated with amyloid-induced toxicity. For this analysis, we used the four *S. cerevisiae* models schematically represented in Figure 32:

i) ALS model, based on the expression of the sequence encoding TDP-43[105] fused to EGFP, in which one copy of the gene was integrated in the yeast genome;
ii) HD model, based on the expression of the sequence encoding the exon 1 of the Htt protein, harbouring a 72-long polyQ expansion (Htt72Q)[240] and fused to the cyan fluorescent protein (CFP);
iii) PD model, based on the expression of the sequence encoding α-syn[108] fused to EGFP, in which two copies of this gene were integrated in the yeast genome;
iv) the so-called AD-like model, based on the integration in the yeast genome of two copies of the sequence encoding for the artificial peptide β23, developed in our laboratory and described in Part I of this PhD thesis.

We decided to analyse and compare not only the transcriptional responses induced by different amyloid proteins, but also the transcriptomic response at different time points, in order to identify transcriptional changes associated with different stages of amyloid structure formation. We resorted to RNA-sequencing (RNA-seq), an advanced method for transcriptomic profiling that provides a quantitative measurement of the frequency of cellular transcripts with relative high accuracy. Although some pathways, like the unfolded protein response (UPR), were modulated in all four yeast models of NDs, enrichment analysis of RNA-seq data, supported by pilot validating experiments, showed a rapid and distinct transcriptomic response associated with the expression of different amyloidogenic (poly)peptides. Defects in mitochondrial functionality, which have already

been repeatedly linked to neurodegeneration, emerged both in AD-like and PD models, but with different trends of modulation and outcomes. We detected extreme alterations of the cell cycle in the AD-like model, and preliminary observations pointed to a potentially deleterious role in the amyloid context for intrinsically disordered proteins (IDPs) involved in the regulation of the cell cycle progression. Transcriptional changes identified in the present work confirmed how *S. cerevisiae* can be greatly informative in the identification of specific mechanisms of neurotoxicity[241]. Since about one third of yeast genes has a human orthologue[242], these models could help untangle the complex interplay between pathological consequences of proteotoxic stress and protective mechanisms and the relative importance of different pathways in the multifactorial contest of neurodegeneration[243].

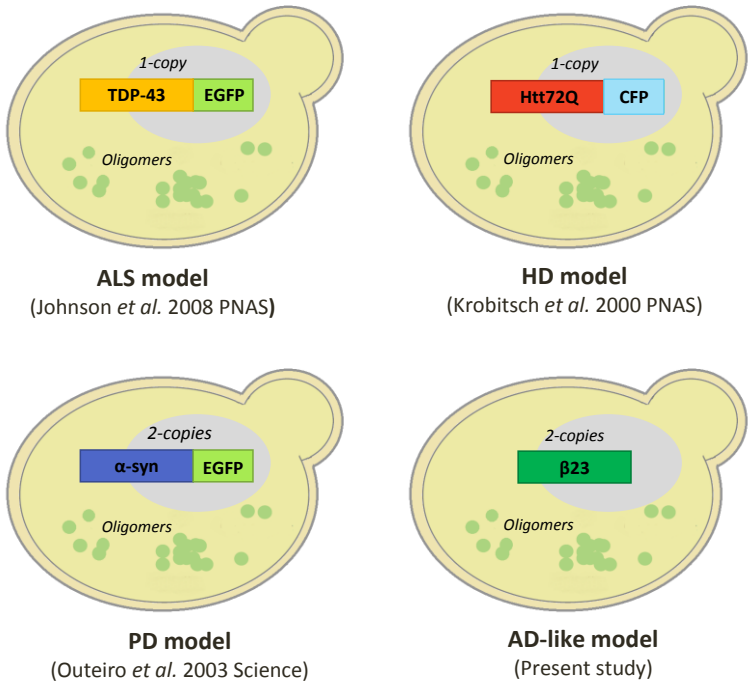

Figure 32. Yeast models for NDs. The inducible expression of different amyloidogenic (poly)peptides leads to the production of toxic oligomers in yeast cells (modified from[89]).

2. RESULTS (PART II)

2.1 Different toxicity profiles were observed in yeast models of NDs

In this study, different yeast models of NDs were used for a comparative analysis of the transcriptional changes occurring following the expression of four different amyloidogenic (poly)peptides. Models for ALS, HD and PD are based on the heterologous expression of the human proteins underlying neurotoxicity[105,108,240], while, in order to study the molecular events associated with amyloid toxicity in AD, we resorted to a newly developed model ('AD-like') based on the expression of the artificial polypeptide β23, which was designed to form amyloid structures[197] and can cause severe toxicity in yeast cells (see Fig. 16). In all four models, the expression of the amyloidogenic (poly)peptides is under the control of a galactose-inducible promoter (*GAL1* promoter) which allows a tight repression of the expression of these proteins in non-inducing conditions (glucose-containing medium).

As previously observed[105,108,120,122,123,130], after switching to galactose-containing medium (inducing conditions), the expression of amyloidogenic (poly)peptides causes a reduction of cellular growth to different extents depending on the yeast model. Serial dilution assay (Fig. 33A) and growth in liquid medium conditions (Fig. 33B) showed a direct correlation between protein toxicity and its expression level and/or properties.

Indeed, in the case of ALS model, in which one copy of the sequence encoding TDP-43 has been integrated in the yeast genome, only a slight reduction in cellular viability was detected, whereas an extreme reduction of yeast viability was observed in the AD-like and the PD models, both based on the integration of two gene copies in the yeast genome. HD model showed a medium-sensitive phenotype that depends on the length of Htt polyQ stretch (72Q)[244].

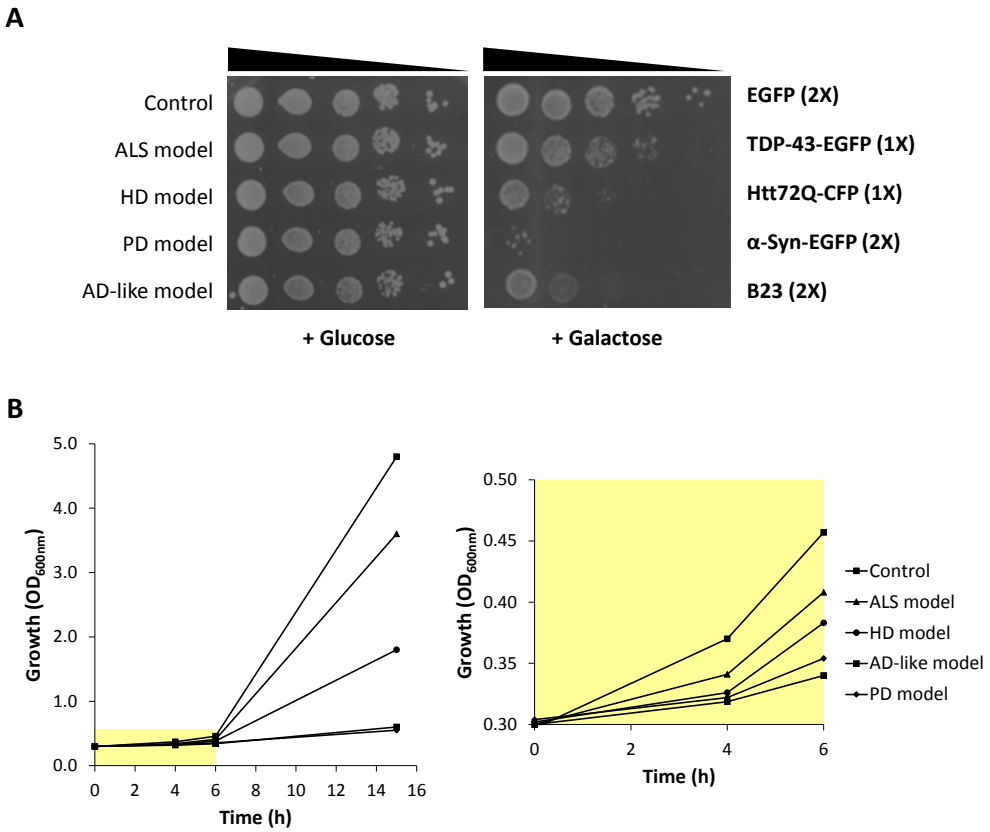

Figure 33. Toxicity induced by amyloidogenic (poly)peptide expression in yeast. A) Serial dilution assays (10-fold input cell dilutions ranging from 10^1 to 10^4) were performed on yeast cells (W303 strain) harbouring one (1X) or two (2X) coding sequences for TDP-43-EGFP, Htt72Q-CFP, α-syn-EGFP or β23 integrated in the genome. Yeast strain expressing EGFP served as control. Cells were spotted on glucose- or galactose-containing agar plates and growth was assessed after 2 days at 30°C. B) Growth curves in liquid medium under inducing (+ galactose) conditions of the yeast models described in A) were collected using OD_{600} (optical density at 600 nm) values. A zoom-in over the 0-6 h period (yellow box) is show in the right panel to highlight differences occurring at early time points.

Growth inhibition was accompanied by the formation of intracellular aggregates that were monitored using fluorescence microscopy in the case of ALS, PD and HD models, since in these strains amyloidogenic proteins are fused to fluorescent proteins (EGFP, for ALS and PD models; CFP, for HD model). As showed in Figure 34, after 4 hours of induction, the toxic proteins are expressed, but the aggregation process is still at preliminary phases. After 15 hours of induction, cytoplasmic aggregates, visible as intracellular fluorescent *foci*, are instead completely formed in amyloidogenic protein-expressing strains. Control strain expressing EGFP was used as reference strain in these experiments.

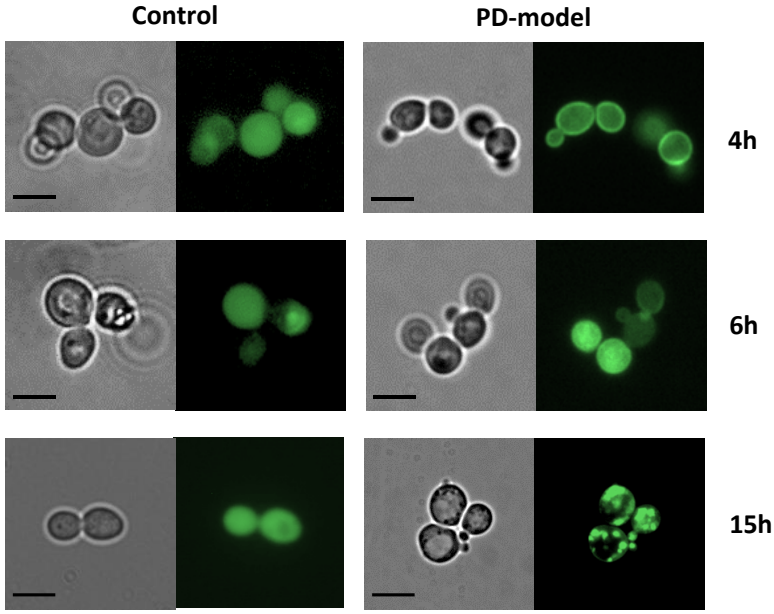

Figure 34. Time-dependent formation of intracellular proteotoxic aggregates. Phase contrast (left-side) and fluorescence (right-side; GFP-filter) microscopy analysis were conducted on a Zeiss Axio Imager.Z2 fluorescence microscope in EGFP-expressing cells ('control' strain; left) and α-syn-expressing cells ('PD model; right) after 4, 6 and 15 hours of induction in galactose-containing medium. Initially associated with membranes (4 hours), α-syn then assume a cytoplasmic localization (6 hours) that prelude to protein aggregation (15 hours). Scale bar: 5 μm.

Microscopy analysis could not be performed for the AD-like model, since the fusion of β23 coding sequence to EGFP leads, on one side, to a drastic reduction of the toxicity observed for the free peptide (Fig. 35), and, on the other side, to the loss of EFGP fluorescence (data not shown), as it happens for the human $A\beta_{42}$ peptide[130] (Fig. 15A). Therefore, the formation of amyloid cytotoxic aggregates in the AD-like model was verified by immune-dot blot analysis with the amyloid-oligomer specific antibody A11 after 6-hour induction, as showed in Figure 17.

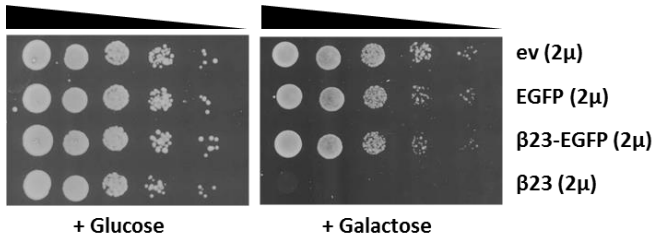

Figure 35. EGFP fusion causes loss of β23 toxicity. Serial dilution assays were performed on yeast cells (W303α strain) transformed with episomal (2μ) constructs containing genes encoding EGFP, β23 or β23-EGFP fusion; empty-vector (ev) transformants served as control.

Given differences in growth performance between the four yeast models and in order to monitor both early and late events associated with the appearance of proteotoxic amyloid aggregates, we set out to evaluate the transcriptional profile of the four ND models at three different time points, namely 4, 6 and 15 hours after inducing protein expression.

2.2 RNA-sequencing analysis

In collaboration with prof. Matteo Pellegrini (UCLA Molecular Biology Institute, Los Angeles) RNA-seq analysis was performed on total RNA extracted from ALS, HD, PD or AD-like models, and from the control strain expressing free EGFP (see 'Materials and Method' for details). *In primis*, we evaluated the expression levels of the amyloidogenic (poly)peptides (Fig. 37) and observed that the number of counts for each "amyloid" gene decreases over time in all four strains, likely due to a decrease of the *GAL1* promoter induction.

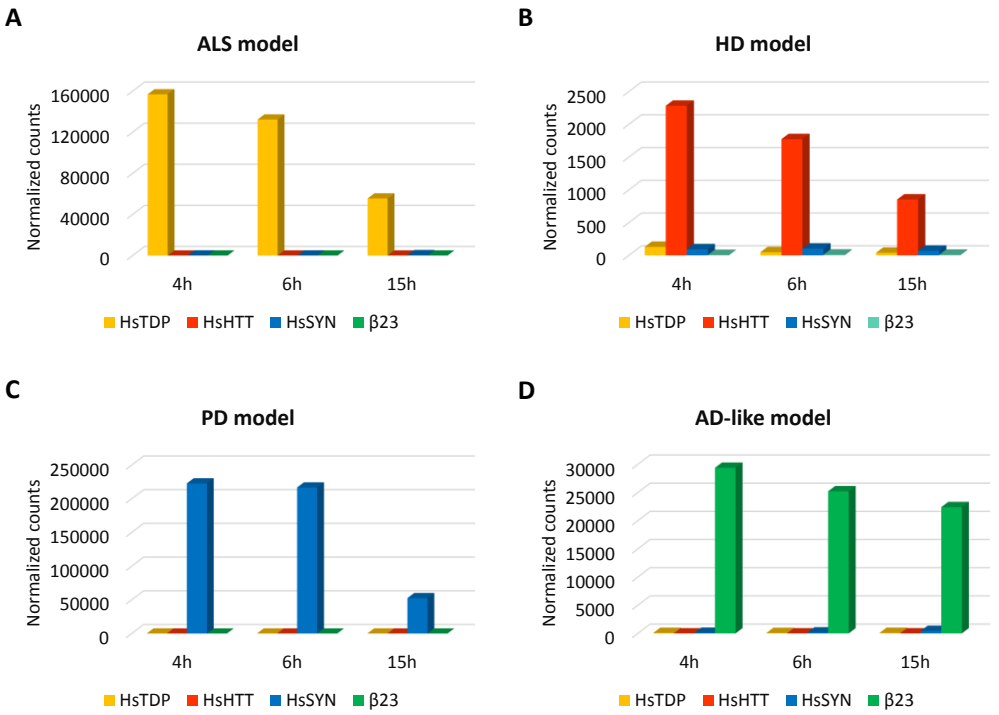

Figure 36 Expression of heterologous proteins in yeast models of NDs. RNA-seq reads were aligned against *Homo sapiens* gene sequences coding for TDP-43 (HsTDP), Huntingtin (HsHTT), α-syn (HsSYN) or against β23 coding sequence. The expression of each sequence in the ALS model (A), HD model (B), PD model (C) or AD-like model (D) is reported as number of normalized read counts (see 'Material and methods' for details) after 4, 6, and 15 hours of induction.

The global expression pattern was characterized using principal component analysis (PCA). The first and second PCA components separated AD-like model samples from

other models. A side cluster was also formed by samples after 15 hours of induction, while samples after 4 and 6 hours of induction were grouped together, with ALS and HD samples clustering closer to the control strain (Fig. 37).

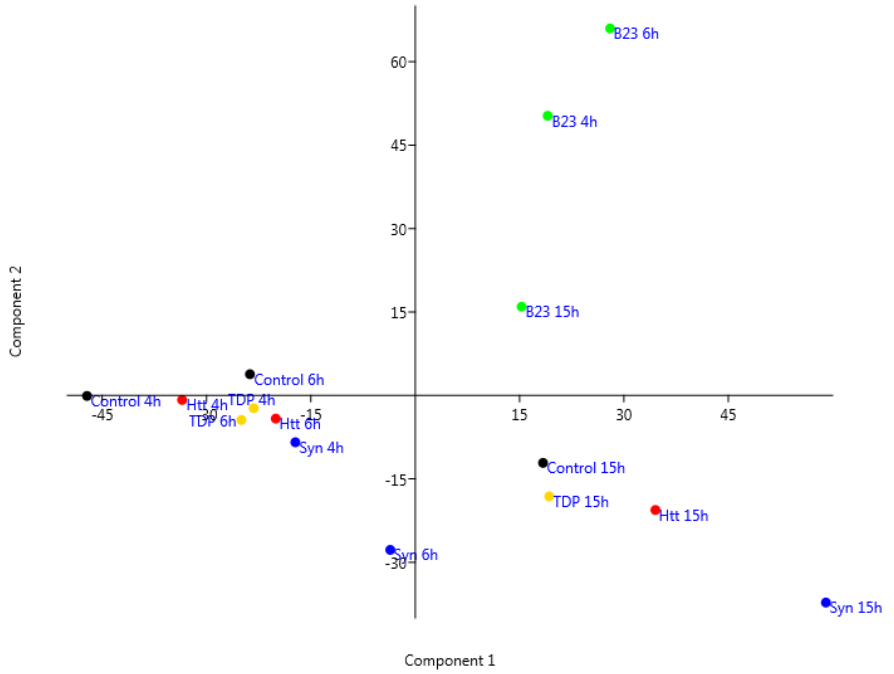

Figure 37. PCA analysis reveals different transcriptomic profiles in yeast models of NDs. Principal component analysis (PCA) on normalized and log-transformed gene counts of different model of NDs and control strain, after 4, 6 and 15 hours of induction (see 'Material and methods' for details). Each dot represents a sample.

For each gene, a $\log_2$ transformed fold change (FC) was calculated to compare the levels of gene expression in each ND model and in the control strain. The total number of differentially expressed genes (DEGs) in the ND models compared to the control strain (see 'Material and Methods' for details) with a FC≥3 was 1967, but only 40 DEGs were common to all strains (Fig. 38A). The less toxic strains (ALS and HD models) elicited the less marked transcriptional response (Fig. 38); in PD and AD-like models, about one-sixth of the total number of ORFs of *S. cerevisiae* genome resulted instead differentially modulated in at least one time point (Fig. 38A). The identification of DEGs even at the earliest time point of induction (4 hours) evidences a rapid yeast response to amyloid protein expression (Fig. 38B-C).

As shown by hierarchical clustering (HC) analysis, a differential modulation profile was observed in different strains: some gene "clusters" were specifically modulated in one model of NDs, others were modulated in more than one strain but with opposite trends of modulation (Fig. 38C).

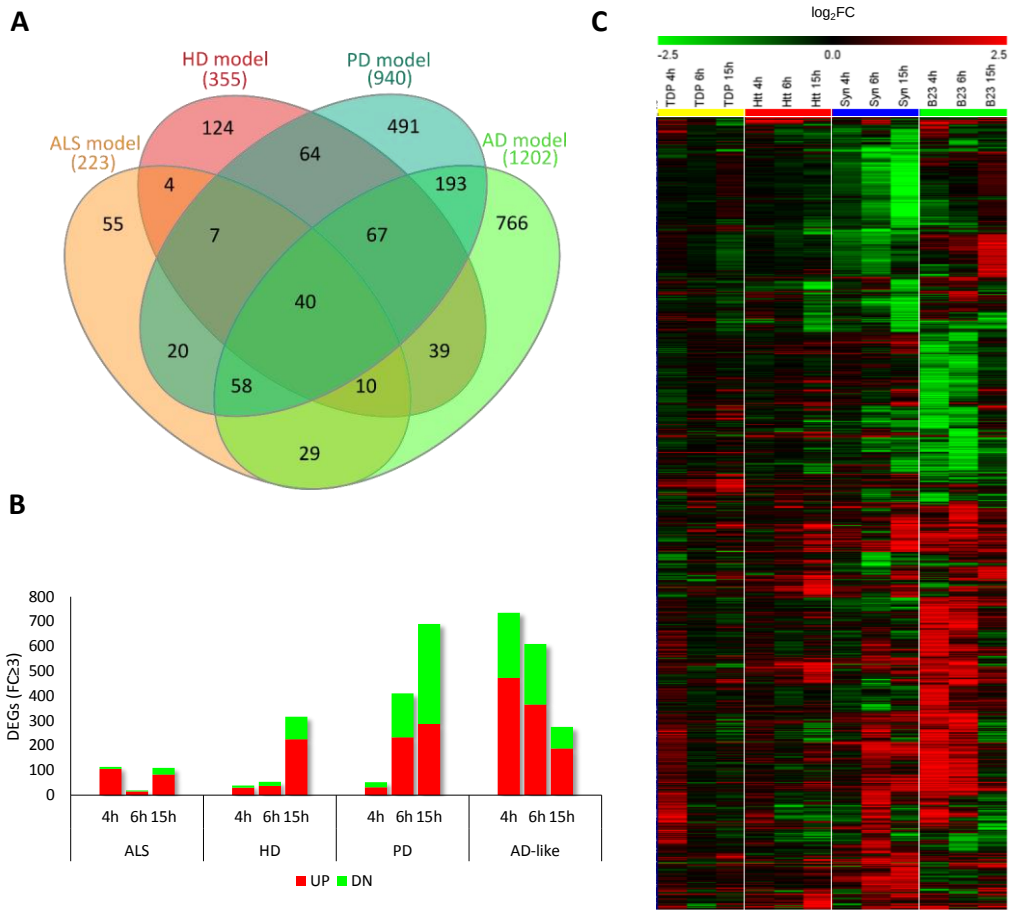

Figure 38. DEGs and transcriptional profiling in yeast model of NDs. A) Venn's diagram[245] showing the number of DEGs in ALS, HD, PD and AD-like model strains, independently from the time point. The total number of DEGs for each model strain is indicated in brackets. B) Bar chart indicating the number of up- ('UP') and down- ('DN') regulated genes in the four different model strains at each time point. C) Hierarchical clustering analysis of 1967 genes exhibiting differential expression (FC≥3) in at least one experiment (compared against control) after 4, 6 and 15 hours of induction of amyloidogenic (poly)peptides. The heat map shows the gene expression level as $\log_2$ FC.

2.3 Enrichment analysis reveals common pathways associated to amyloid aggregate formation in yeast cells

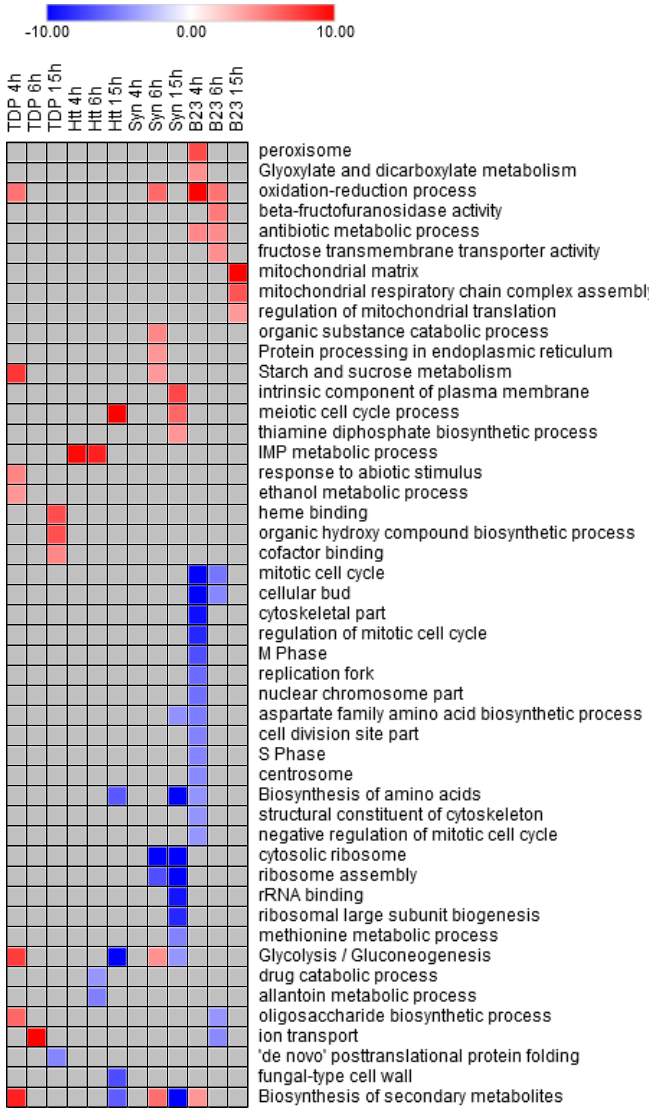

Figure 39. Enrichment analysis shows few common pathways in response to amyloidogenic protein expression in yeast cells. In the heat map are reported the first most significant processes (rank = 1) of each group created by Metascape (see 'Materials and Methods' for details). Red squares indicate samples in which the corresponding process in enriched in upregulated genes, blue squares processes enriched in downregulated genes. Colour intensity is proportional to significativity of the enrichment.

We performed a gene ontology (GO) analysis of DEGs using Metascape tool for gene annotation[246] to identify molecular pathways associated to amyloid aggregate formation in yeast models. Real-time quantitative PCR (qPCR) was used to confirm the modulation of genes belonging to different functional classes (see 'Materials and Methods' for details). Figure 39 shows an overview of the most significantly enriched GO terms.

Several metabolic pathways (such as amino acid biosynthesis or carbohydrate metabolism) resulted significantly enriched in both up- and down-regulated genes in almost all conditions. This dysregulation may not be just a reflection of the switch from glucose- to galactose-containing media or of the progressive nutrients consumption over time, since metabolic factors play key roles in the neurodegenerative process. Amino acids act in the central nervous system as neurotransmitters and neuromodulators[247], the metabolism of purines or some amino acids might represent an alternative way to deal with inadequate energy supply in neurodegeneration[248] and metabolic profiling revealed changes in these pathways in several NDs[249]. Methionine and purine metabolism resulted altered more or less markedly in all model strains (Fig. 40).

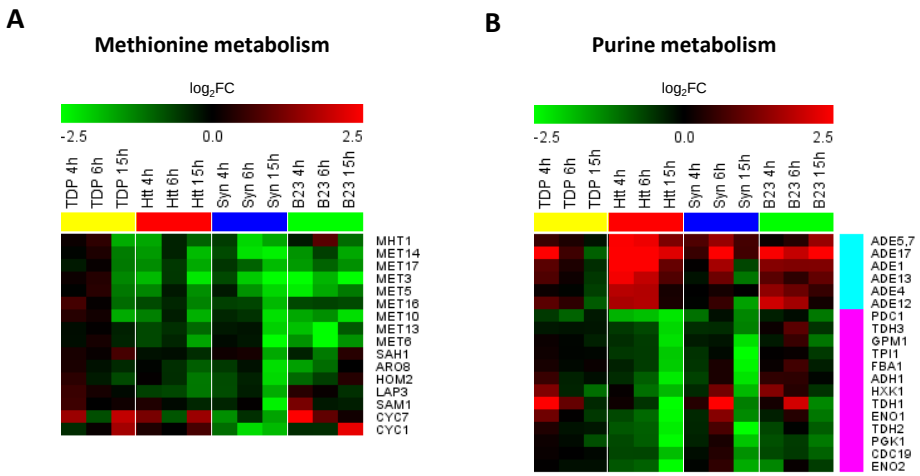

Figure 40. Metabolic pathways are modulated in all model strains. A) Heat map representing the expression profile (log_2 FC) of genes involved in methionine metabolic process. B) Same as in (A) for genes involved in purine metabolism. Cyan bar denotes genes involved in inosine mono-phosphate (IMP) metabolic process and pink bar designates genes participating to purine nucleoside diphosphate metabolism.

Among the dysregulated metabolic pathways, the upregulation of genes involved in the biosynthesis of trehalose (Fig. 41), a non-reducing, highly stable disaccharide, may be linked to its role in resistance against nutritional and environmental stresses, including protein misfolding[250]. In yeast cells, where it can be endogenously synthetized, trehalose can stabilize the native protein conformation and decrease aggregates of denatured proteins[251].

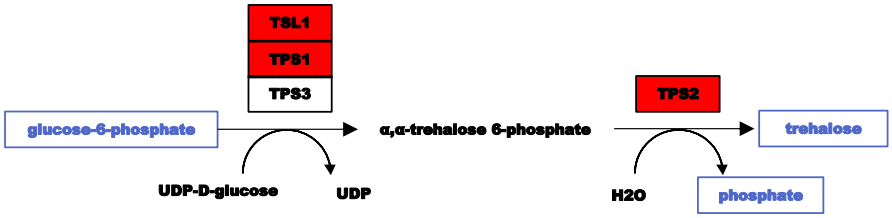

Figure 41. Trehalose biosynthetic pathway in *S. cerevisiae*. Genes positively modulated (especially in the ALS and PD model) are highlighted in red.

In addition, we observed an upregulation of genes involved in oxidative stress response (Fig. 42A) and genes with oxidoreductase activity (whose expression increases in presence of oxidative stress[252]).

As expected in the general response to the proteotoxic stress, genes involved in UPR (Fig. 42B) were modulated (mainly upregulated) in several strains.

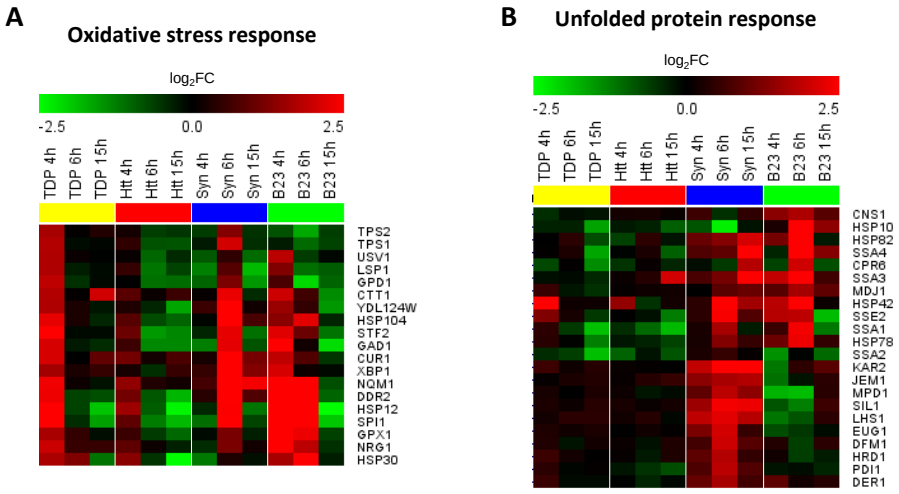

Figure 42. Amyloid (poly)peptide expression elicits stress response in yeast. A) Heat map representing the expression profile (log_2 FC) of genes involved in oxidative stress response. B) Same as in (A) for genes coding for chaperones and other proteins implicated in protein folding, refolding and processing in the ER.

The heat shock protein (Hsp) family plays a major part in defence against protein misfolding and in cellular quality control system. Ssa1 (homologue of human Hsp70) and Hsp82 (homologue of human Hsp90) are ATPases that control protein folding and maturation, but also address misfolded or aggregated proteins to refolding and degradation, together with various co-chaperones. Anyway, their role in neurodegeneration is not fully understood, since in some models Hsp knockdown led to incremented toxicity, while in others Hsp inhibitors worked in reducing toxicity[253]. Ssa1 and Hsp82 resulted transcriptionally upregulated in the AD-like and PD-models and downregulated in ALS and HD models and whether in each case the modulation could represent a defensive mechanism or a pathological consequence is presently unknown.

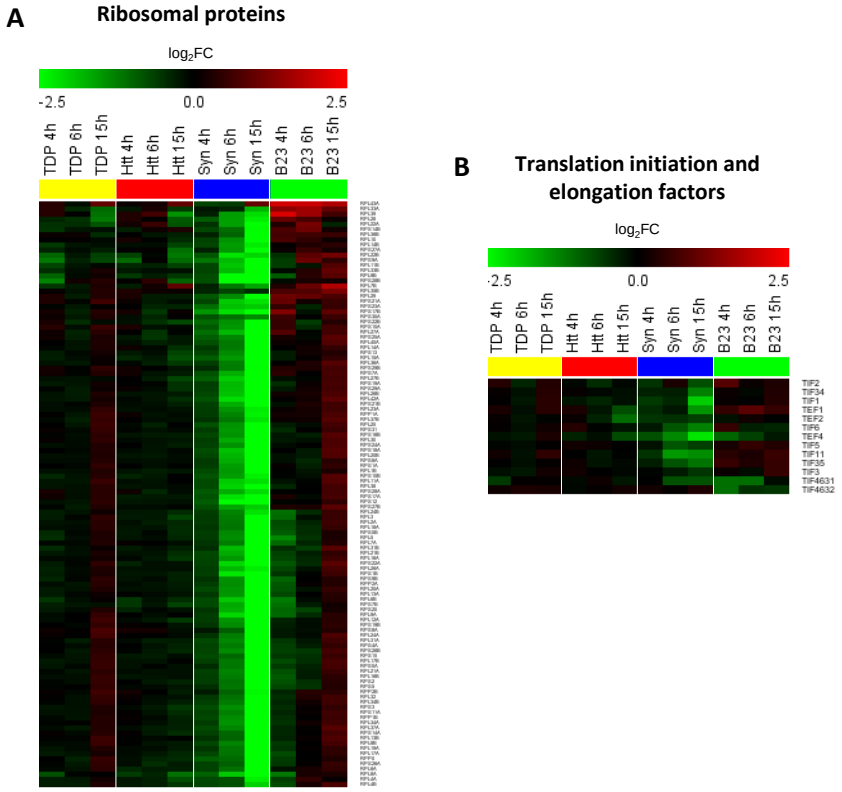

Figure 43. PD model shows global downregulation of genes involved in protein translation. A) Heat map representing the expression profile (log_2 FC) of genes encoding ribosomal proteins of the small or large subunit. B) Same as in (A), for genes encoding translation initiation and elongation factors.

Besides on a correct protein folding, trafficking and degradation, protein homeostasis depends on the regulation of protein synthesis. A breakdown in this balance is characteristic of NDs and, more than as a general symptom of stress, defective translation emerged from our analysis as a signature of α-syn overexpression. The PD model showed a strong downregulation of genes coding for ribosomal proteins - especially of the small subunit - (Fig. 43A) and a less marked downregulation of genes coding for translation initiation and elongation factors (Fig. 43B).

2.4 Iron homeostasis is perturbed upon amyloid protein expression

There is increasing evidence that a perturbation in metal ion homeostasis and compartmentalization can influence protein aggregation through multiple mechanisms. The coordination of metal ions (e.g. iron, copper, zinc, manganese and aluminium) may cause rearrangement of the protein main-chain or induce intermolecular crosslinking, affect protein net charge and destabilize its normal non-pathogenic structure, so triggering misfolding and subsequent accumulation. Furthermore, coordination of redox active metal ions may influence protein accumulation by metal-catalysed chemical modification and promote ROS formation[254]. At the same time, the coordination and possible sequestration into amyloid-like aggregates can cause depletion of metals that are important enzyme co-factors, like iron and copper.

Genes encoding proteins involved in the ion transport and cofactor binding resulted significantly enriched in our analysis; in particular, genes involved in the response to iron deprivation resulted upregulated in the AD-like, PD, and ALS model (Fig. 44A). Expression levels of *FET3* and *FTR1*, coding for two components of the high-affinity iron transporter, were especially upregulated after 15 hours of induction. *FET3* codes for an integral membrane protein that reduces iron ions from Fe(III) to Fe(II), while *FTR1* codes for a transmembrane permease which undergoes a conformational change that allows Fe(II) import into cytoplasm (Fig, 43B). Additionally, other genes involved in iron deprivation response[255] resulted upregulated, including *ARN2* (a membrane permease that mediates nonreductive iron uptake), *FRE1* (that reduces siderophore-bound iron before it is uptaken by transporters), *FIT2* (involved in the retention of siderophore-iron in the cell wall[256]), *CCC2* (necessary for the insertion of copper required for *FET3* functioning) and *HMX1* (an ER-localized heme oxygenase participating to heme degradation during iron starvation[257]) (Fig. 44B).

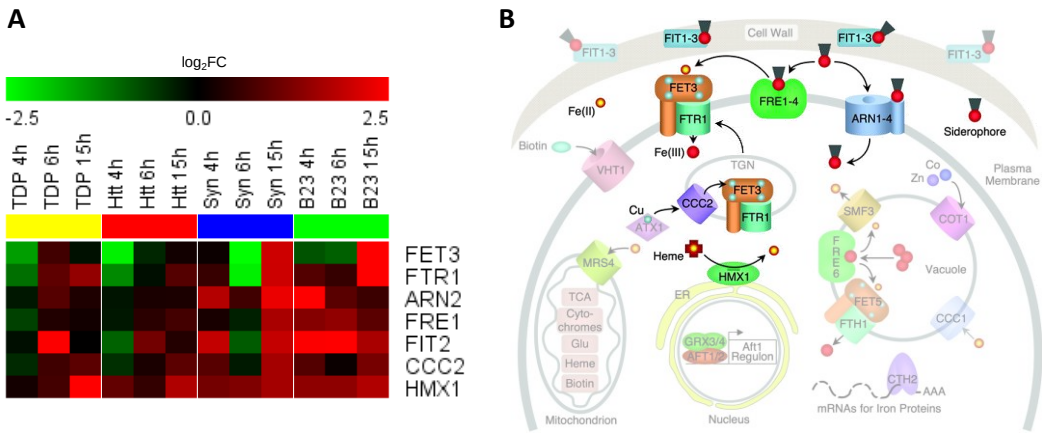

Figure 44. Modulation of genes involved in iron deprivation response. A) Heat map representing the expression profile (log_2 FC) of genes encoding components of the iron deprivation response. B) Iron deprivation response actors and mechanisms. Proteins encoded by genes whose expression pattern is showed in panel (A) are highlighted with brighter colours (modified from[255]).

Since the overexpression of the high-affinity iron transporter could be index of an attempt to compensate for a reduced concentration of this metal due to its sequestration in amyloid structures, we evaluated the effects on cellular viability of an exogenous iron supplementation. Spot assay analysis was performed on galactose-containing media supplemented with different iron concentrations (supplied as iron chloride $FeCl_3$), in a range comprised between 15 and 150 μM. A phenotypic restoration was observed at an intermediate iron concentration (60 μM), both in AD-like and ALS models (Fig. 44), while in the PD model the high toxicity prevented an appreciable viability change. The beneficial effect was abolished at higher iron concentrations, possibly because of the existence of a delicate balance between the compensation of the lack of this essential metal and a surplus that increases aggregation events and toxicity.

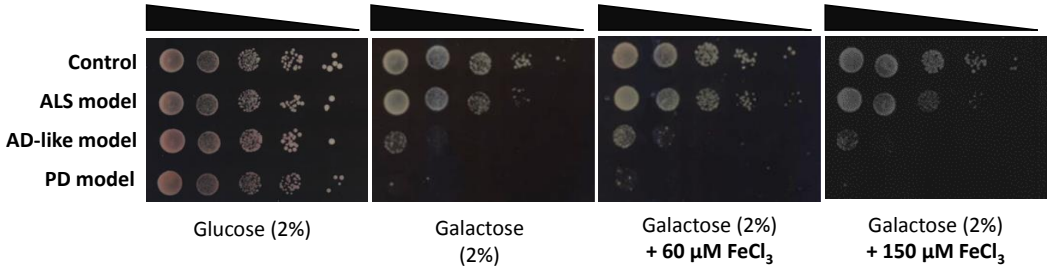

Figure 45. Iron supplementation increases cell viability in ND models. Serial dilution assays (10-fold input cell dilutions ranging from 10^1 to 10^4) were performed on yeast cells (W303 strain) expressing EGFP ('Control'), TDP-43 ('ALS model), β23 ('AD-like model') or α-syn ('PD model') under the control of the galactose-inducible promoter. Cells were spotted on glucose- or galactose-containing agar plates and on galactose-containing plates supplemented with the indicated concentration of $FeCl_3$. Growth was assessed after 2 days at 30°C.

2.5. Mitochondrial functionality is differentially altered in AD-like and PD models

An extensive body of literature supports a role for mitochondrial dysfunction in the pathogenesis of amyloid neurodegenerative pathologies[20,258–260]. Mitochondria play a central role in cell survival since they regulate both energy metabolism and death pathways, with numerous functions spanning from ATP production to lipid and phospholipid metabolism, biosynthesis of heme- and iron-sulfur clusters, calcium homeostasis and regulation of apoptosis. At the same time, mitochondria are the main source of ROS and endogenous toxic free radicals. Functional mitochondria are essential for neuronal cells, which have high energy requirements and poor glycolytic capacity, which makes them mainly rely on aerobic oxidative phosphorylation (OXPHOS). Therefore, neurons are extremely vulnerable to mitochondrial damage. Dysfunctional mitochondria are not able to supply an adequate amount of energy, cause ROS-induced oxidative damage, trigger mitochondrion-mediated apoptosis and may have a pivotal role in ND onset and progression[261,262].

Mitochondrial dysfunction is typical of both sporadic and familial forms of AD[20] and mitochondrial pathways emerged as the most significantly enriched in our analysis (Fig. 46A). Despite the strong upregulation (especially after 15 hours of induction) of genes encoding mitochondrial constituents and proteins for mitochondrial-associated functions, several genes coding for proteins involved in OXPHOS were downregulated (Fig. 46B).

On the other hand, genes for fatty acid (FA) oxidation followed an almost opposite trend (Fig. 46C): induction of FA degradation may be in fact used to fuel the respiratory chain.

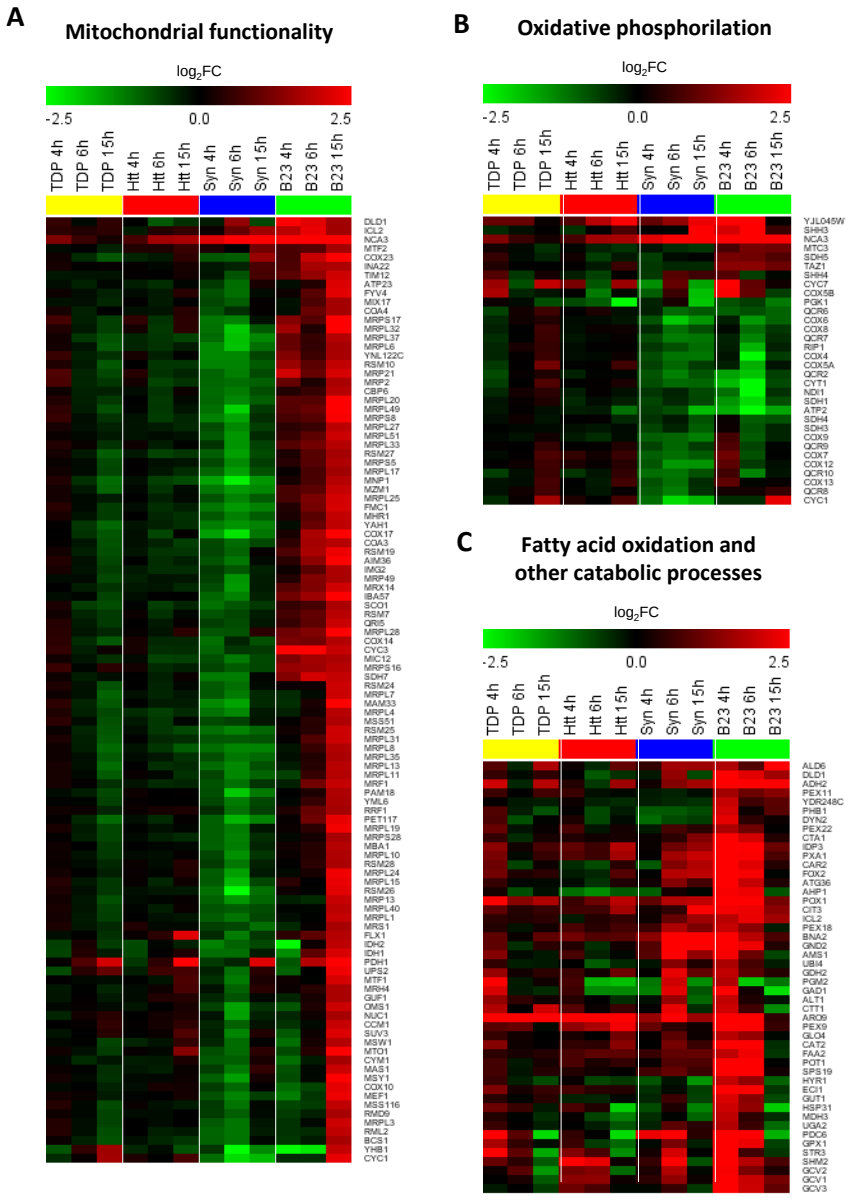

Figure 46. Upregulation of genes involved in mitochondrial functions in AD-like model. A) Heat map representing the expression profile (log_2 FC) of genes encoding mitochondrial proteins. B) Expression profiles of genes involved in OXPHOS. C) Expression profiles of genes involved in FA degradation and other catabolic processes.

Notably, the majority of mitochondrial-related genes that were upregulated in the AD-like model were downregulated in the PD model. The link with mitochondrial damage is recurrent with PD as well and a role for α-syn in mitochondrial dynamics has been repeatedly evidenced[258,259]. Thus, we evaluated the respiratory capacity of the yeast strains. While α-syn-expressing cells retained an almost normal respiration rate (as well as ALS and HD strains), the respiratory capacity of β23-expressing cells was largely compromised (Fig. 47).

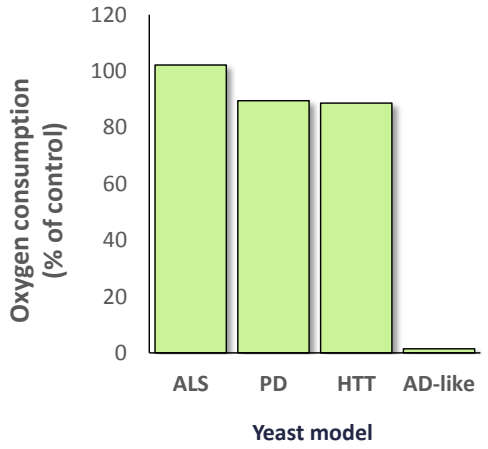

Figure 47. β23 overexpression compromises respiratory capacity. Oxygen consumption was measured using a Clark-type oxygen electrode after 6 hours of protein induction, normalized on cell weight and expressed as percentage of the control.

In line with this result, real-time qPCR analysis revealed a strong downregulation, with almost undetectable levels of expression, of mitochondrially-encoded genes (*COX2* and *COX3*, coding for two subunits of cytochrome c oxidase, the final complex of the respiratory chain with important regulatory functions) in the AD-like model (Fig. 48). Coupled with the respiratory deficiency, this result suggests that the AD-like model may have lost mitochondrial DNA (mtDNA). Nonetheless, Kar2-Aβ_{42}-expressing cells showed the same, even if less pronounced, downregulation of genes encoded by the mitochondrial genome (Fig. 48). On the contrary, *COX2* and *COX3* were upregulated in the PD model (Fig. 48), therefore showing an opposite modulation profile with respect both to the AD-like model and the nuclear-encoded genes.

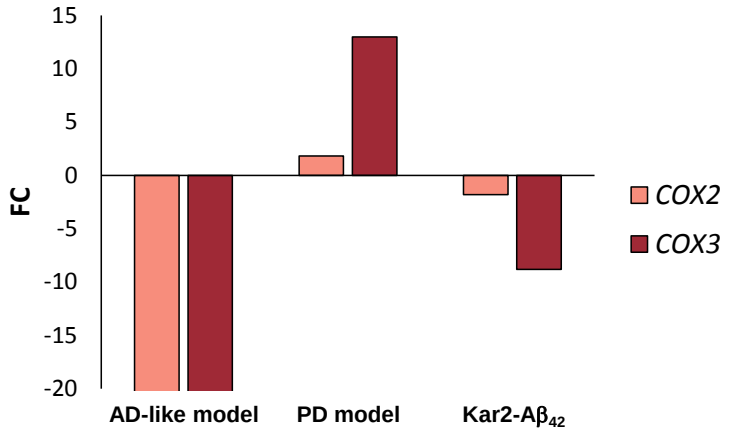

Figure 48. Expression levels of mitochondrially-encoded *COX2* and *COX3* genes were altered in AD-like model. Real-time qPCR was used to measure the expression levels (FC) of mitochondrially-encoded genes in β23- ('AD-like model'), α-syn ('PD model') and Kar2-Aβ_{42}-expressing cells compared to the control strain.

To further investigate differences in the alteration of the mitochondrial functionality in AD-like and PD models, we evaluated mitochondrial structural integrity using a mitochondria-directed red fluorescent protein (mtRFP). For this experiment the strain expressing β23 polypeptide from a multicopy vector was used, since the selectable marker of the plasmid carrying the mtRFP coding sequence (*LEU2*) did not allow selection in the strain bearing two integrated copies of β23 coding sequence (*ade*-) that was used in the rest of the study. The mitochondrial network in the AD-like and PD models was markedly abnormal. Healthy mitochondrial typically exhibit a tubular, ribbon-like architecture, as it was observed in the 90% of the control strain cells (Fig. 49). The AD-like and PD models, besides a high percentage of non-fluorescent cells (60-80%), exhibited a punctuate fluorescence and a fragmented mitochondrial network (Fig. 49). Such fragmented structures are indicative of an enhanced mitochondrial fission.

Fission and fusion are two opposite processes to which mitochondria are continuously subjected in a dynamic equilibrium in order for the cell to maintain a pool of healthy mitochondria and intact mtDNA. Mitochondrial fusion is used to mitigate low but chronic mitochondrial stress by blending oxidative stress into the mitochondrial network and functionally compensate for damaged components, while fission is required to facilitate the removal and turn-over of damaged mitochondria[263,264]. When mitochondria can no

longer be repaired they undergo a selective form of autophagy known as mitophagy[265]. An impaired balance of these processes may induce cell injury and contribute to NDs. In the AD-like model, small, punctuated foci were visible (compatible also with petit mitochondria present in mtDNA-depleted 'ρ0' cells) and vacuoles presented a diffused fluorescence that was not visible in the control cells or in the PD model, a possible sign of increased mitophagy (Fig. 49).

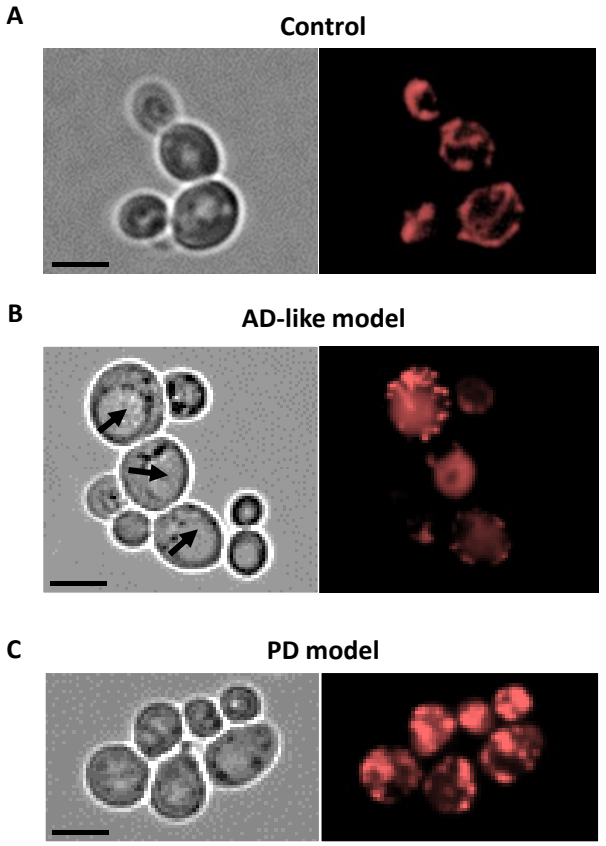

Figure 49. AD-like and PD model exhibit mitochondrial network abnormalities. Phase contrast (left panels) and fluorescence (RFP-filter; right panels) microscopy images of mtRFP-expressing cells. Control cells (A), AD-like (B) and PD models (C) are shown. Arrows denotes cellular vacuoles. Scale bar: 5 μm.

Indeed, positive regulators of mitophagy, like *ATG1* and *ATG33*, resulted upregulated from RNA-seq data, while negative regulators, like *MIP1* and *BRE5*, resulted downregulated. Upregulated were also *ATG11* and *ATG8*, which are required to facilitate

mitochondria fission and autophagosome assembly. The autophagic elimination of dysfunctional mitochondria in some conditions can prove physiologically advantageous and we hypothesize in our model system mitophagy could be activated in an extreme attempt to rescue cell from mitochondrial damage. Nevertheless, we cannot exclude that enhanced autophagy could be due to a break-down in autophagy regulatory pathways. On the other hand, α-syn-induced toxicity could be due to mitochondrial dysfunction for excessive fragmentation, as indicated by previous experiments[266], although mtRFP and α-syn-EGFP fluorescence did not seem to co-localize (Fig. 50).

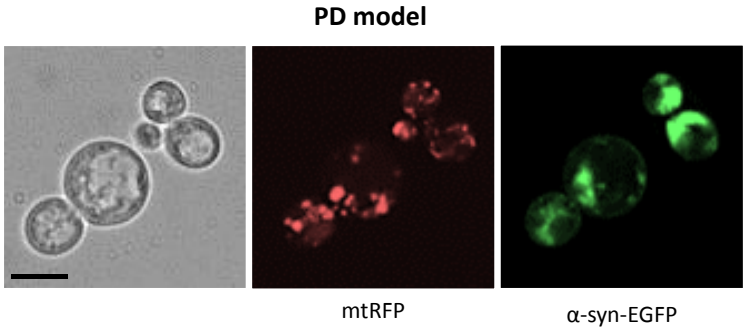

Figure 50. α-Syn-EGFP *foci* are not localized in mitochondria. Phase contrast (left panel) and fluorescent (RFP-filter; central panel; GFP-filter, right panel) microscopy images of the PD model expressing mtRFP. Scale bar: 5 μm.

2.6 An extreme alteration of the cell cycle regulatory pathways is a signature for AD-like model

Microscopy analysis showed an altered shape and morphology of β23-expressing cells, with a high percentage of big (>10 μm diameter), round-shaped cells with a swollen vacuole occupying most of the intracellular space (23% of big cells *versus* 2% in the control strain; Fig. 51).

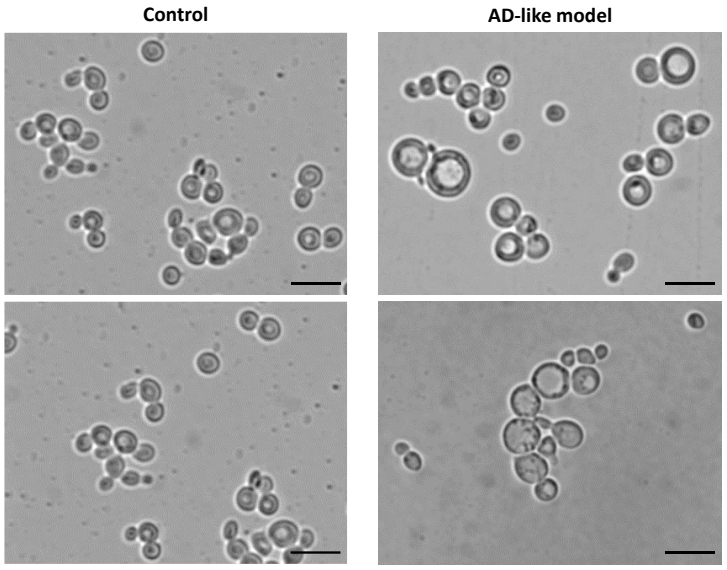

Figure 51. Altered cell morphology in the AD-like model. Contrast phase microscopy images of control cells (left panels) or β23-expressing cells (right panels), after 15-hour induction. Scale bar: 10 μm.

Besides being a consequence of the proteotoxic stress, this phenotype could reflect alterations in the cell division process or in cytoskeletal structures. Indeed, from our enrichment analysis, genes belonging to GO categories concerning mitotic cell cycle resulted globally downregulated in the AD-like model, more markedly at 4 and 6 hours of induction (Fig. 52). These categories included cytoskeletal and microtubule organization (Fig. 52B), cell bud formation (Fig. 52C) and DNA replication and repair (Fig. 52D).

The cell cycle is controlled by an elaborate mechanisms of regulation. Remarkably, as indicated in Fig. 52, several of the downregulated genes (about 35%) are potentially under the control of the transcription factor Mbp1, whose expression does not change appreciably in the ND models.

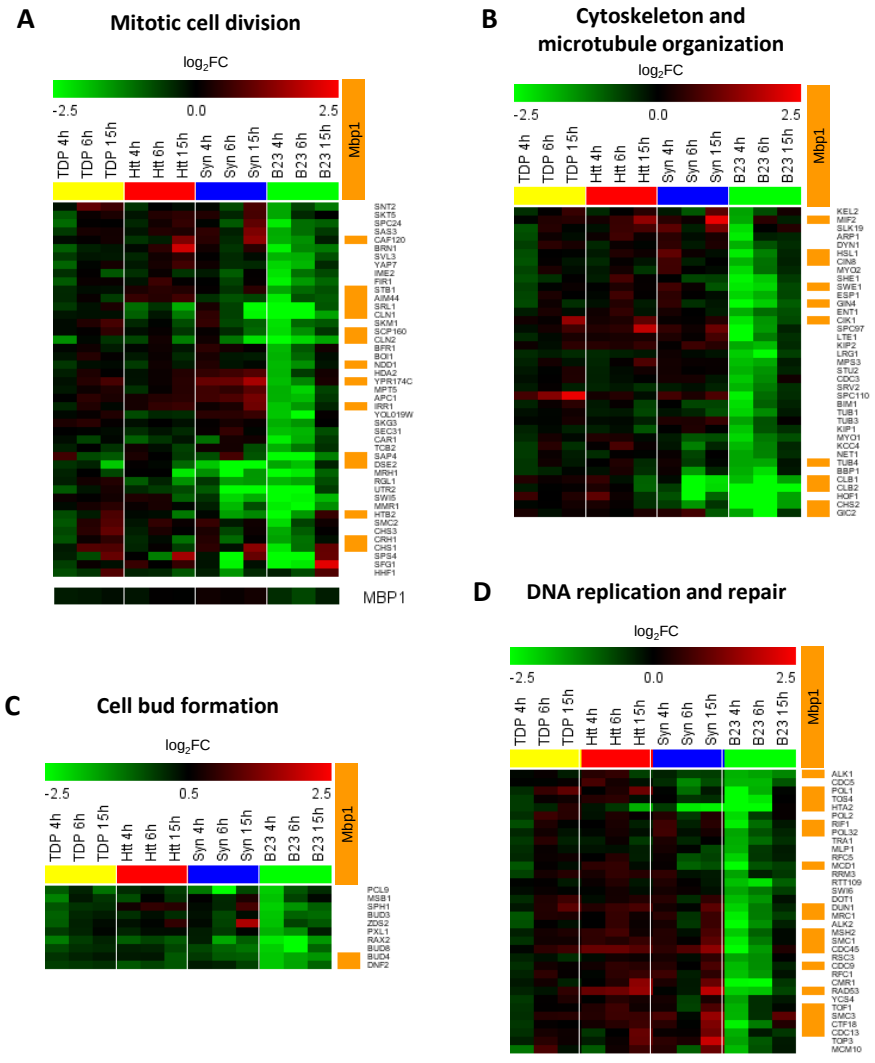

Figure 52. Downregulation of genes involved in regulation of cell cycle in the AD-like model. Heat map of expression levels (log_2 FC) of genes involved in regulation of mitotic cell cycle (A), cytoskeleton and microtubule organization (B), cell bud formation (C) and DNA replication and repair (C). Orange bars highlight genes whose expression is controlled by Mbp1 transcription factor. Last row in panel A shows MBP1 expression levels.

Mbp1 is a key factor in cell cycle progression from G1 to S phase. It forms a complex with Swi6 and, in concert with Swi4, regulates the transcription of late G1-specific targets, like cyclins and genes required for DNA synthesis and repair. In order to explore if there could be a rationale for the enrichment in genes regulated by this transcription

factors, we examined Mbp1 structure, which has been determined only for the DNA-binding domain. Prediction of intrinsically disordered regions using PONDR VSL2 tool showed the presence of segments in the protein sequence characterized by a significant disorder propensity (score > 0.5) (Fig. 53), with an overall 51.7% of disordered residues. A 20% 'consensus' disorder content was evaluated by MobyDB[267] based on the outputs of ten disorder predictors.

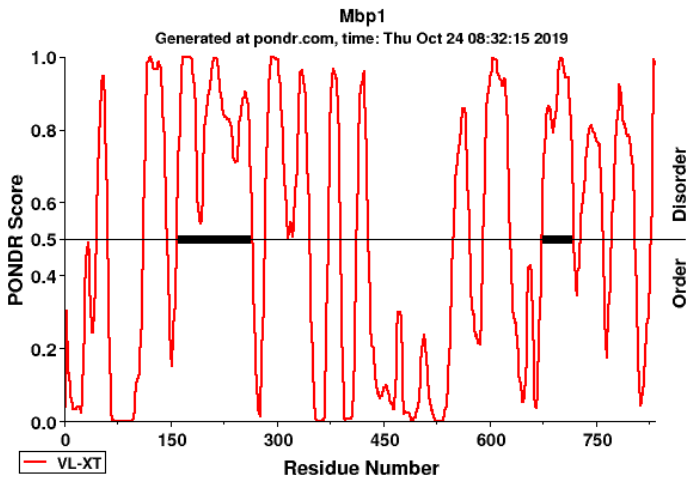

Figure 53. Mbp1 exhibits intrinsically disordered regions. Score prediction for disordered protein regions using PONDR VSL2. Higher score values correspond to higher probability of disorder. The threshold separating order/disorder is set at 0.5.

The presence of intrinsically disordered regions (IDRs) is a common feature of many transcriptional factors, especially if deputed to the regulation of a high number of genes, which allows the flexibility required to interact with multiple targets or proteins and to establish weak yet specific interactions[268]. Nevertheless, in a scenario of amyloid aggregation whose actors are often poorly structured proteins with low complexity regions, IDRs may have also other implications. Indeed, Olzscha *et al.*[198] found that the toxicity associated with β23 polypeptide expression in human cells could be traced back to the sequestration of essential proteins in β23 amyloid-like aggregates and the interactome of β23 was enriched in large-size proteins with long unstructured regions. Additionally, IDRs could facilitate protein inclusion in stress granules (SGs). Stress granules (SGs) are dynamic, membrane-less organelles that transiently form under stress conditions - like oxidative stress - and whose assembly is based on a liquid-liquid

phase separation. They usually contain non-translating mRNAs bound with translation initiation factors, ribosomal subunits, and other proteins affecting mRNA function, and therefore they are believed to represent sites of both mRNA protection from decay and translation stalling, allowing a rapid resume of translation once dissolved. They are critical for stress response, but they have also been linked to the pathogenesis of NDs. It has been proposed that pathological aggregation in NDs could occur through the SG pathway and over-stable SGs could interfere with neuronal function by sequestering and silencing essential transcripts or proteins[269]. All the major players in the nucleation and formation of SGs are either IDPs or proteins containing long IDRs[270]. Therefore, an appealing hypothesis could be that, although not being transcriptionally modulated, Mbp1 could have a higher tendency, conferred by the IDRs, to be sequestered into amyloid-like aggregates or into SGs, in either case becoming inactive and contributing to the decrease in the transcriptional expression levels of its target genes.

2.7 Meiosis-regulatory genes are aberrantly activated in AD-like model

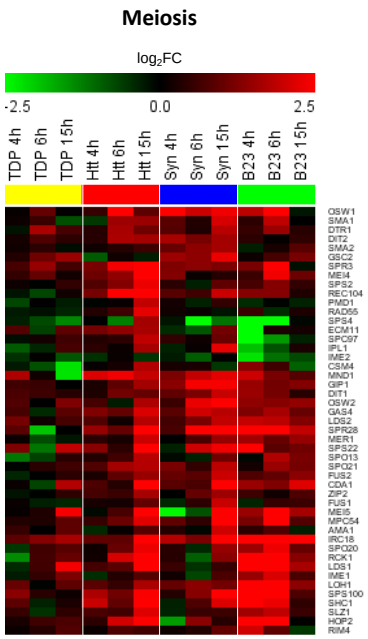

Figure 54. Meiosis-regulatory genes are upregulated in HD, PD and AD-like models. Heat map represents the expression levels (log_2 FC) of genes involved in meiotic and gametogenesis processes.

Unexpectedly, genes involved in regulation of meiotic cell cycle and gametogenesis were found significantly upregulated in the AD-like, PD and HD models (Fig. 54).

Particularly significant is the upregulation of *IME1* in the AD-like model (Fig. 55A), since it can force haploid cells to enter in meiosis I without being able to successfully complete it, lacking homologous chromosomes, and resulting in a meiotic catastrophe[271]. *IME1* is known as "master regulator of meiosis" and codes for a transcriptional factor that activates the expression of early meiotic genes. RNA-seq data showed the upregulation not only of *IME1,* but also of one of its targets, *RIM4* (Fig. 55). The stability of both Ime1 and Rim4 is regulated by the protein kinase Ime2, which promotes their degradation at the onset of meiosis II and whose expression was downregulated at transcriptional level in the AD-like model (Fig. 55). Importantly, Ime2 presents a functional homolog in the human Cdk2 protein[272], a kinase whose misregulation is associated to several neurological disorders, including AD[273].

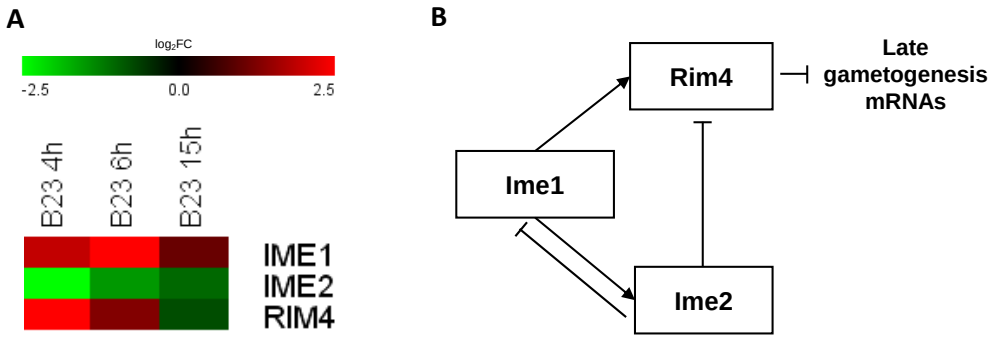

Figure 55. Transcriptional activation of *IME1* and *RIM4* is an early signature for AD-like model. A) Heat map represents the expression levels (log_2 FC) of *IME1*, *IME2* and *RIM4* in the AD-like model. B) Schematic representation of the activation/repression relationship between Ime1, Ime2 and Rim4.

Rim4 is a RNA-binding protein bearing low-complexity regions (Fig. 56A) and Berchowitz *et al.*[274] showed that, upon sporulation initiation, Rim4 switches from a monomeric to an amyloid-like aggregated conformation crucially involved in the regulation of the gametogenesis progression (Fig. 56B). During meiosis I, Rim4 aggregates repress the translation of mRNAs encoding proteins which are involved in medium-late stages of gametogenesis.

Possibly the exposure to β23-amyloid aggregates in AD-like model pushes aggregation-prone proteins as Rim4, but also Mbp1, to accumulate, potentially by cross-seeding[275] and in turn they could interact incorrectly with other cellular components, promoting pathological processes.

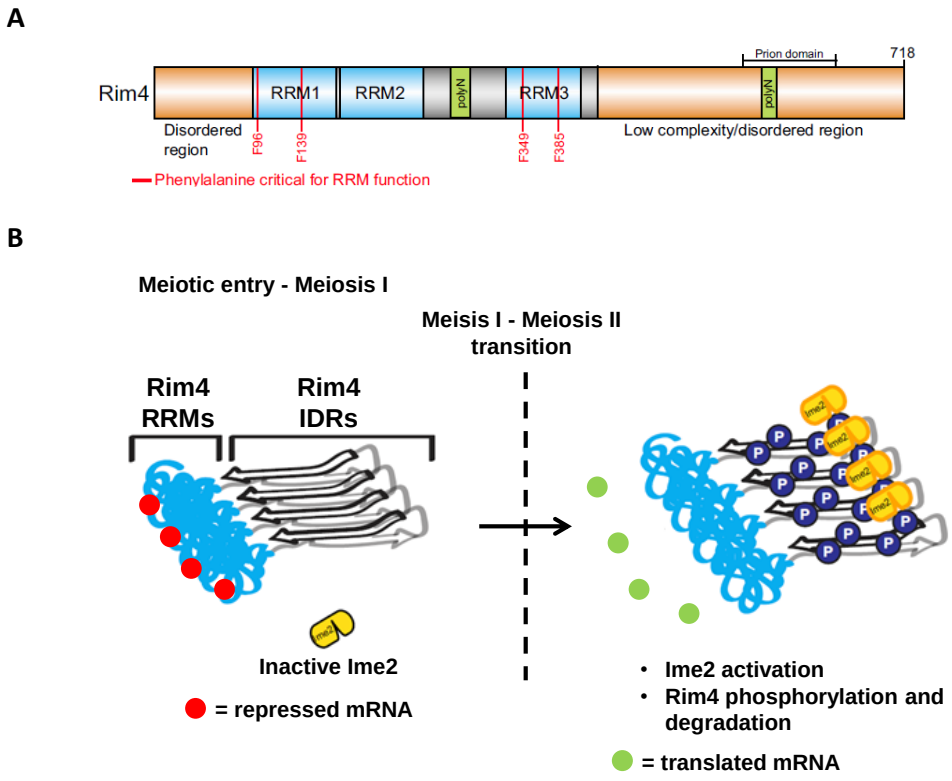

Figure 56. Rim4 possesses low-complexity regions and becomes active upon forming amyloid-like structures. A) Schematic structure of Rim4, containing three N-terminal RNA recognition motifs (RRMs) that are required for RNA binding, a C-terminal low-complexity (LC) region, two poly-N stretches and a computationally predicted prion domain[274]. B) Amyloid-like aggregates of Rim4 repress the translation of medium-late gametogenesis mRNAs and the progression into meiosis II requires Rim4 degradation through a process controlled by Ime2 (modified from[276]).

3. DISCUSSION (PART II)

Humanized yeast models have been employed to study proteins and cellular pathways involved in NDs, such as ALS[105], HD[277], PD[108] and AD[116]. Studying amyloid protein aggregation in yeast cells offers the advantage to couple the simplification of the system (compared to animal or mammalian cell models) with the *in vivo* expression of the protein, so as to reproduce aggregation and pathological effects occurring in human neurons.

Yeast models have been used for several overexpression screenings of genetic modifiers of amyloid toxicity[109,120,142,277–281], but, to our knowledge, mRNA profiling has been performed only in a limited number of studies[141,266,282]. Although complementary, these two approaches can provide different kinds of information, being genetic hits usually biased toward regulatory proteins and transcriptional data toward metabolic responses[279]. We then compared transcriptional profiles of four different yeast models for amyloid neurodegenerative pathologies and found that yeast cells rapidly and differentially modulated gene expression in response to proteotoxic stress caused by different amyloidogenic peptides.

The decline in cellular proteostasis that is typical of NDs was accompanied by the activation of common pathways related to protein folding and oxidative stress, including trehalose biosynthesis. Trehalose has a protective role in stress tolerance and protein stabilization[251] and increased levels have been detected also in yeast cells constitutively expressing secretory $A\beta_{42}$, in which, as resulted by genome-wide expression analysis, a strong endoplasmic reticulum stress and UPR were triggered[141]. Trehalose was reported also to act in more indirect ways, e.g. reducing Htt and α-syn aggregates in treated mammalian cell lines through autophagy induction[283].

An alteration of the metal ion homeostasis is another factor likely contributing to oxidative stress[284] and neurodegeneration. Increased burden of iron and other metals has been found in specific brain regions of PD[285] and AD patients[286] as well as in ALS cerebrospinal fluid[287] and the requirement of metal ions for normal synaptic functioning[288] has stimulated the development of therapeutic strategies aimed at re-establishing the correct metal balance[289–291]. In our study, this pathway was affected in almost all models tested (AD-like, PD, ALS).

In a previous transcriptional profiling in the α-syn-expressing strain, Su *et al.*[266] identified not only an increase in transcripts of genes with oxidoreductase activity and the

alteration of metal ion homeostasis, but also a global downregulation in the expression of ribosomal gene and genes involved in function and maintenance of mitochondria. Both these results were confirmed in our analysis.

Even though Su *et al.* initially considered the decrease in ribosomal transcripts a general index of a yeast stressful condition, in our experiment is rather seemed a specific feature of α-syn overexpression. This is in accordance with the observations by Khurana *et al.*[292], who identified several genetic modifiers specific of α-syn toxicity related to mRNA translation, including initiation factors and ribosomal subunits, and found a reduced incorporation of radiolabelled amino acids in PD-patient-derived neurons. α-Syn has been found to interact with proteins involved in protein biosynthesis - including translation initiation factors and ribosomal proteins - in neurons[293] and mutations in the translation initiation factor EIF4G1 (PARK18) have been linked to autosomal dominant PD[294]. Intriguingly, although without a prove of a direct association, a positive correlation between α-syn oligomer abundance and altered protein synthesis machinery has been found in post-mortem brains of PD patients at different stages of disease[295].

Downregulated genes in PD model were also enriched in genes coding for mitochondria-localized proteins, but interestingly, the AD-like model had an almost opposite response. Being human brain activity responsible for a high portion of total energy consumption, mitochondrial abnormalities endanger neuronal activity and may participate to ND pathology[296]. In yeasts expressing β23 polypeptide there was a specific upregulation of mitochondrial transcripts encoded by the nuclear genome that was in opposition with a strong downregulation of mitochondrial-encoded transcripts, along with the almost total suppression of the respiration capacity. Reduced energy metabolism is one of the best documented anomalies in AD[297]. Chen *et al.*[140,141] reported a decreased respiration capacity and a reduced growth in presence of an exclusively respirable carbon source in yeast cells constitutively expressing secretory $A\beta_{42}$. A strong impairment of total respiration have been found in APP human neuroblastoma cells[298] and several investigators have documented that COX activity is systematically decreased in AD subjects[299]. A reduction in the number of mitochondria have been identified as an early feature of AD in the analysis of biopsy specimens[300] and a high degree of mtDNA deletion was found in vascular walls from human AD brains and APP transgenic mice[301]. Not only directly Aβ, but also metal ions might be responsible for the toxic insult[299], given the deep interrelation between these pathways.

Analogously to the findings in the AD-like model, but in opposition to the upregulation observed in the PD model, we found downregulation of mitochondrial-encoded genes also in a strain expressing secretory $A\beta_{42}$, thus confirming β23 as an effective surrogate to study Aβ toxicity.

Aβ has been reported to accumulate in mitochondria and directly interact with mitochondrial proteins[302–304], affecting respiration, ROS generation and organelle morphology[298,299]. Here, we reported similar responses for β23-expressing cells. Fluorescence microscopy detected aberrant mitochondrial structures, similar to those that have been observed in brain tissue from AD patients and neuronal cells expressing mutant APP[300,305] and some evidences seem to point to an increased mitophagy, possibly with protective effects. Upregulation of mitophagy-linked transcripts and high levels of mtDNA in autophagosomes in AD subjects have been reported [300,306] and a protective role for mitophagy is supported by the recent study by Fang *et al.*[307], who evidenced how mitophagy stimulation could reverse memory impairments in AD models. α-Syn appeared to not localize into yeast mitochondria but to impair them in more indirect ways[266,308] (differently from other experimental models[309–315]), but, even if respiration was not significantly impacted in α-syn-expressing cells, mitochondrial morphology was clearly affected. The round, fragmented mitochondria we observed in the PD yeast model have been observed upon α-syn overexpression in previous studies both in yeast[316] and in different model systems[28,315]. Several studies have reported a role for α-syn as a promoter of mitochondrial fragmentation in response to mitochondrial stress, even in physiological conditions[317], but it is clear that a prolonged or unchecked activation of α-syn would lead to excessive mitochondrial fission, mitochondrial failure and eventually neuronal cell death and PD[317]. A PD model based on α-syn expression in aged cells showed that abrogation of mtDNA reduced α-syn-induced ROS formation and apoptosis, demonstrating a strict requirement of functional mitochondria[318]. The downregulation of nuclear-encoded mitochondrial genes could thus be interpreted as a protective mechanism. On the other hand, the upregulation of nuclear-encoded mitochondrial transcripts in the AD-like model could be aimed at recovering mitochondrial function following β23-induced mitochondrial loss, in concert with increased mitophagy.

Our analysis revealed deep alterations of the cell cycle, that have already been documented in AD[319,320]. Cells expressing β23 were characterized by a marked

downregulation of functional and structural proteins involved in the mitotic cell cycle. AβOs have been found to directly impair mitotic spindle assembly and mitotic microtubule motor proteins, generating defective mitotic structures[321]. The overexpression of a prion protein in yeast have been reported to cause the downregulation of genes involved in cytokinesis and to arrest the cell cycle sequestering a spindle body component[322].

Since yeast regulatory proteins are generally not detected by transcriptional analyses either because their differential expression is transient, making changes hard to measure, or they are mainly regulated post-transcriptionally[279], we evaluated if a significant enrichment could be found in targets of specific transcriptional factors. This analysis led to the identification of Mbp1, whose structure presents IDRs that could promote its interaction with amyloid aggregates formed inside the cell or its inclusion in SGs. The percentage of disorder that we found in Mbp1 is comparable to that of TDP-43, an amyloidogenic protein that has a 57.2% of disordered residues predicted with PONDR VLS2 and a 37% of consensus disorder predicted with MobyDB and, when cytoplasmically mislocalized, has been found in SGs[270]. An analogous disorder composition can be found also in Rim4 (53% disordered residues with PONDR VLS2; 33% with MobyDB), an RNA binding protein that resulted upregulated in the AD-like model. Rim4 acts at early stages of meiosis and is able to form functional amyloid aggregates that bind specific mRNAs repressing their translation[274]. The presence of RNA binding domains can facilitate protein recruitment in SGs that may function in "cross-seed" and trap proteins with low-complexity regions[323]. According to Protter *et al.*[324], promiscuous interactions established by IDRs can synergize with specific protein-protein or RNA-protein interactions that lead to granule assembly. We speculate that, in a persistent stress condition, the presence of pathological amyloid proteins could enhance the formation of over-reactive SGs that may, on one side, drive the transition of normally non-pathological proteins towards irreversible amyloid conformations and, on the other side, interfere with cellular function by sequestering important proteins and silencing transcripts.

Finally, our work evidenced a general activation of meiotic cellular pathways in HD, PD and AD-like models. More than an effect directly translatable on human gametes, this result highlights the aberrant occurrence of cell cycle events in cells that should not undergo such processes. Increasing evidences have shown that cells that entered G_0 -

and so are no longer mitotically active, as are many hippocampal neurons - are erroneously reactivated in AD and other NDs. They are forced to go through a cell cycle they are not able to complete, some even reaching S phase, but they cannot return in G_0 and so undergo apoptosis[320]. Analogously, when haploid yeast cells go through meiosis, either they are not able to proceed through nuclear division or aneuploidy occurs, in both cases resulting in cell death[271].

Overall, our results furtherly confirmed the specificity of yeast response to different amyloid proteins and the power of this simple model organism to study complex human diseases.

4. MATERIALS AND METHODS (PART II)

Yeast strains for transcriptional analysis

Yeast strains and genotypes used in transcriptional experiments are listed in Table 10. ALS model was kindly provided by Prof. Aaron D. Gitler. HD model, PD model and EGFP control strain were kindly provided by the laboratory of Susan Lindquist. For the construction of the AD-like model with two integrated copies of β23 coding sequence, see Part I, 'Material and Methods'. All the sequencing coding for amyloidogenic proteins/peptides are under the control of a galactose-inducible (*GAL1*) promoter. Isogenic strains for ALS, HD and AD-like models were used as additional controls in real-time qPCR experiments. For the generation of ALS and HD model isogenic strains, either pMW#3 vector (Addgene; *URA3* selectable marker) or pMW#2 vector (Addgene; *HIS3* selectable marker) were integrated, respectively, in the *his3* or *ura3* locus of the W303a strain (ATCC), using a standard, lithium acetate-based transformation protocol[229]. The resulting transformants were selected on SD medium supplemented with 2% (w/v) glucose lacking either uracil or histidine. For the generation of the AD-like model isogenic strain model bearing pFL26 and pMW#2 empty vectors, see Part I, 'Material and methods'.

Table 10. ***S. cerevisiae*** **strains used for transcriptional analyses.**

Strain[a]	Description[b]	Genotype
Strains used for RNA-sequencing		
1xTDP-43-EGFP W303a	ALS model	*MATa can1-100, his3-11,15, leu2-3,112, ade2-1, trp1-1, URA3, Gal-TDP-43-EGFP*
1xHtt72Q-CFP W303a	HD model	*MATα can1-100, leu2-3,112, ade2-1, trp1-1, ura3-1, HIS3, Gal-FLAG-Htt72Q-CFP*
2x4-6-α-Syn-EGFP *pdr1Δpdr3Δ* W303α	PD model	*MATα can1-100, his3-11,15, leu2.3,112, ade 2-1, TRP1, Gal-4-6-α-Syn-GFP, URA3, Gal-4-6-α-Syn-EGFP, pdr1::KAN, pdr3::KAN*
2xβ23 *pdr1Δpdr3Δ* W303α	AD-like model	*MATα can1-100, HIS3, Gal-Myc-β23, LEU2, Gal-Myc-β23, ade 2-1, TRP1, Gal vector, URA3, Gal vector, pdr1::KAN, pdr3::KAN*
2xEGFP *pdr1Δpdr3Δ* W303α	EGFP control (PD model isogenic strain)	*MATα can1-100, his3-11,15, leu2.3,112, ade 2-1, TRP1, Gal-EGFP, URA3, Gal-EGFP, pdr1::KAN, pdr3::KAN*

Table 10 (continued).

Additional strains used for real-time quantitative PCR		
1xev$_{(URA3)}$ W303a	Control (ALS model isogenic strain)	*MATa can1-100, his3-11,15, leu2-3,112, ade2-1, trp1-1, URA3, empty vector*
1xev$_{(HIS3)}$ W303a	Control (HD model isogenic strain)	*MATα can1-100, his3-11,15, leu2-3,112, ade2-1, trp1-1, ura3-1, HIS3, empty vector*
2xev$_{(LEU2,HIS3)}$ *pdr1Δpdr3Δ* W303α	Control (AD-like model isogenic strain)	*MATα can1-100, HIS3, pMW#2 vector, LEU2, pFL26 vector, ade 2-1, TRP1, empty vector, URA3, empty vector, pdr1::KAN, pdr3::KAN*

[a]TDP-43, TAR DNA binding protein 43; EGFP, enhanced green fluorescent protein; Htt, Huntingtin; CFP, cyan fluorescent protein; α-Syn, α-Synuclein; ev, empty vector.

[b]ALS, amyotrophic lateral sclerosis; HD, Huntington's disease, PD, Parkinson's disease; AD, Alzheimer's disease.

Yeast strains expressing β23 polypeptide, free EGFP and β23-EGFP fusion in pYES2 vector

Yeast codon-optimized β23 coding sequence (see Table 8) was cloned in the multicopy yeast expression vector pYES2 (Thermo Fisher Scientific, *URA3* selectable marker) and transformed into the wild-type *S. cerevisiae* strain W303α (ATCC, see Table 9) as described in Part I, 'Materials and methods'.

To generate pYES2-EGFP plasmid, the EGFP coding sequence was PCR amplified using plasmid pXY212-EGFP as template[227] and oligonucleotides #R and #S as primers (Table 11). The resulting amplicon was then cloned into the *Bam*HI-*Xba*I restriction sites of the pYES2 vector.

To produce the β23-EGFP fusion protein, a variant β23 sequence lacking a terminal stop codon was PCR amplified using plasmid β23-pYES2 as template and oligonucleotides #T and #U as primers (Table 11). The resulting amplicon was then inserted into the *Hind*III-*Bam*HI restriction sites of the pYES2-EGFP vector.

After sequence verification, the resulting construct was transformed into the wild-type *S. cerevisiae* strain W303α using a standard, lithium acetate-based transformation protocol[229]. Yeast transformants were selected under non-inducing conditions on SD medium containing 2% (w/v) glucose plus histidine, leucine, adenine and tryptophan, but without uracil. The same yeast strain transformed with the empty pYES2 vector served as a control.

Table 11. Oligonucleotides used for yeast strain generation.

Primer name	Primer sequence[a]
#R	FW: 5'-TAAATATAAAGGATCCTCTGGTATGAGTAAAGGAGAAGAACTTTTC-3'
#S	RE: 5'-AATTATTTTATCTAGATTATTTGTATAGTTCATCCATGCC-3'
#T	FW: 5'-TAAATATAAAAAGCTTGCCACCATGGAGCAAAAAC-3'
#U	RE: 5'-AATTATTTTAGGATCCATGCATGTCGATCTGCAGTTCTCCAC-3'

[a]FW, forward primer; RE, reverse primer.

Yeast strains expressing mtRFP

For analysis of mitochondrial morphotypes, pYX142-mtRFP plasmid (*LEU2* selectable marker) was transformed using a standard yeast electroporation protocol[325] in PD model strain, in EGFP model strain and in the DY strain previously transformed with yeast codon-optimized β23 coding sequence cloned into *Hind*III-*Xba*I restriction site of pYES3 vector (Thermo Fisher Scientific, *TRP1* selectable marker). The resulting transformants were selected on SD medium supplemented with 2% (w/v) glucose lacking leucine.

Cytotoxicity assays in yeast

For growth curve analysis, yeast cells were cultured at 30°C in SD medium supplemented with 2% (w/v) glucose ('non-inducing conditions') - plus the appropriate amino acids and/or nucleobases according to the strain auxotrophies - for 24 h, washed and diluted to an OD_{600} of 0.3 in selective minimal medium supplemented with 2% (w/v) galactose ('inducing conditions'). Cell growth was monitored for 4, 6 and 15 hours by OD_{600} measurements.

For serial dilution 'spot' assays performed on solid media, yeast pre-cultures were washed, adjusted to an OD_{600} value of 1.0 and serially diluted in ten-fold increments, prior to spotting (4 µl aliquots for each dilution) onto glucose- or galactose-containing, selective minimal medium agar plates. Yeast growth was examined by visual inspection (and photographically recorded) after incubation at 30°C for two days.

Microscopy analysis

For imaging of living yeast cells, yeast strains were grown overnight in non-inducing conditions. After 24 h, cells were washed, diluted to 0.3 OD_{600}/ml in galactose-containing medium and incubated for 4, 6 or 15 hours at 30°C. To visualize mitochondrial network, mtRFP-transformed strains were prepared as above and grown for 15 hours in inducing

conditions. Cell were then imaged with a Zeiss Axio Imager.Z2 microscope for acquisition and Axiovision Software. For visualization of EGFP and CFP-fusion proteins, GFP and cyan filters were used. mtRFP fluorescence was detected at 588 nm with an RFP filter.

Total RNA extraction from yeast models

For total RNA purification, yeast strains (ALS model, HD model, PD model, AD-like model, EGFP control, see Table 10) were cultured at 30°C overnight in 'non-inducing' conditions. The next morning, cells were diluted to 0.3 OD_{600}/ml into 'inducing' medium, grown at 30°C and harvested by centrifugation at 4 or 6 hours post-induction. For 15-hour induction, cells were diluted from overnight cultures to different OD600/ml into inducing medium (0.01 OD_{600}/ml for the control strain; 0.04 OD_{600}/ml for ALS model; 0.1 OD_{600}/ml for HD model; 0.3 OD_{600}/ml for both PD and AD-like models) and harvested by centrifugation at 15 hours post induction, when all strains reached 0.5 OD_{600}/ml. From each sample, 10 OD_{600} of yeast cells were resuspended in RLT buffer (Qiagen), supplemented with an equal volume of acid-washed glass beads (0.5 mm diameter) and were lysed by five rounds of vigorous vortexing (1 minute stroke followed by 1 minute incubation on ice) with a Mini-Beadbeater 16 (BioSpec Products Inc.). Total RNA extraction was performed using RNeasy Mini Kit (Qiagen), following manufacturer's instructions, and RNA concentration was measured with the Qubit RNA Assay (Thermo Fisher Scientific). RNA purity was assessed by the OD_{260}/OD_{280} ratio and the overall quality of the RNA preparation was verified by denaturing electrophoresis on formaldehyde agarose gel.

Yeast libraries preparation and RNA-sequencing

Total RNA integrity was assessed using Agilent TapeStation 2200 (Agilent Technologies) and quantified using the Qubit BR RNA assay. 50 ng of total RNA was used to prepare stranded mRNA-seq libraries using the Illumina NeoPrep Library Prep System.

Libraries were sequenced as in Morselli *et al.*[326] with an Illumina HiSeq 4000 using 50 bp single-end reads. Reads were aligned using STAR-RNA (version 2.3.1) against the *S. cerevisiae* genome (sacCer3) supplemented with the plasmid construct sequences using the following parameters: --outFilterMismatchNoverLmax 0.04 --outFilterMultimapNmax 1

Data analysis

Out of the original 6365 genes from RNA-seq data, 5831 were included in the analysis since they passed the threshold of 100 counts (number of reads aligned against a gene) in at least one sample. The threshold of 100 gene counts - under which a transcript was considered undetectable - was chosen evaluating the number of counts for genes coding for the amyloidogenic proteins in the untransformed strain (control conditions), where they, given their human or synthetic origin, should not be expressed. Data were normalized (DEseq2 implemented normalization[327]), log-transformed (log_2) and gene expression modulation, defined as FC, was determined by the ratio between the gene counts in a specific model strain and gene counts in the control strain at the same time point. Genes were defined as DEGs either with FC ≥ 3 or FC ≤ -3. Genes related to genetic background differences among strains, e.g. genes related to mating-type, auxotrophies and deletions of *PDR1* and *PDR3*, were removed before further analysis. PCA was performed using Past software (ver. 3.20). HC analysis was performed using MultiExperiment Viewer (MeV) software (ver. 4.9). Enrichment analysis was conducted on gene lists of DEGs (up- or down-regulated) using Metascape Bioinformatics Resources for gene annotation and analysis[246] (q-value < 10^{-4}). Transcription factor analysis was performed comparing gene lists of DEGs with gene lists of transcription factor targets [http://www.yeastract.com/]. Significant enrichment in targets of a specific transcription was evaluated using Fisher's exact test (p-value < 10^{-10}). Transcriptional factors with more than 1000 targets were excluded from the analysis.

Real-time qPCR

Real-time qPCR was used to evaluate and confirm the relative expression of specific genes. To exclude any bias deriving from genetic differences between the strains, like auxotrophies, mating-type and deletion of *PDR1* and *PDR3* genes, real-time qPCR confirmation was performed using the isogenic control for each strain that are listed in Table 10. Briefly, 1 µg of total RNA from each strain was reverse transcribed using iScript cDNA Synthesis Kit (Bio-Rad) according to manufacturer's instructions. An equal amount of cDNA was used for each qPCR reaction, using primers listed in Table 12. Melting curve analyses were conducted to check for amplification specificity. Each reaction was set up in triplicate and a no template control was included. Relative transcript abundances were determined by using the comparative C_T method[328] and standardization to a reference gene (*UBC6*[329,330]).

Table 12. Genes tested in real-time qPCR experiments and oligonucleotides used.

Gene	Gene brief description[a]	Primer sequence[b]
APJ1	Chaperone with a role in SUMO-mediated protein degradation	FW: 5'-GCTCTACGCCGAGCTTCTCC-3'
		RE: 5'-AGGGCCTCTATCCAAATGATGG-3'
BTN2	v-SNARE binding protein	FW: 5'-GAAGGTGGCATCAACGAACCA-3'
		RE: 5'-CTTCTTCCTCCTTCAAAGATTCA-3'
CLB2	B-type cyclin involved in cell cycle progression	FW: 5'-GCAGCTGCGATGTTTATGTCG-3'
		RE: 5'-CGGGCGCAAGTTCTTCTTTAG-3'
ERO1	Thiol oxidase required for oxidative protein folding in the ER	FW: 5'-TCATTTTGGGACGCCAACG-3'
		RE: 5'-TCTCAGGCTGCCAGTACTCAGG-3'
FET3	Ferro-O_2-oxidoreductase	FW: 5'-GATGCTCATTCTCAACAACTCAG-3'
		RE: 5'-TTAAATCCAGTGTATTGGCAGCG-3'
HOF1	Protein that regulates actin cytoskeleton organization	FW: 5'-GTCAGGGATAGAGGTATTACTG-3'
		RE: 5'-CCAGGTGCCTCATTTCCAATC-3'
HSP12	Plasma membrane protein involved in maintaining membrane organization	FW: 5'-ACTCTGCCGAAAAAGGCAAGG-3'
		RE: GACGGCATCGTTCAACTTGG-3'
HSP26	sHSP with chaperone activity	FW: 5'-GGTTCCTGGTGTCAAAAGCAAG-3'
		RE: 5'-CTCTCTTCATTCAAGGTAGATGG-3'
HXT2	High-affinity glucose transporter of the major facilitator superfamily	FW: 5'-TCAACTTCGCATCCACTTTCG-3'
		RE: 5'-ATGGCCATGGAAGCAGAACC-3'
IME1	Master regulator of meiosis that is active only during meiotic events	RE: FW: 5'-CGTTGAAAAATCACCACCGCCA-3'
		RE: 5'-CTGAAGGAGTAAGCCGCAGCA-3'
IME2	Serine/threonine protein kinase involved in activation of meiosis	FW: 5'-ACGGCCTACGTTTCCACAAGAT-3'
		RE: 5'-CCACGCACCCGAATGCCCAA-3'
MCD4	Protein involved in GPI anchor synthesis	FW: 5'-TCAAAGATGGCGCTTCTGACC-3'
		RE: 5'-TCCAGCTCGATGGAAGATTGC-3'
MET14	Adenylylsulfate kinase	FW: 5'-CCATTAGAAGTCGCTGAGCAAAGG-3'
		RE: 5'-CGCTTCATATGGGGCAGAAATACC-3'
MND1	Protein required for recombination and meiotic nuclear division	FW: 5'-TGAAGACGGCGTCATTTCG-3'
		RE: 5'-CTCGCTTGAATCATACAATTTTTGC-3'
MRPL49	Mitochondrial ribosomal protein of the large subunit	FW: 5'-ACTTTAAAAGCAACCGTTGTTGG-3'
		RE: 5'-TCACCTTTACTCTTTGCATGACG-3'
MRPL6	Mitochondrial ribosomal protein of the large subunit	FW: 5'-CTTTTTCTGCGCTCTCAAGTGG-3'
		RE: 5'-TTTTCTGATAATCCTGGGCATGG-3'
MXR1	Methionine-S-sulfoxide reductase	FW: 5'-ACAGTATCGCAGTGGATTGTTCG-3'
		RE: 5'-GGCAATCTTATTACCCCATTTTGG-3'

Table 12 (continued).

MXR2	Methionine-R-sulfoxide reductase	FW: 5'-CCACTGAAAGGCCCAACACC-3'
		RE: 5'-TGGCCTTGCTCGAATACAACG-3'
OYE3	Conserved NADPH oxidoreductase containing FMN	FW: 5'-GCGGAACGATCGAAAACAGG-3'
		RE: 5'-GTACGGCGACAACCTCAAACC-3'
PHO89	Plasma membrane Na^+/Pi cotransporter	FW: 5'-TTCTGGCTTATGGTGGTGTTGC-3'
		RE: 5'-AGCCTCTTGATGGCGACTGC-3'
PIC2	Mitochondrial copper and phosphate carrier	FW: 5'-GTTTGTGGAATGGGTTAATGGTGAGAATTG-3'
		RE: 5'-TAACCGGTGGTTGGTAAGCCTACATAAG-3'
POR1	Mitochondrial porin (voltage-dependent anion channel)	FW: 5'-CGCCAATGGCATTAAGTTCTC-3'
		RE: 5'-CTTGTCATTCAACTTTGCTTCCAC-3'
POT1	3-ketoacyl-CoA thiolase with broad chain length specificity	FW: 5'-ACTGGCGCAAGGCAAGTAGC-3'
		RE: 5'-GCGGCACCCATACCAGTACC-3'
POX1	Fatty-acyl CoA oxidase	FW: 5'-CGCGTGGGTGTACACTTGG-3'
		RE: 5'-GGCACCTCTCTCCTGCAACC-3'
RIM4	Putative RNA-binding protein	FW: 5'-GGCAAAACATTTACAGGGCCAG-3'
		RE: 5'-GCTTTCCTGCTGGGATCCGC-3'
SPO1	Meiosis-specific prospore protein	FW: 5'-TGGATTATCAGGCGGAAGTTGG-3'
		RE: 5'-TCCTCTTCAAGGTCCCACTCTT-3'
SPO20	Meiosis-specific subunit of the t-SNARE complex	FW: 5'-AACGTAGCCGACCGAAAGATTG-3'
		RE: 5'-TCTGGTCTCGCTTTTCTCTCTC-3'
SSA4	Heat shock protein that is highly induced upon stress	FW: 5'-AATGGTAAAGAACCAAACCGTTC-3'
		RE: 5'-GACTGGTCACCCGTTAAGATG-3'
TSL1	Large subunit of trehalose 6-phosphate synthase/phosphatase complex	FW: 5'-CAAGGTTCGGCCTCCTCTGG-3'
		RE: 5'-ACGCTGTTTTGCAGCAGACG-3'
UBC6	Ubiquitin-conjugating enzyme involved in ERAD	FW: 5'-CAAGGGCGGTCAATATCACG-3'
		RE: 5'-GGGCTTGAAACGTCCATTCG-3'
VMA16	Subunit c'' of the vacuolar ATPase	FW: 5'-TTCTGGGCAGGTATCACTGTCG-3'
		RE: 5'-AATCAGCAGCATCGGAAATGG-3'

[a]SUMO, small ubiquitin-like modifier; v-SNARE, vesicle SNAP REceptor; ER, endoplasmic reticulum; sHSP, small heat shock protein; GPI, glycosylphosphatidylinositol; FMN, flavin mononucleotide; Pi, inorganic phosphate; CoA, coenzyme A; t-SNARE, target SNAP REceptor; ERAD, ER-associated protein degradation.

[b]FW, forward primer; RE, reverse primer.

Determination of respiratory capacity

Yeast cells were grown for 6 hours in 'inducing' selective minimal medium (2% galactose), harvested and washed twice prior measurements. Oxygen uptake was measured at 30°C using a Clark-type oxygen electrode in a 1 ml stirred chamber containing 1 ml of air-saturated respiration buffer (0.1 m phthalate–KOH, pH 5.0), 10 mM glucose (Oxygraph System Hansatech Instruments England) starting the reaction with the addition of 20 mg of wet weight of cells as previously described[331].

CONCLUSIONS AND FUTURE PERSPECTIVES

Despite progresses made in the last years, our understanding of the complex pathobiology of age-related NDs is still inadequate and treatments are not resolutive. In the present thesis work, I used *S. cerevisiae* to investigate the molecular basis of amyloid-associated toxicity and screen compounds able to rescue cellular viability.

Resorting to the inducible expression of the artificial polypeptide β23, I introduced a new model for AD, which was confirmed as a reliable model to reproduce toxic effects associated with oligomer formation from the human amyloid peptide $A\beta_{42}$.

Although Aβ-unrelated AD causative agents are being actively sought, within the so-called β-amyloid oligomer cascade hypothesis soluble amyloid oligomeric aggregates are considered the most neurotoxic species, responsible for various cytotoxic effects culminating in neuroinflammation and cognitive impairment. In spite of that, therapies have been mainly developed with the aim to inhibit amyloid fibril formation or to promote their dissolution and clearance, with potentially deleterious effects deriving from oligomer release. β23-based model proved to be a valuable tool to study intracellular cytotoxicity of prefibrillar β-oligomers and to select compounds specifically targeting these species.

Using a novel approach, I tested dietary polyphenolic compounds known for their antioxidant and neuroprotective properties not only as their plant precursors, but also, and especially, as the human metabolites generated by human phase II and gut microbial enzymes, which are the truly circulating species reaching the *in vivo* concentrations that could account for their beneficial effects.

Screenings in the AD-like model identified PVLs, the main circulating flavan-3-ol metabolites in humans, as a class of compounds able to increase cellular viability. The (4'-OH)-PVL metabolite proved to be particularly effective and displayed a selective anti-Aβ oligomer activity in both *in vivo* and *in vitro* experiments. (4'-OH)-PVL was devoid of effects on fibrils and able to prevent cognitive decline and neuroinflammation in an acute AD mouse model.

The molecular basis of this action are likely centred on oligomer remodelling and detoxification and preliminary *in silico* and *in vitro* data suggest that (4'-OH)-PVL (and some other PVL metabolites) could be able to cross the BBB, an important issue that needs to be addressed in perspective of a nutraceutical or pharmaceutical use of PVLs.

Other PVL metabolites (especially the sulfated derivatives) were nearly as effective as (4'-OH)-PVL and therefore their activity deserves to be more extensively investigated.
In future, it would be also interesting to evaluate differences linked to individual gut microbiota composition in the production of these compounds, several of which display an anti-microbial activity and can in turn contribute to determine microbiota composition. All the more so because gut dysbiosis may increase the permeability both of the intestine and of the BBB by stimulating the inflammatory response and growing evidences implicate the resident microbiota in the neurodegenerative process.
Besides an anti-oligomer action, other PVL activities are conceivable and should be explored in next experiments, possibly evaluating the modulation of specific pathways (e.g. the unfolded protein response or the oxidative stress response) following treatment with compounds.

Indeed, the second part of this PhD project concerned the transcriptomic analysis of four yeast ND models, which I performed from data obtained using the RNA-seq technology. This analysis revealed a fast and differential response of yeast cells to the expression of different amyloidogenic (poly)peptides that, despite their differences in sequence, size and physiological function, are able to form aggregates with remarkably similar structural features. The yeast response, which involved the transcriptional activation of the unfolded protein response and the onset of mitochondrial dysfunctions (associated with transcriptional response to ROS generation and mitochondrial network morphological changes), corroborated previous findings about the relevance of these pathways in NDs. Nevertheless, the comparative analysis of different models allowed me to highlight the different nature of the mitochondrial alterations that were detectable both in the AD-like and PD model, pointing in one case to an increased mitophagy, with a more severe loss of mitochondrial functionality, and in the other to an augmented mitochondrial fission process. The alteration of metal ion homeostasis evidenced the delicate equilibrium between the beneficial and detrimental action of essential metal ions and, more in general, the intersection between causative factors and pathological consequence of amyloid aggregation. Even if yeast does not have a homologue of the microtubule-associated protein tau, the downregulation of cytoskeleton- and cell-cycle-associated genes in the AD-like model suggests that the link between these processes and amyloid toxicity goes beyond the specific protein. Moreover, the dysregulation of genes involved

not only in mitosis but also in meiosis is index of a profound damage in the cell division process that has been found also in neurons undergoing neurodegeneration.

Future experiments will deeper investigate the role of proteins harbouring intrinsically disordered regions and stress granules, which recurrently emerged from our observations of the transcriptional changes, and will move forward with characterizing the involvement of different cellular components and pathways in amyloid toxicity.

ABBREVIATIONS

(4'-OH)-PVL, 5-(4'-hydroxyphenyl)-γ-valerolactone metabolite

3-HBA, 3-hydroxybenzoic acid

3-HPP, hydroxyphenylpropionic acid

AD, Alzheimer's disease

ADDL, Aβ-derived diffusible ligand

AFM, atomic force microscopy

ALS, amyotrophic lateral sclerosis

AMPA, amino-3-hydroxy-5-methyl-4-isoxazole

APOE, apolipoprotein E

APP, amyloid precursor protein

Aβ, amyloid-β peptide

AβO, amyloid-β oligomer

BBB, blood-brain barrier

CFP, cyan fluorescent protein

CNS, central nervous system

CQ, clioquinol

CSF, cerebrospinal fluid

DEG, differentially expressed gene

DMEM, Dulbecco's modified essential medium

EC, epicatechin

EC_{50}, half-maximal effective concentration

EGCG, (-)-epigallocatechin gallate

EGFP, enhanced green fluorescent protein

ER, endoplasmic reticulum

ESCRT, endosomal sorting complexes required for transport

FA, fatty acid

FC, fold change

FUS, FUsed in Sarcoma

GFP, green fluorescent protein

GO, gene ontology

GuHCl, guanidine hydrochloride

HC, hierarchical clustering

HD, Huntington's disease

Htt, huntingtin

ICV, intra-cerebroventricular

IDP, intrinsically disordered protein

IDR, intrinsically disordered region

LTP, long term potentiation

mAb, monoclonal antibody

mtDNA, mitochondrial DNA

mtRFP, mitochondria-directed red fluorescent protein

NAC, non-Aβ component

ND, neurodegenerative disease

NMDA, N-methyl-D-aspartate

NORT, novel object recognition test

ORF, open reading frame

OXPHOS, oxidative phosphorylation

PCA, principal component analysis

PD, Parkinson's disease

PEI, polyethylenimine

PICUP, photo-induced crosslinking of unmodified proteins

polyQ, polyglutamine

PRD, prolin-rich domain

PVL, phenyl-γ-valerolactone

qPCR, quantitative PCR

RBD, RNA-binding domain

RNA-seq, RNA-sequencing

ROS, oxygen reactive species

SD, synthetic defined dextrose

SEC, size-exclusion chromatography

SG, stress granule

SOD1, superoxide dismutase 1

TBS, Tris-buffered saline

TDP-43, TAR DNA-binding protein 43

TFA, trifluoroacetic acid

Tg, transgenic

Th-T, Thioflavin-T

Trx, thioredoxin

UPR, unfolded protein response

α-Syn, α-Synuclein

REFERENCES

1. Reeve, A., Simcox, E. & Turnbull, D. Ageing and Parkinson's disease: Why is advancing age the biggest risk factor? *Ageing Res. Rev.* **14**, 19–30 (2014).
2. Prince, M. *et al.* World Alzheimer Report 2015: The Global Impact of Dementia | Alzheimer's Disease International. *Alzheimer's Dis. Int. (ADI), London* 1–87 (2015).
3. United Nation. Ageing. Available at: https://www.un.org/en/sections/issues-depth/ageing/.
4. World Health Organization. Dementia. Available at: https://www.who.int/en/news-room/fact-sheets/detail/dementia.
5. Soto, C. & Pritzkow, S. Protein misfolding, aggregation, and conformational strains in neurodegenerative diseases. *Nat. Neurosci.* **21**, 1332–1340 (2018).
6. Soto, C. Unfolding the role of protein misfolding in neurodegenerative diseases. *Nat. Rev. Neurosci.* **4**, 49 (2003).
7. Gremer, L. *et al.* Fibril structure of amyloid- β(1-42) by cryoelectron microscopy. *Science* **358**, 116–119 (2017).
8. Haass, C. & Selkoe, D. J. Soluble protein oligomers in neurodegeneration: Lessons from the Alzheimer's amyloid β-peptide. *Nat. Rev. Mol. Cell Biol.* **8**, 101–112 (2007).
9. Cline, E. N., Bicca, M. A., Viola, K. L. & Klein, W. L. The Amyloid-β Oligomer Hypothesis: Beginning of the Third Decade. *J. Alzheimer's Dis.* **64**, S567–S610 (2018).
10. Chiti, F. & Dobson, C. M. Protein Misfolding, Functional Amyloid, and Human Disease. *Annu. Rev. Biochem.* **75**, 333–366 (2006).
11. Tenreiro, S., Munder, M. C., Alberti, S. & Outeiro, T. F. Harnessing the power of yeast to unravel the molecular basis of neurodegeneration. *J. Neurochem.* **127**, 438–52 (2013).
12. Sweeney, P. *et al.* Protein misfolding in neurodegenerative diseases: Implications and strategies. *Transl. Neurodegener.* **6**, 1–13 (2017).
13. Valastyan, J. S. & Lindquist, S. Mechanisms of protein-folding diseases at a glance. *Dis. Model. Mech.* **7**, 9–14 (2014).
14. Hartl, F. U. & Hayer-Hartl, M. Converging concepts of protein folding in vitro and in vivo. *Nat. Struct. Mol. Biol.* **16**, 574 (2009).

15. Fu, H., Hardy, J. & Duff, K. E. Selective vulnerability in neurodegenerative diseases. *Nat. Neurosci.* **21**, 1350–1358 (2018).
16. Drew, L. An age-old story of dementia. *Nature* **559**, S2 (2018).
17. Chen, G. F. *et al.* Amyloid beta: Structure, biology and structure-based therapeutic development. *Acta Pharmacol. Sin.* **38**, 1205–1235 (2017).
18. Kumar, D. *et al.* Amyloid-β Peptide Protects Against Microbial Infection In Mouse and Worm Models of Alzheimer's Disease. *Sci. Transl. Med.* **8**, 340ra72 (2016).
19. Steiner, H. & Haass, C. Intramembrane proteolysis by presenilins. *Nat. Rev. Mol. cell Biol.* **1**, 217 (2000).
20. Moreira, P. I., Carvalho, C., Zhu, X., Smith, M. A. & Perry, G. Mitochondrial dysfunction is a trigger of Alzheimer's disease pathophysiology. *Biochim. Biophys. Acta - Mol. Basis Dis.* **1802**, 2–10 (2010).
21. Brandt, R. & Bakota, L. Microtubule dynamics and the neurodegenerative triad of Alzheimer's disease: The hidden connection. *J. Neurochem.* **143**, 409–417 (2017).
22. Small, S. A., Simoes-Spassov, S., Mayeux, R. & Petsko, G. A. Endosomal Traffic Jams Represent a Pathogenic Hub and Therapeutic Target in Alzheimer's Disease. *Trends Neurosci.* **40**, 592–602 (2017).
23. Kanekiyo, T., Xu, H. & Bu, G. ApoE and Aβ in Alzheimer's disease: Accidental encounters or partners? *Neuron* **81**, 740–754 (2014).
24. Selkoe, D. J. & Hardy, J. The amyloid hypothesis of Alzheimer's disease at 25 years. *EMBO Mol. Med.* **8**, 595–608 (2016).
25. Elbaz, A., Carcaillon, L., Kab, S. & Moisan, F. Epidemiology of Parkinson's disease. *Rev. Neurol. (Paris).* **172**, 14–26 (2016).
26. Stefanis, L. α-Synuclein in Parkinson's Disease. *Cold Spring Harb. Perspect. Med.* **2**, a009399 (2012).
27. Lööv, C., Scherzer, C. R., Hyman, B. T., Breakefield, X. O. & Ingelsson, M. α-Synuclein in Extracellular Vesicles: Functional Implications and Diagnostic Opportunities. *Cell. Mol. Neurobiol.* **36**, 437–448 (2016).
28. Nakamura, K. *et al.* Direct membrane association drives mitochondrial fission by the Parkinson disease-associated protein α-synuclein. *J. Biol. Chem.* **286**, 20710–20726 (2011).
29. Lindersson, E. *et al.* Proteasomal Inhibition by α-Synuclein Filaments and

Oligomers. *J. Biol. Chem.* **279**, 12924–12934 (2004).

30. Ross, C. A. & Tabrizi, S. J. Huntington's disease: From molecular pathogenesis to clinical treatment. *Lancet Neurol.* **10**, 83–98 (2011).
31. Saudou, F. & Humbert, S. The Biology of Huntingtin. *Neuron* **89**, 910–926 (2016).
32. Arndt, J. R., Chaibva, M. & Legleiter, J. The emerging role of the first 17 amino acids of huntingtin in Huntington's disease. *Biomol. Concepts* **6**, 33–46 (2015).
33. Gusella, J. F. & MacDonald, M. E. Huntington's disease: the case for genetic modifiers. *Genome Med.* **1**, 80 (2009).
34. Valko, K. & Ciesla, L. Amyotrophic lateral sclerosis. *Prog. Med. Chem.* **58**, 63–117 (2019).
35. Couratier, P. *et al.* Epidemiology of amyotrophic lateral sclerosis: A review of literature. *Rev. Neurol. (Paris).* **172**, 37–45 (2016).
36. Chen-Plotkin, A. S., Lee, V. M. Y. & Trojanowski, J. Q. TAR DNA-binding protein 43 in neurodegenerative disease. *Nat. Rev. Neurol.* **6**, 211–220 (2010).
37. Lee, E. B., Lee, V. M. Y. & Trojanowski, J. Q. Gains or losses: Molecular mechanisms of TDP43-mediated neurodegeneration. *Nat. Rev. Neurosci.* **13**, 38–50 (2012).
38. Prasad, A., Bharathi, V., Sivalingam, V., Girdhar, A. & Patel, B. K. Molecular mechanisms of TDP-43 misfolding and pathology in amyotrophic lateral sclerosis. *Front. Mol. Neurosci.* **12**, 1–36 (2019).
39. Russo, A. *et al.* Increased cytoplasmic TDP-43 reduces global protein synthesis by interacting with Rack1 on polyribosomes. *Hum. Mol. Genet.* **26**, 1407–1418 (2017).
40. Amlie-Wolf, A. *et al.* Transcriptomic changes due to cytoplasmic TDP-43 expression reveal dysregulation of histone transcripts and nuclear chromatin. *PLoS One* **10**, 1–20 (2015).
41. Liu, G. *et al.* Endocytosis regulates TDP-43 toxicity and turnover. *Nat. Commun.* **8**, (2017).
42. Leibiger, C. *et al.* TDP-43 controls lysosomal pathways thereby determining its own clearance and cytotoxicity. *Hum. Mol. Genet.* **27**, 1593–1607 (2018).
43. Duan, W. *et al.* Mutant TAR DNA-binding protein-43 induces oxidative injury in motor neuron-like cell. *Neuroscience* **169**, 1621–1629 (2010).
44. Dang, T. N. T. *et al.* Increased metal content in the TDP-43A315T transgenic

mouse model of frontotemporal lobar degeneration and amyotrophic lateral sclerosis. *Front. Aging Neurosci.* **6**, 1–8 (2014).

45. Breydo, L. & Uversky, V. N. Structural, morphological, and functional diversity of amyloid oligomers. *FEBS Lett.* **589**, 2640–2648 (2015).
46. Lee, S. J. C., Nam, E., Lee, H. J., Savelieff, M. G. & Lim, M. H. Towards an understanding of amyloid-β oligomers: Characterization, toxicity mechanisms, and inhibitors. *Chem. Soc. Rev.* **46**, 310–323 (2017).
47. Terry, R. D. *et al.* Physical basis of cognitive alterations in Alzheimer's disease: synapse loss is the major correlate of cognitive impairment. *Ann. Neurol. Off. J. Am. Neurol. Assoc. Child Neurol. Soc.* **30**, 572–580 (1991).
48. Lambert, M. P. *et al.* Diffusible, nonfibrillar ligands derived from Aβ 1-42 are potent central nervous system neurotoxins. *Proc. Natl. Acad. Sci.* **95**, 6448–6453 (1998).
49. Balducci, C. *et al.* Synthetic amyloid-β oligomers impair long-term memory independently of cellular prion protein. *Proc. Natl. Acad. Sci.* **107**, 2295–2300 (2010).
50. Xiao, C. *et al.* Brain transit and ameliorative effects of intranasally delivered anti-amyloid-β oligomer antibody in 5XFAD mice. *J. Alzheimer's Dis.* **35**, 777–788 (2013).
51. Klyubin, I. *et al.* Amyloid β protein immunotherapy neutralizes Aβ oligomers that disrupt synaptic plasticity in vivo. *Nat. Med.* **11**, 556–561 (2005).
52. Lesné, S. *et al.* A specific amyloid-β protein assembly in the brain impairs memory. *Nature* **440**, 352–357 (2006).
53. Lesné, S. E. *et al.* Brain amyloid-β oligomers in ageing and Alzheimer's disease. *Brain* **136**, 1383–1398 (2013).
54. Amar, F. *et al.* The amyloid-beta oligomer Abeta*56 induces specific alterations in neuronal signaling that lead to tau phosphorylation and aggregation. *Sci. Signal.* **10**, (2017).
55. Gong, Y. *et al.* Alzheimer's disease-affected brain: Presence of oligomeric Aβ ligands (ADDLs) suggests a molecular basis for reversible memory loss. *Proc. Natl. Acad. Sci.* **100**, 10417–10422 (2003).
56. Kayed, R. *et al.* Common Structure of Soluble Amyloid Oligomers Implies Common Mechanism of Pathogenesis. *Science* **300**, 486–489 (2003).
57. Kayed, R. *et al.* Fibril specific, conformation dependent antibodies recognize a

generic epitope common to amyloid fibrils and fibrillar oligomers that is absent in prefibrillar oligomers. *Mol. Neurodegener.* **2**, 1–11 (2007).

58. Matsumura, S. *et al.* Two distinct amyloid β-protein (Aβ) assembly pathways leading to oligomers and fibrils identified by combined fluorescence correlation spectroscopy, morphology, and toxicity analyses. *J. Biol. Chem.* **286**, 11555–11562 (2011).
59. Necula, M., Kayed, R., Milton, S. & Glabe, C. G. Small molecule inhibitors of aggregation indicate that amyloid β oligomerization and fibrillization pathways are independent and distinct. *J. Biol. Chem.* **282**, 10311–10324 (2007).
60. Cohen, S. I. A. *et al.* Proliferation of amyloid-β42 aggregates occurs through a secondary nucleation mechanism. *Proc. Natl. Acad. Sci.* **110**, 9758–9763 (2013).
61. De, S. *et al.* Soluble aggregates present in cerebrospinal fluid change in size and mechanism of toxicity during Alzheimer's disease progression. *Acta Neuropathol. Commun.* **7**, 1–13 (2019).
62. Yang, T. *et al.* A highly sensitive novel immunoassay specifically detects low levels of soluble Aβ oligomers in human cerebrospinal fluid. *Alzheimer's Res. Ther.* **7**, 1–16 (2015).
63. Jin, M. *et al.* Soluble amyloid β-protein dimers isolated from Alzheimer cortex directly induce Tau hyperphosphorylation and neuritic degeneration. *Proc. Natl. Acad. Sci.* **108**, 5819–5824 (2011).
64. Bode, D. C., Baker, M. D. & Viles, J. H. Ion channel formation by amyloid-β42 oligomers but not amyloid-β40 in cellular membranes. *J. Biol. Chem.* **292**, 144–1413 (2017).
65. Snyder, E. M. *et al.* Regulation of NMDA receptor trafficking by amyloid-β. *Nat. Neurosci.* **8**, 1051–1058 (2005).
66. Zhao, W. Q. *et al.* Inhibition of calcineurin-mediated endocytosis and α-amino-3-hydroxy- 5-methyl-4-isoxazolepropionic acid (AMPA) receptors prevents amyloid β oligomer-induced synaptic disruption. *J. Biol. Chem.* **285**, 7619–7632 (2010).
67. Yang, W. N. *et al.* Mitogen-activated protein kinase signaling pathways are involved in regulating α7 nicotinic acetylcholine receptor-mediated amyloid-β uptake in SH-SY5Y cells. *Neuroscience* **278**, 276–290 (2014).
68. Esbjörner, E. K. *et al.* Direct observations of amyloid β Self-assembly in live cells provide insights into differences in the kinetics of Aβ(1-40) and Aβ(1-42)

aggregation. *Chem. Biol.* **21**, 732–742 (2014).

69. Zheng, L. *et al.* Intracellular localization of amyloid-β peptide in SH-SY5Y neuroblastoma cells. *J. Alzheimer's Dis.* **37**, 713–733 (2013).
70. Goldberg, M. S. & Lansbury Jr, P. T. Is there a cause-and-effect relationship between α-synuclein fibrillization and Parkinson's disease? *Nat. Cell Biol.* **2**, E115–E119 (2000).
71. Conway, K. A. *et al.* Acceleration of oligomerization, not fibrillization, is a shared property of both α-synuclein mutations linked to early-onset Parkinson's disease: Implications for pathogenesis and therapy. *Proc. Natl. Acad. Sci.* **97**, 571–576 (2000).
72. Winner, B. *et al.* In vivo demonstration that α-synuclein oligomers are toxic. *Proc. Natl. Acad. Sci.* **108**, 4194–4199 (2011).
73. Sivanesam, K. & Andersen, N. H. Modulating the Amyloidogenesis of alpha-Synuclein. *Curr. Neuropharmacol.* **14**, 226–237 (2016).
74. Conway, K. A., Rochet, J.-C., Bieganski, R. M. & Lansbury, P. T. Kinetic Stabilization of the α-Synuclein Protofibril by a Dopamine-α-Synuclein Adduct. *Science* **294**, 1346–1349 (2001).
75. Saudou, F., Finkbeiner, S., Devys, D. & Greenberg, M. E. Huntingtin Acts in the Nucleus to Induce Apoptosis but Death Does Not Correlate with the Formation of Intranuclear Inclusions. *Cell* **95**, 55–66 (1998).
76. Arrasate, M., Mitra, S., Schweitzer, E. S., Segal, M. R. & Finkbeiner, S. Inclusion body formation reduces levels of mutant huntingtin and the risk of neuronal death. *Nature* **431**, 805–810 (2004).
77. Fang, Y. *et al.* Full-length TDP-43 forms toxic amyloid oligomers that are present in frontotemporal lobar dementia-TDP patients. *Nat. Commun.* **5**, 1–13 (2014).
78. French, R. L. *et al.* Detection of TAR DNA-binding protein 43 (TDP-43) oligomers as initial intermediate species during aggregate formation. *J. Biol. Chem.* **294**, 6696–6709 (2019).
79. Bitan, G., Fradinger, E. A., Spring, S. M. & Teplow, D. B. Neurotoxic protein oligomers—what you see is not always what you get. *Amyloid* **12**, 88–95 (2005).
80. Pujol-Pina, R. *et al.* SDS-PAGE analysis of Aβ oligomers is disserving research into Alzheimer s disease: appealing for ESI-IM-MS. *Sci. Rep.* **5**, 14809 (2015).
81. Upadhaya, A. R., Lungrin, I., Yamaguchi, H., Fändrich, M. & Thal, D. R. High-

molecular weight Aβ oligomers and protofibrils are the predominant Aβ species in the native soluble protein fraction of the AD brain. *J. Cell. Mol. Med.* **16**, 287–295 (2012).

82. Pryor, N. E., Moss, M. A. & Hestekin, C. N. Unraveling the early events of amyloid-β protein (Aβ) aggregation: techniques for the determination of Aβ aggregate size. *Int. J. Mol. Sci.* **13**, 3038–3072 (2012).
83. Bitan, G. *et al.* Amyloid β-protein (Aβ) assembly: Aβ40 and Aβ42 oligomerize through distinct pathways. *Proc. Natl. Acad. Sci.* **100**, 330–335 (2003).
84. Ono, K., Condron, M. M. & Teplow, D. B. Structure–neurotoxicity relationships of amyloid β-protein oligomers. *Proc. Natl. Acad. Sci.* **106**, 14745–14750 (2009).
85. Hayden, E. Y., Conovaloff, J. L., Mason, A., Bitan, G. & Teplow, D. B. Preparation of pure populations of covalently stabilized amyloid β-protein oligomers of specific sizes. *Anal. Biochem.* **518**, 78–85 (2017).
86. Jan, A., Hartley, D. M. & Lashuel, H. A. Preparation and characterization of toxic Aβ aggregates for structural and functional studies in Alzheimer's disease research. *Nat. Protoc.* **5**, 1186 (2010).
87. Hodgson, J. Thousands of amyloids may foil Alzheimer's drugs. *Nat. Biotechnol.* **37**, 114–115 (2019).
88. Finder, V. H., Vodopivec, I., Nitsch, R. M. & Glockshuber, R. The recombinant amyloid-β peptide Aβ1–42 aggregates faster and is more neurotoxic than synthetic Aβ1–42. *J. Mol. Biol.* **396**, 9–18 (2010).
89. Pereira, C., Bessa, C., Soares, J., Leo, M. & Saraiva, L. Contribution of yeast models to neurodegeneration research. *J. Biomed. Biotechnol.* **2012**, (2012).
90. Matlack, K. E. S. *et al.* Clioquinol promotes the degradation of metal-dependent amyloid-β (Aβ) oligomers to restore endocytosis and ameliorate Aβ toxicity. *Proc. Natl. Acad. Sci.* **111**, 4013–8 (2014).
91. Bagriantsev, S. & Liebman, S. Modulation of Aβ 42 low-n oligomerization using a novel yeast reporter system. *BMC Biol.* **4**, 32 (2006).
92. Pearce, D. A. & Sherman, F. A yeast model for the study of Batten disease. *Proc. Natl. Acad. Sci.* **95**, 6915–6918 (1998).
93. Babcock, M. *et al.* Regulation of mitochondrial iron accumulation by Yfh1p, a putative homolog of frataxin. *Science* **276**, 1709–1712 (1997).
94. Wilson, R. B. & Roof, D. M. Respiratory deficiency due to loss of mitochondrial

DNA in yeast lacking the frataxin homologue. *Nat. Genet.* **16**, 352 (1997).

95. Sanchez, Y. *et al.* Regulation of RAD53 by the ATM-like kinases MEC1 and TEL1 in yeast cell cycle checkpoint pathways. *Science (80-.).* **271**, 357–360 (1996).
96. Fritz, E., Friedl, A. A., Zwacka, R. M., Eckardt-Schupp, F. & Meyn, M. S. The yeast TEL1 gene partially substitutes for human ATM in suppressing hyperrecombination, radiation-induced apoptosis and telomere shortening in AT cells. *Mol. Biol. Cell* **11**, 2605–2616 (2000).
97. Zhang, S. *et al.* Ncr1p, the yeast ortholog of mammalian Niemann Pick C1 protein, is dispensable for endocytic transport. *Traffic* **5**, 1017–1030 (2004).
98. Berger, A. C., Hanson, P. K., Wylie Nichols, J. & Corbett, A. H. A yeast model system for functional analysis of the Niemann–Pick type C protein 1 homolog, Ncr1p. *Traffic* **6**, 907–917 (2005).
99. Nolden, M. *et al.* The m-AAA protease defective in hereditary spastic paraplegia controls ribosome assembly in mitochondria. *Cell* **123**, 277–289 (2005).
100. Nishida, C. R., Gralla, E. B. & Valentine, J. S. Characterization of three yeast copper-zinc superoxide dismutase mutants analogous to those coded for in familial amyotrophic lateral sclerosis. *Proc. Natl. Acad. Sci. U. S. A.* **91**, 9906–9910 (1994).
101. Bach, S. *et al.* Isolation of drugs active against mammalian prions using a yeast-based screening assay. *Nat. Biotechnol.* **21**, 1075 (2003).
102. Apodaca, J., Kim, I. & Rao, H. Cellular tolerance of prion protein PrP in yeast involves proteolysis and the unfolded protein response. *Biochem. Biophys. Res. Commun.* **347**, 319–326 (2006).
103. Ma, J. & Lindquist, S. De novo generation of a PrP Sc-like conformation in living cells. *Nat. Cell Biol.* **1**, 358 (1999).
104. Tank, E. M. H., Harris, D. A., Desai, A. A. & True, H. L. Prion protein repeat expansion results in increased aggregation and reveals phenotypic variability. *Mol. Cell. Biol.* **27**, 5445–5455 (2007).
105. Johnson, B. S., McCaffery, J. M., Lindquist, S. & Gitler, A. D. A yeast TDP-43 proteinopathy model: Exploring the molecular determinants of TDP-43 aggregation and cellular toxicity. *Proc. Natl. Acad. Sci.* **105**, 6439–44 (2008).
106. Fushimi, K. *et al.* Expression of human FUS/TLS in yeast leads to protein aggregation and cytotoxicity, recapitulating key features of FUS proteinopathy.

Protein Cell **2**, 141–149 (2011).

107. Ju, S. *et al.* A Yeast Model of FUS/TLS-Dependent Cytotoxicity. *PLoS Biol.* **9**, (2011).
108. Outeiro, T. F. & Lindquist, S. Yeast cells provide insight into alpha-synuclein biology and pathobiology. *Science* **302**, 1772–1775 (2003).
109. Cooper, A. A. *et al.* α-Synuclein Blocks ER-Golgi Traffic and Rab1 Rescues Neuron Loss in Parkinson's Models. *Science (80-.).* **313**, 324–328 (2006).
110. Chen, Q., Thorpe, J. & Keller, J. N. α-synuclein alters proteasome function, protein synthesis, and stationary phase viability. *J. Biol. Chem.* **280**, 30009–30017 (2005).
111. Dixon, C., Mathias, N., Zweig, R. M., Davis, D. A. & Gross, D. S. Alpha-synuclein targets the plasma membrane via the secretory pathway and induces toxicity in yeast. *Genetics* **170**, 47–59 (2005).
112. Sharma, N. *et al.* α-synuclein budding yeast model. *J. Mol. Neurosci.* **28**, 161–178 (2006).
113. Flower, T. R., Chesnokova, L. S., Froelich, C. A., Dixon, C. & Witt, S. N. Heat Shock Prevents Alpha-synuclein-induced Apoptosis in a Yeast Model of Parkinson's Disease. *J. Mol. Biol.* **351**, 1081–1100 (2005).
114. Xiong, Y. *et al.* GTPase activity plays a key role in the pathobiology of LRRK2. *PLoS Genet.* **6**, e1000902 (2010).
115. Chacińska, A. *et al.* Effects of beta-amyloid on proliferation and morphology of yeast Saccharomyces cerevisiae. *Lett. Pept. Sci.* **9**, 197–201 (2002).
116. Zhang, H., Komano, H., Fuller, R. S., Gandy, S. E. & Frail, D. E. Proteolytic processing and secretion of human beta-amyloid precursor protein in yeast. Evidence for a yeast secretase activity. *J. Biol. Chem.* **269**, 27799–27802 (1994).
117. Caine, J. *et al.* Alzheimer's Aβ fused to green fluorescent protein induces growth stress and a heat shock response. *FEMS Yeast Res.* **7**, 1230–1236 (2007).
118. Von Der Haar, T., Jossé, L., Wright, P., Zenthon, J. & Tuite, M. F. Development of a novel yeast cell-based system for studying the aggregation of Alzheimer's disease-associated Aβ peptides in vivo. *Neurodegener. Dis.* **4**, 136–147 (2007).
119. Middendorp, O., Lüthi, U., Hausch, F. & Barberis, A. Searching for the most effective screening system to identify cell-active inhibitors of β-secretase. *Biological Chemistry* **385**, 481 (2004).
120. Treusch, S. *et al.* Functional Links Between Aβ Toxicity, Endocytic Trafficking,

and Alzheimer's Disease Risk Factors in Yeast. *Science* **334**, 1241–1245 (2011).

121. Vandebroek, T., Terwel, D., Van Helmont, T., Winderickx, J. & Van Leuven, F. Phosphorylation and aggregation of protein tau in humanized yeast cells and in transgenic mouse brain. *New Trends Alzheimer Park. Relat. Disord.* **256**, 15–19 (2005).
122. Krobitsch, S. & Lindquist, S. Aggregation of huntingtin in yeast varies with the length of the polyglutamine expansion and the expression of chaperone proteins. *Proc. Natl. Acad. Sci.* **97**, 1589–1594 (2000).
123. Meriin, A. B. *et al.* Huntingtin toxicity in yeast model depends on polyglutamine aggregation mediated by a prion-like protein Rnq1. *J. Cell Biol.* **157**, 997–1004 (2002).
124. LaFerla, F. M., Green, K. N. & Oddo, S. Intracellular amyloid-β in Alzheimer's disease. *Nature Reviews Neuroscience* **8**, 499–509 (2007).
125. Bharadwaj, P., Waddington, L., Varghese, J. & Macreadie, I. G. A new method to measure cellular toxicity of non-fibrillar and fibrillar Alzheimer's Abeta using yeast. *J. Alzheimers. Dis.* **13**, 147–150 (2008).
126. Luu, Y. & Macreadie, I. Development of convenient system for detecting yeast cell stress, including that of amyloid beta. *Int. J. Mol. Sci.* **19**, 2136 (2018).
127. Vetrivel, K. S. & Thinakaran, G. Amyloidogenic processing of β-amyloid precursor protein in intracellular compartments. *Neurology* **66**, S69–S73 (2006).
128. Suzuki, T., Araki, Y., Yamamoto, T. & Nakaya, T. Trafficking of Alzheimer's Disease–Related Membrane Proteins and Its Participation in Disease Pathogenesis. *J. Biochem.* **139**, 949–955 (2006).
129. Glabe, C. Intracellular mechanisms of amyloid accumulation and pathogenesis in Alzheimer's disease. *J. Mol. Neurosci.* **17**, 137–145 (2001).
130. D'Angelo, F. *et al.* A yeast model for amyloid-β aggregation exemplifies the role of membrane trafficking and PICALM in cytotoxicity. *Dis. Model. Mech.* **6**, 206–216 (2013).
131. Villar-Piqué, A. & Ventura, S. Protein aggregation propensity is a crucial determinant of intracellular inclusion formation and quality control degradation. *Biochim. Biophys. Acta (BBA)-Molecular Cell Res.* **1833**, 2714–2724 (2013).
132. Macreadie, I. *et al.* Validation of folate in a convenient yeast assay suited for identification of inhibitors of Alzheimer's amyloid-beta aggregation. *J. Alzheimers.*

Dis. **15**, 391–396 (2008).

133. Wurth, C., Guimard, N. K. & Hecht, M. H. Mutations that reduce aggregation of the Alzheimer's Aβ42 peptide: an unbiased search for the sequence determinants of Aβ amyloidogenesis. *J. Mol. Biol.* **319**, 1279–1290 (2002).
134. Kim, W. *et al.* A high-throughput screen for compounds that inhibit aggregation of the Alzheimer's peptide. *ACS Chem. Biol.* **1**, 461–469 (2006).
135. Nair, S., Traini, M., Dawes, I. W. & Perrone, G. G. Genome-wide analysis of Saccharomyces cerevisiae identifies cellular processes affecting intracellular aggregation of Alzheimer's amyloid-β42: importance of lipid homeostasis. *Mol. Biol. Cell* **25**, 2235–2249 (2014).
136. Porzoor, A. *et al.* Anti-amyloidogenic properties of some phenolic compounds. *Biomolecules* **5**, 505–527 (2015).
137. Dhakal, S., Subhan, M., Fraser, J. M., Gardiner, K. & Macreadie, I. Simvastatin Efficiently Reduces Levels of Alzheimer's Amyloid Beta in Yeast. *Int. J. Mol. Sci.* **20**, 3531 (2019).
138. Park, S.-K. *et al.* Development and validation of a yeast high-throughput screen for inhibitors of Aβ42 oligomerization. *Dis. Model. Mech.* **4**, 822–831 (2011).
139. Park, S.-K., Ratia, K., Ba, M., Valencik, M. & Liebman, S. W. Inhibition of Aβ42 oligomerization in yeast by a PICALM ortholog and certain FDA approved drugs. *Microb. Cell* **3**, 53 (2016).
140. Chen, X. & Petranovic, D. Amyloid-β peptide-induced cytotoxicity and mitochondrial dysfunction in yeast. *FEMS Yeast Res.* **15**, (2015).
141. Chen, X. *et al.* Interplay of energetics and ER stress exacerbates Alzheimer's amyloid-β (Aβ) toxicity in yeast. *Front. Mol. Neurosci.* **10**, 232 (2017).
142. Fruhmann, G. *et al.* The impact of ESCRT on Aβ1-42 induced membrane lesions in a yeast model for Alzheimer's disease. *Front. Mol. Neurosci.* **11**, 406 (2018).
143. Verduyckt, M. *et al.* Yeast as a model for Alzheimer's disease: latest studies and advanced strategies. in *Systems Biology of Alzheimer's Disease* 197–215 (Springer, 2016).
144. Forloni, G. & Balducci, C. Alzheimer's disease, oligomers, and inflammation. *J. Alzheimer's Dis.* **62**, 1261–1276 (2018).
145. Hara, H. *et al.* An Oral Aβ Vaccine Using a Recombinant Adeno-Associated Virus Vector in Aged Monkeys: Reduction in Plaque Amyloid and Increase in Aβ

Oligomers. *J. Alzheimer's Dis.* **54**, 1047–1059 (2016).

146. Panza, F., Lozupone, M., Logroscino, G. & Imbimbo, B. P. A critical appraisal of amyloid-β-targeting therapies for Alzheimer disease. *Nat. Rev. Neurol.* **15**, 73–88 (2019).
147. Grant, W. B. Using Multicountry Ecological and Observational Studies to Determine Dietary Risk Factors for Alzheimer's Disease. *J. Am. Coll. Nutr.* **35**, 476–489 (2016).
148. Knekt, P. *et al.* Flavonoid intake and risk of chronic diseases. *Am. J. Clin. Nutr.* **76**, 560–568 (2002).
149. Bondonno, N. P. *et al.* Flavonoid intake is associated with lower mortality in the Danish Diet Cancer and Health Cohort. *Nat. Commun.* **10**, 1–10 (2019).
150. Ehrnhoefer, D. E. *et al.* EGCG redirects amyloidogenic polypeptides into unstructured, off-pathway oligomers. *Nat. Struct. Mol. Biol.* **15**, 558–566 (2008).
151. Bieschke, J. *et al.* EGCG remodels mature α-synuclein and amyloid-β fibrils and reduces cellular toxicity. *PNAS* **107**, 7710–7715 (2010).
152. Ladiwala, A. R. A. *et al.* Polyphenolic Glycosides and Aglycones Utilize Opposing Pathways To Selectively Remodel and Inactivate Toxic Oligomers of Amyloid β. *ChemBioChem* **12**, 1749–1758 (2011).
153. Wang, J. *et al.* Brain-Targeted Proanthocyanidin Metabolites for Alzheimer's Disease Treatment. *J. Neurosci.* **32**, 5144–5150 (2012).
154. Nehlig, A. The neuroprotective effects of cocoa flavanol and its influence on cognitive performance. *Br. J. Clin. Pharmacol.* **75**, 716–727 (2013).
155. Dubner, L., Wang, J., Ho, L., Ward, L. & Pasinetti, G. M. Recommendations for development of new standardized forms of cocoa breeds and cocoa extract processing for the prevention of Alzheimer's disease: Role of cocoa in promotion of cognitive resilience and healthy brain aging. *J. Alzheimer's Dis.* **48**, 879–889 (2015).
156. Moreira, A., Diógenes, M. J., De Mendonça, A., Lunet, N. & Barros, H. Chocolate Consumption is Associated with a Lower Risk of Cognitive Decline. *J. Alzheimer's Dis.* **53**, 85–93 (2016).
157. Socci, V., Tempesta, D., Desideri, G., De Gennaro, L. & Ferrara, M. Enhancing Human Cognition with Cocoa Flavonoids. *Front. Nutr.* **4**, 1–7 (2017).
158. Mena, P. *et al.* Phenyl-γ-valerolactones and phenylvaleric acids, the main colonic

metabolites of flavan-3-ols: Synthesis, analysis, bioavailability, and bioactivity. *Nat. Prod. Rep.* **36**, 714–752 (2019).

159. Jaeger, B. N., Parylak, S. L. & Gage, F. H. Mechanisms of dietary flavonoid action in neuronal function and neuroinflammation. *Mol. Aspects Med.* **61**, 50–62 (2018).
160. Takagaki, A., Otani, S. & Nanjo, F. Antioxidative Activity of Microbial Metabolites of (−)-Epigallocatechin Gallate Produced in Rat Intestines. *Biosci. Biotechnol. Biochem.* **75**, 582–585 (2011).
161. Unno, K. *et al.* Blood–Brain Barrier Permeability of Green Tea Catechin Metabolites and their Neuritogenic Activity in Human Neuroblastoma SH-SY5Y Cells. *Mol. Nutr. Food Res.* **61**, 1–7 (2017).
162. Brickman, A. M. *et al.* Enhancing dentate gyrus function with dietary flavanols improves cognition in older adults. *Nat. Neurosci.* **17**, 1798–1803 (2014).
163. Wang, D. *et al.* Role of intestinal microbiota in the generation of polyphenol derived phenolic acid mediated attenuation of Alzheimer's disease β-amyloid oligomerization. *Mol. Nutr. Food Res.* **59**, 1025–1040 (2015).
164. Del Rio, D. *et al.* Bioavailability and catabolism of green tea flavan-3-ols in humans. *Nutrition* **26**, 1110–1116 (2010).
165. Ottaviani, J. I. *et al.* The metabolome of [2-14C](-)-epicatechin in humans: Implications for the assessment of efficacy, safety, and mechanisms of action of polyphenolic bioactives. *Sci. Rep.* **6**, 1–10 (2016).
166. Ottaviani, J. I. *et al.* Evaluation at scale of microbiome-derived metabolites as biomarker of flavan-3-ol intake in epidemiological studies. *Sci. Rep.* **8**, 1–11 (2018).
167. Borges, G., Ottaviani, J. I., van der Hooft, J. J. J., Schroeter, H. & Crozier, A. Absorption, metabolism, distribution and excretion of (−)-epicatechin: A review of recent findings. *Mol. Aspects Med.* **61**, 18–30 (2018).
168. Brindani, N. *et al.* Synthetic and analytical strategies for the quantification of phenyl-γ-valerolactone conjugated metabolites in human urine. *Mol. Nutr. Food Res.* **61**, 6–10 (2017).
169. Dal-Pan, A. *et al.* Cognitive-enhancing effects of a polyphenols-rich extract from fruits without changes in neuropathology in an animal model of Alzheimer's disease. *J. Alzheimer's Dis.* **55**, 115–135 (2017).
170. Palhano, F. L., Lee, J., Grimster, N. P. & Kelly, J. W. Toward the molecular

mechanism (s) by which EGCG treatment remodels mature amyloid fibrils. *J. Am. Chem. Soc.* **135**, 7503–7510 (2013).

171. Hyung, S.-J. *et al.* Insights into antiamyloidogenic properties of the green tea extract (−)-epigallocatechin-3-gallate toward metal-associated amyloid-β species. *Proc. Natl. Acad. Sci.* **110**, 3743–3748 (2013).
172. Rezai-Zadeh, K. *et al.* Green tea epigallocatechin-3-gallate (EGCG) modulates amyloid precursor protein cleavage and reduces cerebral amyloidosis in Alzheimer transgenic mice. *J. Neurosci.* **25**, 8807–8814 (2005).
173. Rezai-Zadeh, K. *et al.* Green tea epigallocatechin-3-gallate (EGCG) reduces β-amyloid mediated cognitive impairment and modulates tau pathology in Alzheimer transgenic mice. *Brain Res.* **1214**, 177–187 (2008).
174. Choi, Y.-T. *et al.* The green tea polyphenol (−)-epigallocatechin gallate attenuates β-amyloid-induced neurotoxicity in cultured hippocampal neurons. *Life Sci.* **70**, 603–614 (2001).
175. Reznichenko, L. *et al.* Reduction of iron-regulated amyloid precursor protein and β-amyloid peptide by (–)-epigallocatechin-3-gallate in cell cultures: implications for iron chelation in Alzheimer's disease. *J. Neurochem.* **97**, 527–536 (2006).
176. Bastianetto, S., Yao, Z., Papadopoulos, V. & Quirion, R. Neuroprotective effects of green and black teas and their catechin gallate esters against β-amyloid-induced toxicity. *Eur. J. Neurosci.* **23**, 55–64 (2006).
177. Ortiz-López, L. *et al.* Green tea compound epigallo-catechin-3-gallate (EGCG) increases neuronal survival in adult hippocampal neurogenesis in vivo and in vitro. *Neuroscience* **322**, 208–220 (2016).
178. Yamamoto, N. *et al.* Epigallocatechin gallate induces extracellular degradation of amyloid β-protein by increasing neprilysin secretion from astrocytes through activation of ERK and PI3K pathways. *Neuroscience* **362**, 70–78 (2017).
179. Chang, X. *et al.* (−)-Epigallocatechin-3-gallate attenuates cognitive deterioration in Alzheimer′ s disease model mice by upregulating neprilysin expression. *Exp. Cell Res.* **334**, 136–145 (2015).
180. Sul, D. *et al.* Protective effect of caffeic acid against beta-amyloid-induced neurotoxicity by the inhibition of calcium influx and tau phosphorylation. *Life Sci.* **84**, 257–262 (2009).
181. Oboh, G., Agunloye, O. M., Akinyemi, A. J., Ademiluyi, A. O. & Adefegha, S. A.

Comparative study on the inhibitory effect of caffeic and chlorogenic acids on key enzymes linked to Alzheimer's disease and some pro-oxidant induced oxidative stress in rats' brain-in vitro. *Neurochem. Res.* **38**, 413–419 (2013).

182. Yan, J. *et al.* Protection against β-amyloid peptide toxicity in vivo with long-term administration of ferulic acid. *Br. J. Pharmacol.* **133**, 89–96 (2001).
183. Ono, K., Hirohata, M. & Yamada, M. Ferulic acid destabilizes preformed β-amyloid fibrils in vitro. *Biochem. Biophys. Res. Commun.* **336**, 444–449 (2005).
184. Bramanti, E., Fulgentini, L., Bizzarri, R., Lenci, F. & Sgarbossa, A. β-Amyloid amorphous aggregates induced by the small natural molecule ferulic acid. *J. Phys. Chem. B* **117**, 13816–13821 (2013).
185. Meng, G. *et al.* Application of ferulic acid for Alzheimer's disease: combination of text mining and experimental validation. *Front. Neuroinform.* **12**, 31 (2018).
186. Picone, P. *et al.* Ferulic acid inhibits oxidative stress and cell death induced by Ab oligomers: improved delivery by solid lipid nanoparticles. *Free Radic. Res.* **43**, 1133–1145 (2009).
187. Mori, T., Koyama, N., Guillot-Sestier, M.-V., Tan, J. & Town, T. Ferulic acid is a nutraceutical β-secretase modulator that improves behavioral impairment and alzheimer-like pathology in transgenic mice. *PLoS One* **8**, e55774 (2013).
188. Kim, H.-S. *et al.* Inhibitory effects of long-term administration of ferulic acid on microglial activation induced by intracerebroventricular injection of β-amyloid peptide (1—42) in mice. *Biol. Pharm. Bull.* **27**, 120–121 (2004).
189. Ono, K. *et al.* Phenolic compounds prevent amyloid β-protein oligomerization and synaptic dysfunction by site-specific binding. *J. Biol. Chem.* **287**, 14631–43 (2012).
190. Cui, L. *et al.* Ferulic Acid Inhibits the Transition of Amyloid-β 42 Monomers to Oligomers but Accelerates the Transition from Oligomers to Fibrils. *J. Alzheimer's Dis.* **37**, 19–28 (2013).
191. Cho, J.-Y. *et al.* Inhibitory effects of long-term administration of ferulic acid on astrocyte activation induced by intracerebroventricular injection of β-amyloid peptide (1–42) in mice. *Prog. Neuro-Psychopharmacology Biol. Psychiatry* **29**, 901–907 (2005).
192. Yan, J.-J. *et al.* Protective effects of ferulic acid in amyloid precursor protein plus presenilin-1 transgenic mouse model of Alzheimer disease. *Biol. Pharm. Bull.* **36**,

140–143 (2013).

193. Szwajgier, D. Inhibition of cholinesterases by phenolic acids detected in beer: A dose-response model approach. *African J. Biotechnol.* **12**, 1675–1681 (2013).
194. Jagota, S. & Rajadas, J. Effect of phenolic compounds against Aβ aggregation and Aβ-induced toxicity in transgenic C. elegans. *Neurochem. Res.* **37**, 40–48 (2012).
195. Verzelloni, E. *et al.* Antiglycative and neuroprotective activity of colon-derived polyphenol catabolites. *Mol. Nutr. Food Res.* **55**, S35–S43 (2011).
196. Yuan, T. *et al.* Pomegranate's Neuroprotective Effects against Alzheimer's Disease Are Mediated by Urolithins, Its Ellagitannin-Gut Microbial Derived Metabolites. *ACS Chem. Neurosci.* **7**, 26–33 (2016).
197. West, M. W. *et al.* De novo amyloid proteins from designed combinatorial libraries. *Proc. Natl. Acad. Sci. U. S. A.* **96**, 11211–11216 (1999).
198. Olzscha, H. *et al.* Amyloid-like aggregates sequester numerous metastable proteins with essential cellular functions. *Cell* **144**, 67–78 (2011).
199. Nilsberth, C. *et al.* The'Arctic'APP mutation (E693G) causes Alzheimer's disease by enhanced Aβ protofibril formation. *Nat. Neurosci.* **4**, 887 (2001).
200. Adlard, P. A. *et al.* Rapid restoration of cognition in Alzheimer's transgenic mice with 8-hydroxy quinoline analogs is associated with decreased interstitial Aβ. *Neuron* **59**, 43–55 (2008).
201. LeVine III, H., Ding, Q., Walker, J. A., Voss, R. S. & Augelli-Szafran, C. E. Clioquinol and other hydroxyquinoline derivatives inhibit Aβ (1–42) oligomer assembly. *Neurosci. Lett.* **465**, 99–103 (2009).
202. Grossi, C. *et al.* Clioquinol decreases amyloid-β burden and reduces working memory impairment in a transgenic mouse model of Alzheimer's disease. *J. Alzheimer's Dis.* **17**, 423–440 (2009).
203. Ryan, T. M. *et al.* Stabilization of nontoxic Aβ-oligomers: insights into the mechanism of action of hydroxyquinolines in Alzheimer's disease. *J. Neurosci.* **35**, 2871–2884 (2015).
204. Qin, X.-Y., Cheng, Y. & Yu, L.-C. Potential protection of green tea polyphenols against intracellular amyloid beta-induced toxicity on primary cultured prefrontal cortical neurons of rats. *Neurosci. Lett.* **513**, 170–173 (2012).
205. Espín, J. C., Larrosa, M., García-Conesa, M. T. & Tomás-Barberán, F. Biological

significance of urolithins, the gut microbial ellagic acid-derived metabolites: the evidence so far. *Evidence-Based Complement. Altern. Med.* **2013**, (2013).

206. Xu, J. *et al.* Urolithins Attenuate LPS-Induced Neuroinflammation in BV2Microglia via MAPK, Akt, and NF-κB Signaling Pathways. *J. Agric. Food Chem.* **66**, 571–580 (2018).
207. Lee, G., Park, J. S., Lee, E. J., Ahn, J. H. & Kim, H. S. Anti-inflammatory and antioxidant mechanisms of urolithin B in activated microglia. *Phytomedicine* **55**, 50–57 (2019).
208. Ladiwala, A. R. A. *et al.* Resveratrol selectively remodels soluble oligomers and fibrils of amyloid Aβ into off-pathway conformers. *J. Biol. Chem.* **285**, 24228–24237 (2010).
209. Balducci, C. *et al.* Toll-like receptor 4-dependent glial cell activation mediates the impairment in memory establishment induced by β-amyloid oligomers in an acute mouse model of Alzheimer's disease. *Brain. Behav. Immun.* **60**, 188–197 (2017).
210. Heneka, M. T. *et al.* Neuroinflammation in Alzheimer's disease. *Lancet Neurol.* **14**, 388–405 (2015).
211. Xiong, H., Buckwalter, B. L., Shieh, H.-M. & Hecht, M. H. Periodicity of polar and nonpolar amino acids is the major determinant of secondary structure in self-assembling oligomeric peptides. *Proc. Natl. Acad. Sci.* **92**, 6349–6353 (1995).
212. Wang, Z.-X., Tan, L., Liu, J. & Yu, J.-T. The essential role of soluble Aβ oligomers in Alzheimer's disease. *Mol. Neurobiol.* **53**, 1905–1924 (2016).
213. Chafekar, S. M., Baas, F. & Scheper, W. Oligomer-specific Aβ toxicity in cell models is mediated by selective uptake. *Biochim. Biophys. Acta (BBA)-Molecular Basis Dis.* **1782**, 523–531 (2008).
214. Umeda, T. *et al.* Intraneuronal amyloid β oligomers cause cell death via endoplasmic reticulum stress, endosomal/lysosomal leakage, and mitochondrial dysfunction in vivo. *J. Neurosci. Res.* **89**, 1031–1042 (2011).
215. Lee, M.-H. *et al.* Somatic APP gene recombination in Alzheimer's disease and normal neurons. *Nature* **563**, 639 (2018).
216. Lee, C. C. *et al.* 5-(3′, 4′-Dihydroxyphenyl-γ-valerolactone), a major microbial metabolite of proanthocyanidin, attenuates THP-1 monocyte-endothelial adhesion. *Int. J. Mol. Sci.* **18**, 1363 (2017).
217. Kitazawa, M., Oddo, S., Yamasaki, T. R., Green, K. N. & LaFerla, F. M.

Lipopolysaccharide-induced inflammation exacerbates tau pathology by a cyclin-dependent kinase 5-mediated pathway in a transgenic model of Alzheimer's disease. *J. Neurosci.* **25**, 8843–8853 (2005).

218. Gimenez-Llort, L. *et al.* Modeling behavioral and neuronal symptoms of Alzheimer's disease in mice: a role for intraneuronal amyloid. *Neurosci. Biobehav. Rev.* **31**, 125–147 (2007).
219. Nortley, R. *et al.* Amyloid beta oligomers constrict human capillaries in Alzheimer's disease via signaling to pericytes. *Science* **9518**, (2019).
220. Pasinetti, G. M. *et al.* The role of the gut microbiota in the metabolism of polyphenols as characterized by gnotobiotic mice. *J. Alzheimer's Dis.* **63**, 409–421 (2018).
221. Steinmann, J., Buer, J., Pietschmann, T. & Steinmann, E. Anti-infective properties of epigallocatechin-3-gallate (EGCG), a component of green tea. *Br. J. Pharmacol.* **168**, 1059–1073 (2013).
222. Koutsos, A., Tuohy, K. M. & Lovegrove, J. A. Apples and cardiovascular health—is the gut microbiota a core consideration? *Nutrients* **7**, 3959–3998 (2015).
223. Espín, J. C., González-Sarrías, A. & Tomás-Barberán, F. A. The gut microbiota: A key factor in the therapeutic effects of (poly)phenols. *Biochem. Pharmacol.* **139**, 82–93 (2017).
224. Cardona, F., Andrés-Lacueva, C., Tulipani, S., Tinahones, F. J. & Queipo-Ortuño, M. I. Benefits of polyphenols on gut microbiota and implications in human health. *J. Nutr. Biochem.* **24**, 1415–1422 (2013).
225. Curti, C. *et al.* Catalytic, Enantioselective Vinylogous Mukaiyama Aldol Reaction of Furan-Based Dienoxy Silanes: A Chemodivergent Approach to γ-Valerolactone Flavan-3-ol Metabolites and δ-Lactone Analogues. *Adv. Synth. Catal.* **357**, 4082–4092 (2015).
226. Moretto, N. *et al.* Conformation-sensitive antibodies against Alzheimer amyloid-β by immunization with a thioredoxin-constrained B-cell epitope peptide. *J. Biol. Chem.* **282**, 11436–11445 (2007).
227. Levati, E., Sartini, S., Bolchi, A., Ottonello, S. & Montanini, B. Moonlighting transcriptional activation function of a fungal sulfur metabolism enzyme. *Sci. Rep.* **6**, 25165 (2016).
228. Higuchi, R., Krummel, B. & Saiki, R. A general method of in vitro preparation and

specific mutagenesis of DNA fragments: study of protein and DNA interactions. *Nucleic Acids Res.* **16**, 7351–7367 (1988).

229. Ito, H., Fukuda, Y., Murata, K. & Kimura, A. Transformation of intact yeast cells treated with alkali cations. *J. Bacteriol.* **153**, 163–168 (1983).
230. Tardiff, D. F., Tucci, M. L., Caldwell, K. a, Caldwell, G. a & Lindquist, S. Different 8-hydroxyquinolines protect models of TDP-43 protein, α-synuclein, and polyglutamine proteotoxicity through distinct mechanisms. *J. Biol. Chem.* **287**, 4107–20 (2012).
231. Beeg, M., Stravalaci, M., Bastone, A., Salmona, M. & Gobbi, M. A modified protocol to prepare seed-free starting solutions of amyloid-β (Aβ)1-40 and Aβ1-42 from the corresponding depsipeptides. *Anal. Biochem.* **411**, 297–299 (2011).
232. Messa, M. *et al.* The peculiar role of the A2V mutation in amyloid-β (Aβ) 1–42 molecular assembly. *J. Biol. Chem.* **289**, 24143–24152 (2014).
233. Habchi, J. *et al.* Systematic development of small molecules to inhibit specific microscopic steps of Aβ42 aggregation in Alzheimer's disease. *Proc. Natl. Acad. Sci.* **114**, E200–E208 (2017).
234. Balducci, C. *et al.* Doxycycline counteracts neuroinflammation restoring memory in Alzheimer's disease mouse models. *Neurobiol. Aging* **70**, 128–139 (2018).
235. Polymeropoulos, M. H. *et al.* Mutation in the α-synuclein gene identified in families with Parkinson's disease. *Science (80-.).* **276**, 2045–2047 (1997).
236. MacDonald, M. E. *et al.* A novel gene containing a trinucleotide repeat that is expanded and unstable on Huntington's disease chromosomes. *Cell* **72**, 971–983 (1993).
237. Sreedharan, J. *et al.* TDP-43 mutations in familial and sporadic amyotrophic lateral sclerosis. *Science* **319**, 1668–1672 (2008).
238. Scheuner, D. *et al.* Secreted amyloid β–protein similar to that in the senile plaques of Alzheimer's disease is increased in vivo by the presenilin 1 and 2 and APP mutations linked to familial Alzheimer's disease. *Nat. Med.* **2**, 864 (1996).
239. Khurana, V. & Lindquist, S. Modelling neurodegeneration in Saccharomyces cerevisiae: Why cook with baker's yeast? *Nat. Rev. Neurosci.* **11**, 436–449 (2010).
240. Colby, D. W. *et al.* Potent inhibition of huntingtin aggregation and cytotoxicity by a disulfide bond-free single-domain intracellular antibody. *Proc. Natl. Acad. Sci.* **101**, 17616–17621 (2004).

241. Braun, R. J., Büttner, S., Ring, J., Kroemer, G. & Madeo, F. Nervous yeast: modeling neurotoxic cell death. *Trends Biochem. Sci.* **35**, 135–144 (2010).

242. Kachroo, A. H. *et al.* Systematic humanization of yeast genes reveals conserved functions and genetic modularity. *Science* **348**, 921–925 (2015).

243. Sheikh, S., Haque, E. & Mir, S. S. Neurodegenerative diseases: multifactorial conformational diseases and their therapeutic interventions. *J. Neurodegener. Dis.* **2013**, (2013).

244. Duennwald, M. L., Jagadish, S., Muchowski, P. J. & Lindquist, S. Flanking sequences profoundly alter polyglutamine toxicity in yeast. *Proc. Natl. Acad. Sci. U. S. A.* **103**, 11045–11050 (2006).

245. Heberle, H., Meirelles, G. V., da Silva, F. R., Telles, G. P. & Minghim, R. InteractiVenn: a web-based tool for the analysis of sets through Venn diagrams. *BMC Bioinformatics* **16**, 169 (2015).

246. Zhou, Y. *et al.* Metascape provides a biologist-oriented resource for the analysis of systems-level datasets. *Nat. Commun.* **10**, 1523 (2019).

247. Socha, E., Koba, M. & Kośliński, P. Amino acid profiling as a method of discovering biomarkers for diagnosis of neurodegenerative diseases. *Amino Acids* **51**, 367–371 (2019).

248. Kori, M., Aydın, B., Unal, S., Arga, K. Y. & Kazan, D. Metabolic biomarkers and neurodegeneration: a pathway enrichment analysis of Alzheimer's disease, Parkinson's disease, and amyotrophic lateral sclerosis. *Omi. a J. Integr. Biol.* **20**, 645–661 (2016).

249. Kaddurah-Daouk, R. *et al.* Alterations in metabolic pathways and networks in Alzheimer's disease. *Transl. Psychiatry* **3**, e244 (2013).

250. Elbein, A. D., Pan, Y. T., Pastuszak, I. & Carroll, D. New insights on trehalose: A multifunctional molecule. *Glycobiology* **13**, 17–27 (2003).

251. Singer, M. a & Lindquist, S. Multiple effects of trehalose on protein folding in vitro and in vivo. *Mol. Cell* **1**, 639–648 (1998).

252. Attfield, P. V. Stress tolerance: the key to effective strains of industrial baker's yeast. *Nat. Biotechnol.* **15**, 1351 (1997).

253. Lackie, R. E. *et al.* The Hsp70/Hsp90 chaperone machinery in neurodegenerative diseases. *Front. Neurosci.* **11**, 1–23 (2017).

254. Viles, J. H. Metal ions and amyloid fiber formation in neurodegenerative diseases.

Copper, zinc and iron in Alzheimer's, Parkinson's and prion diseases. *Coordination Chemistry Reviews* **256**, 2271–2284 (2012).

255. Philpott, C. C. & Protchenko, O. Response to iron deprivation in Saccharomyces cerevisiae. *Eukaryot. Cell* **7**, 20–27 (2008).
256. Philpott, C. C., Protchenko, O., Kim, Y. W., Boretsky, Y. & Shakoury-Elizeh, M. The response to iron deprivation in Saccharomyces cerevisiae: expression of siderophore-based systems of iron uptake. *Biochem. Soc. Trans.* **30**, 698–702 (2002).
257. Protchenko, O. & Philpott, C. C. Regulation of intracellular heme levels by HMX1, a homologue of heme oxygenase, in Saccharomyces cerevisiae. *J. Biol. Chem.* **278**, 36582–36587 (2003).
258. Braun, R. J. Mitochondrion-mediated cell death: dissecting yeast apoptosis for a better understanding of neurodegeneration. *Front. Oncol.* **2**, 182 (2012).
259. Pozo Devoto, V. M. & Falzone, T. L. Mitochondrial dynamics in Parkinson's disease: a role for α-synuclein? *Dis. Model. Mech.* **10**, 1075–1087 (2017).
260. Haelterman, N. A. *et al.* A Mitocentric View of Parkinson's Disease. *Annu. Rev. Neurosci.* **37**, 137–159 (2014).
261. Martin, L. J. Mitochondrial pathobiology in ALS. *J. Bioenerg. Biomembr.* **43**, 569–579 (2011).
262. Correia, S. C. *et al.* Mitochondrial importance in Alzheimer's, Huntington's and Parkinson's diseases. in *Neurodegenerative diseases* 205–221 (Springer, 2012).
263. Westermann, B. Mitochondrial fusion and fission in cell life and death. *Nat. Rev. Mol. cell Biol.* **11**, 872 (2010).
264. Youle, R. J. & Van Der Bliek, A. M. Mitochondrial fission, fusion, and stress. *Science* **337**, 1062–1065 (2012).
265. Youle, R. J. & Narendra, D. P. Mechanisms of mitophagy. *Nat. Rev. Mol. cell Biol.* **12**, 9 (2011).
266. Su, L. J. *et al.* Compounds from an unbiased chemical screen reverse both ER-to-Golgi trafficking defects and mitochondrial dysfunction in Parkinson's disease models. *Dis. Model. Mech.* **3**, 194–208 (2010).
267. Di Domenico, T., Walsh, I., Martin, A. J. M. & Tosatto, S. C. E. MobiDB: a comprehensive database of intrinsic protein disorder annotations. *Bioinformatics* **28**, 2080–2081 (2012).

268. Singh, G. P. & Dash, D. Intrinsic disorder in yeast transcriptional regulatory network. *Proteins Struct. Funct. Bioinforma.* **68**, 602–605 (2007).

269. Wolozin, B. Regulated protein aggregation: stress granules and neurodegeneration. *Mol. Neurodegener.* **7**, 56 (2012).

270. Uversky, V. N., Kuznetsova, I. M., Turoverov, K. K. & Zaslavsky, B. Intrinsically disordered proteins as crucial constituents of cellular aqueous two phase systems and coacervates. *FEBS Lett.* **589**, 15–22 (2015).

271. Mitchell, A. P. & Bowdish, K. S. Selection for Early Meiotic Mutants in Yeast. *Genetics* **151**, 65–72 (1992).

272. Szwarcwort-Cohen, M., Kasulin-Boneh, Z., Sagee, S. & Kassir, Y. Human Cdk2 is a functional homolog of budding yeast Ime2, the meiosis-specific Cdk-like kinase. *Cell Cycle* **8**, 647–654 (2009).

273. Nguyen, M. D., Mushynski, W. E. & Julien, J. P. Cycling at the interface between neurodevelopment and neurodegeneration. *Cell Death Differ.* **9**, 1294 (2002).

274. Berchowitz, L. E. *et al.* Regulated Formation of an Amyloid-like Translational Repressor Governs Gametogenesis. *Cell* **163**, 406–418 (2015).

275. Juhl, D. W. *et al.* Conservation of the Amyloid Interactome Across Diverse Fibrillar Structures. *Sci. Rep.* **9**, 3863 (2019).

276. Carpenter, K., Bell, R. B., Yunus, J., Amon, A. & Berchowitz, L. E. Phosphorylation-mediated clearance of amyloid-like assemblies in meiosis. *Dev. Cell* **45**, 392–405 (2018).

277. Giorgini, F., Guidetti, P., Nguyen, Q., Bennett, S. C. & Muchowski, P. J. A genomic screen in yeast implicates kynurenine 3-monooxygenase as a therapeutic target for Huntington disease. *Nat. Genet.* **37**, 526–531 (2005).

278. Willingham, S., Outeiro, T. F., DeVit, M. J., Lindquist, S. L. & Muchowski, P. J. Yeast genes that enhance the toxicity of a mutant huntingtin fragment or alpha-synuclein. *Science* **302**, 1769–1772 (2003).

279. Yeger-Lotem, E. *et al.* Bridging high-throughput genetic and transcriptional data reveals cellular responses to alpha-synuclein toxicity. *Nat. Genet.* **41**, 316 (2009).

280. Flower, T. R. *et al.* YGR198w (YPP1) targets A30P α-synuclein to the vacuole for degradation. *J. Cell Biol.* **177**, 1091–1104 (2007).

281. Liang, J. *et al.* Novel suppressors of α-synuclein toxicity identified using yeast. *Hum. Mol. Genet.* **17**, 3784–3795 (2008).

282. Hughes, R. E. *et al.* Altered transcription in yeast expressing expanded polyglutamine. *Proc. Natl. Acad. Sci. U. S. A.* **98**, 13201–13206 (2001).

283. Sarkar, S., Davies, J. E., Huang, Z., Tunnacliffe, A. & Rubinsztein, D. C. Trehalose, a novel mTOR-independent autophagy enhancer, accelerates the clearance of mutant huntingtin and α-synuclein. *J. Biol. Chem.* **282**, 5641–5652 (2007).

284. Crichton, R. R., Dexter, D. T. & Ward, R. J. Metal based neurodegenerative diseases-From molecular mechanisms to therapeutic strategies. *Coord. Chem. Rev.* **252**, 1189–1199 (2008).

285. Götz, M. E., Double, K. A. Y., Gerlach, M., Youdim, M. B. H. & Riederer, P. The relevance of iron in the pathogenesis of Parkinson's disease. *Ann. N. Y. Acad. Sci.* **1012**, 193–208 (2004).

286. Lovell, M. A., Robertson, J. D., Teesdale, W. J., Campbell, J. L. & Markesbery, W. R. Copper, iron and zinc in Alzheimer's disease senile plaques. *J. Neurol. Sci.* **158**, 47–52 (1998).

287. Roos, P. M., Vesterberg, O., Syversen, T., Flaten, T. P. & Nordberg, M. Metal concentrations in cerebrospinal fluid and blood plasma from patients with amyotrophic lateral sclerosis. *Biol. Trace Elem. Res.* **151**, 159–170 (2013).

288. Tamano, H. & Takeda, A. Dynamic action of neurometals at the synapse. *Metallomics* **3**, 656–661 (2011).

289. Crouch, P. J. & Barnham, K. J. Therapeutic redistribution of metal ions to treat Alzheimer's disease. *Acc. Chem. Res.* **45**, 1604–1611 (2012).

290. C Badrick, A. & E Jones, C. Reorganizing metals: the use of chelating compounds as potential therapies for metal-related neurodegenerative disease. *Curr. Top. Med. Chem.* **11**, 543–552 (2011).

291. Crichton, R. R., Ward, R. J. & Hider, R. C. The Efficacy of Iron Chelators for Removing Iron from Specific Brain Regions and the Pituitary—Ironing out the Brain. *Pharmaceuticals* **12**, 138 (2019).

292. Khurana, V. *et al.* Genome-Scale Networks Link Neurodegenerative Disease Genes to α-Synuclein through Specific Molecular Pathways. *Cell Syst.* **4**, 157–170 (2017).

293. Chung, C. Y. *et al.* In situ peroxidase labeling and mass-spectrometry connects alpha-synuclein directly to endocytic trafficking and mRNA metabolism in

neurons. *Cell Syst.* **4**, 242–250 (2017).

294. Deng, H., Wu, Y. & Jankovic, J. The EIF 4G1 gene and Parkinson's disease. *Acta Neurol. Scand.* **132**, 73–78 (2015).
295. Garcia-Esparcia, P. *et al.* Altered machinery of protein synthesis is region-and stage-dependent and is associated with α-synuclein oligomers in Parkinson's disease. *Acta Neuropathol. Commun.* **3**, 76 (2015).
296. Moreira, P. I., Duarte, A. I., Santos, M. S., Rego, A. C. & Oliveira, C. R. An integrative view of the role of oxidative stress, mitochondria and insulin in Alzheimer's disease. *J. Alzheimer's Dis.* **16**, 741–761 (2009).
297. Moreira, P. I. *et al.* The key role of oxidative stress in Alzheimer's disease. *Oxidative Stress Neurodegener. Disord.* **451**, 466 (2007).
298. Rhein, V. *et al.* Amyloid-beta leads to impaired cellular respiration, energy production and mitochondrial electron chain complex activities in human neuroblastoma cells. *Cell. Mol. Neurobiol.* **29**, 1063 (2009).
299. Selfridge, J. E., Lezi, E., Lu, J. & Swerdlow, R. H. Role of mitochondrial homeostasis and dynamics in Alzheimer's disease. *Neurobiol. Dis.* **51**, 3–12 (2013).
300. Hirai, K. *et al.* Mitochondrial abnormalities in Alzheimer's disease. *J. Neurosci.* **21**, 3017–3023 (2001).
301. Aliyev, A. *et al.* Mitochondria DNA deletions in atherosclerotic hypoperfused brain microvessels as a primary target for the development of Alzheimer's disease. *J. Neurol. Sci.* **229**, 285–292 (2005).
302. Manczak, M. *et al.* Mitochondria are a direct site of Aβ accumulation in Alzheimer's disease neurons: implications for free radical generation and oxidative damage in disease progression. *Hum. Mol. Genet.* **15**, 1437–1449 (2006).
303. Pagani, L. & Eckert, A. Amyloid-Beta interaction with mitochondria. *Int. J. Alzheimer's Dis.* **2011**, (2011).
304. Pavlov, P. F. *et al.* Mitochondrial γ-secretase participates in the metabolism of mitochondria-associated amyloid precursor protein. *FASEB J.* **25**, 78–88 (2011).
305. Wang, X. *et al.* Amyloid-β overproduction causes abnormal mitochondrial dynamics via differential modulation of mitochondrial fission/fusion proteins. *Proc. Natl. Acad. Sci.* **105**, 19318–19323 (2008).
306. Sorrentino, V. *et al.* Enhancing mitochondrial proteostasis reduces amyloid-β

proteotoxicity. *Nature* **552**, 187–193 (2017).

307. Fang, E. F. *et al.* Mitophagy inhibits amyloid-β and tau pathology and reverses cognitive deficits in models of Alzheimer's disease. *Nat. Neurosci.* **22**, 401 (2019).
308. Gitler, A. D. *et al.* The Parkinson's disease protein α-synuclein disrupts cellular Rab homeostasis. *Proc. Natl. Acad. Sci.* **105**, 145–150 (2008).
309. Martin, L. J. *et al.* Parkinson's disease α-synuclein transgenic mice develop neuronal mitochondrial degeneration and cell death. *J. Neurosci.* **26**, 41–50 (2006).
310. Li, W.-W. *et al.* Localization of α-synuclein to mitochondria within midbrain of mice. *Neuroreport* **18**, 1543–1546 (2007).
311. Devi, L., Raghavendran, V., Prabhu, B. M., Avadhani, N. G. & Anandatheerthavarada, H. K. Mitochondrial import and accumulation of α-synuclein impair complex I in human dopaminergic neuronal cultures and Parkinson disease brain. *J. Biol. Chem.* **283**, 9089–9100 (2008).
312. Cole, N. B., DiEuliis, D., Leo, P., Mitchell, D. C. & Nussbaum, R. L. Mitochondrial translocation of α-synuclein is promoted by intracellular acidification. *Exp. Cell Res.* **314**, 2076–2089 (2008).
313. Shavali, S., Brown-Borg, H. M., Ebadi, M. & Porter, J. Mitochondrial localization of alpha-synuclein protein in alpha-synuclein overexpressing cells. *Neurosci. Lett.* **439**, 125–128 (2008).
314. Chinta, S. J., Mallajosyula, J. K., Rane, A. & Andersen, J. K. Mitochondrial alpha-synuclein accumulation impairs complex I function in dopaminergic neurons and results in increased mitophagy in vivo. *Neurosci. Lett.* **486**, 235–239 (2010).
315. Kamp, F. *et al.* Inhibition of mitochondrial fusion by α-synuclein is rescued by PINK1, Parkin and DJ-1. *EMBO J.* **29**, 3571–3589 (2010).
316. Sampaio-Marques, B. *et al.* SNCA (α-synuclein)-induced toxicity in yeast cells is dependent on sirtuin 2 (Sir2)-mediated mitophagy. *Autophagy* **8**, 1494–1509 (2012).
317. Norris, K. L. *et al.* Convergence of Parkin, PINK1 and alpha-synuclein on Stress-induced Mitochondrial Morphological Remodeling. **290**, 13862–13874 (2015).
318. Büttner, S. *et al.* Functional mitochondria are required for α-synuclein toxicity in aging yeast. *J. Biol. Chem.* **283**, 7554–7560 (2008).
319. Moh, C. *et al.* Cell cycle deregulation in the neurons of Alzheimer's disease. in

Cell Cycle in Development 565–576 (Springer, 2011).

320. Bonda, D. J. *et al.* Cell cycle aberrations and neurodegeneration. *Neuropathol. Appl. Neurobiol.* **36**, 157–163 (2010).
321. Borysov, S. I., Granic, A., Padmanabhan, J., Walczak, C. E. & Potter, H. Alzheimer Aβ disrupts the mitotic spindle and directly inhibits mitotic microtubule motors. *Cell Cycle* **10**, 1397–1410 (2011).
322. Treusch, S. & Lindquist, S. An intrinsically disordered yeast prion arrests the cell cycle by sequestering a spindle pole body component. *J Cell Biol* **197**, 369–379 (2012).
323. Furukawa, Y. & Nukina, N. Functional diversity of protein fibrillar aggregates from physiology to RNA granules to neurodegenerative diseases. *Biochim. Biophys. Acta (BBA)-Molecular Basis Dis.* **1832**, 1271–1278 (2013).
324. Protter, D. S. W. *et al.* Intrinsically disordered regions can contribute promiscuous interactions to RNP granule assembly. *Cell Rep.* **22**, 1401–1412 (2018).
325. Becker, D. M. & Guarente, L. [12] High-efficiency transformation of yeast by electroporation. in *Methods in enzymology* **194**, 182–187 (Elsevier, 1991).
326. Morselli, M. *et al.* In vivo targeting of de novo DNA methylation by histone modifications in yeast and mouse. *Elife* **4**, e06205 (2015).
327. Anders, S. & Huber, W. Differential expression analysis for sequence count data. *Genome Biol.* **11**, R106 (2010).
328. Schmittgen, T. D. & Livak, K. J. Analyzing real-time PCR data by the comparative C T method. *Nat. Protoc.* **3**, 1101 (2008).
329. Teste, M.-A., Duquenne, M., François, J. M. & Parrou, J.-L. Validation of reference genes for quantitative expression analysis by real-time RT-PCR in Saccharomyces cerevisiae. *BMC Mol. Biol.* **10**, 99 (2009).
330. Nadai, C., Campanaro, S., Giacomini, A. & Corich, V. Selection and validation of reference genes for quantitative real-time PCR studies during Saccharomyces cerevisiae alcoholic fermentation in the presence of sulfite. *Int. J. Food Microbiol.* **215**, 49–56 (2015).
331. Ferrero, I., Viola, A.-M. & Goffeau, A. Induction by glucose of an antimycin-insensitive, azide-sensitive respiration in the yeast Kluyveromyces lactis. *Antonie Van Leeuwenhoek* **47**, 11–24 (1981).